What is the Relationship between Tensor Factorizations and Circuits (and How Can We Exploit it)?

Anonymous authors
Paper under double-blind review

Abstract

This paper establishes a rigorous connection between circuit representations and tensor factorizations, two seemingly distinct yet fundamentally related areas. By connecting these fields, we highlight a series of opportunities that can benefit both communities. Our work generalizes popular tensor factorizations within the circuit language, and unifies various circuit learning algorithms under a single, generalized hierarchical factorization framework. Specifically, we introduce a modular "Lego block" approach to build tensorized circuit architectures. This, in turn, allows us to systematically construct and explore various circuit and tensor factorization models while maintaining tractability. This connection not only clarifies similarities and differences in existing models, but also enables the development of a comprehensive pipeline for building and optimizing new circuit/tensor factorization architectures. We show the effectiveness of our framework through extensive empirical evaluations, and highlight new research opportunities for tensor factorizations in probabilistic modeling.

1 Introduction

This paper aims at bridging two apparently distant, but in fact intimately related fields: *circuit representations* (Darwiche & Marquis, 2002; Choi et al., 2020; Vergari et al., 2021) and *tensor factorizations* (Kolda, 2006; Sidiropoulos et al., 2017). Specifically, we establish a formal connection between the two representations and show how the latter can bring a unified perspective on the many learning algorithms devised to learn the former, as well as create research opportunities for both communities.

Tensors are multidimensional generalizations of matrices that are extensively used to represent high-dimensional data (Kroonenberg, 2007). Tensor factorizations are well-understood mathematical objects to compactly represent tensors in terms of simple operations acting on lower-dimensional tensors (Kolda, 2006). They have been extensively applied in ML and AI, e.g., in computer vision (Vasilescu & Terzopoulos, 2002; Savas & Eldén, 2007; Panagakis et al., 2021), graph analysis (Kolda et al., 2005), computational neuroscience (Vos et al., 2007; Tresp et al., 2021), neuro-symbolic AI (Nickel et al., 2015; Balazevic et al., 2019; Gema et al., 2023; Loconte et al., 2023), language modeling (Ma et al., 2019; Hu et al., 2022; Xu et al., 2023), and as ways to encode probability distributions (Jaini et al., 2018b; Novikov et al., 2021; Amiridi et al., 2022; Hood & Schein, 2024). While usually defined in terms of *shallow factorizations*, tensor factorizations can be also expressed as a hierarchy of factorizations (Grasedyck, 2010), sometimes represented in the graphical formalism of tensor networks (Orús, 2013; Glasser et al., 2019).

Circuit representations (Darwiche & Marquis, 2002; Choi et al., 2020; Vergari et al., 2021), on the other hand, are structured computational graphs introduced in the context of logical reasoning and probabilistic modeling (Darwiche, 2003; Poon & Domingos, 2011; Kisa et al., 2014). *Probabilistic circuits* (PCs) (Vergari et al., 2019b; Choi et al., 2020), in particular, are circuits that encode tractable probability distributions. They support a number of applications requiring exact and efficient inference routines, e.g., lossless compression (Liu et al., 2022), biomedical generative modeling (Dang et al., 2022b), reliable neuro-symbolic AI (Ahmed et al., 2022; Loconte et al., 2023) and constrained text generation (Zhang et al., 2023). Many algorithms to learn PCs from data have been proposed in the past (see e.g., Sidheekh & Natarajan (2024) for a review), with one paradigm emerging: building *overparameterized* circuits, comprising millions or even bil-

lions of parameters (Liu et al., 2023a; Gala et al., 2024a), and training these parameters by gradient-ascent, expectation-maximization (Peharz et al., 2016; 2020c), or regularized variants (Dang et al., 2022a).

Both hierarchical tensor factorizations and PCs have been introduced as alternative representations of probabilistic graphical models (Song et al., 2013; Robeva & Seigal, 2017; Glasser et al., 2020; Bonnevie & Schmidt, 2021), and the connection between certain circuits and factorizations has been hinted in some works (Jaini et al., 2018b; Glasser et al., 2019). However, they mainly differ in how they are applied: tensor factorizations are usually used in tasks where a ground-truth tensor to approximate is available or a dimensionality reduction problem can be formulated (aka *tensor sketch*), whereas PCs are usually learned from data in the same spirit generative models are trained. Similar to tensor factorizations, however, modern PC representations are overparameterized and usually encoded as a collection of tensors as to leverage parallelism and modern deep learning frameworks (Vergari et al., 2019a; Peharz et al., 2020c; Mari et al., 2023). This begs the question: Is there any formal and systematic connection between circuits and tensor factorizations? Our answer is affirmative as we show that *a circuit can be cast as a generalized sparse hierarchical tensor factorization*, where its parameters encode the lower-dimensional tensors of the factorization itself. Or alternatively, *a hierarchical tensor factorization is a special case of a deep circuit with a particular tensorized architecture*. When it comes to PCs, this implies decomposing probability distributions represented as non-negative tensors (Cichocki & Phan, 2009). At the same time, classical tensor factorizations can be exactly encoded as (shallow) circuits. By affirming the duality of tensor factorizations and circuits, we systematize previous results in the literature, open up new perspectives in representing and learning circuits, and suggest possible ways to construct new and extend existing (probabilistic) factorizations.

Specifically, in this paper we will first derive a compact way to denote several tensorized circuit architectures, and represent them as computational graphs using a *"Lego blocks"* approach that stacks (locally) dense tensor factorizations while preserving the structural properties of circuits required for tractability. This enables us to use novel "blocks" in a plug-and-play manner. Then, we unify the many different algorithms for learning PCs that have been proposed in the literature so far (Peharz et al., 2020c;a; Liu & Van den Broeck, 2021b), which come from different perspectives and yield circuits that are considered as different models. In particular, we show that their differences reduce to factorizations and syntactic transformations of their tensor parameters, since they can be understood under the same generalized (hierarchical) factorization based on the Tucker tensor factorization (Tucker, 1966) and its specializations (Kolda & Bader, 2009). Therefore, we argue the different performances that are often reported in the literature are actually the result of different hyperparameters and learning methods more than different inductive biases (Liu et al., 2023b).

Furthermore, after making this connection, we exploit tensor factorizations to further compress the parameters of modern PC architectures already represented in tensor format. By doing so, we introduce PCs that are more parameter-efficient than previous ones, and we show that finding the best circuit architecture for a certain setting is far from solved. Lastly, we highlight how this connection with circuits can spawn interesting research opportunities for the tensor factorization community (highlighted as boxes throughout the paper): ranging from learning to decompose tensors from data, to interpreting tensor factorizations as latent-variable probabilistic models, to inducing sparsity via the specification of background knowledge.

Contributions. **i)** We generalize popular tensor factorization methods and their hierarchical formulation into the language of *circuits* (Section 2). **ii)** We connect PCs to non-negative tensor factorizations and highlight how the latter can be interpreted as latent variable models, and as such they can be used as generative models and for neuro-symbolic AI (Section 3). **iii)** Within our framework, we abstract away the many options used to build and learn modern overparameterized architectures to arrive at a general algorithmic pipeline (Section 4) to represent and learn hierarchical tensor factorizations as tensorized circuits. **iv)** This allows us to analyze how existing, different parameterizations of circuits are related to each other by leveraging tensor factorizations, while proposing more parameter-efficient modeling choices that retain some of the expressiveness (Section 5). **v)** We evaluate several algorithmic choices in our framework on a wide range of distribution estimation tasks, highlighting the major trade-offs in terms of time and space complexity, and resulting performance (Section 6).

2 From Tensor Factorizations to Circuits

Symbols notation. We will adapt most of the notation and nomenclature from Kolda & Bader (2009). We denote sets of random variables with $\mathbf{X}$, $\mathbf{Y}$ and $\mathbf{Z}$, and we use $[n]$ to express the set $\{1, 2, \ldots, n\}$ with $n > 0$. The domain of a variable X is denoted as $\mathsf{dom}(X)$, and we denoted as $\mathsf{dom}(\mathbf{X}) = \mathsf{dom}(X_1) \times \cdots \times \mathsf{dom}(X_n)$ the joint domain of variables $\mathbf{X} = \{X_i\}_{i=1}^n$. We denote scalars with lower-case letters (e.g., $a \in \mathbb{R}$), vectors with boldface lower-case letters (e.g., $\mathbf{a} \in \mathbb{R}^N$), matrices with boldface upper-case letters (excluding those used for variables, e.g., $\mathbf{A} \in \mathbb{R}^{M \times N}$), and tensors with boldface calligraphic letters (e.g., $\boldsymbol{\mathcal{A}} \in \mathbb{R}^{I_1 \times I_2 \times I_3}$). Moreover, we use subscripts to denote entries of tensors (e.g., a_{ijk} is the (i, j, k)-th entry in $\boldsymbol{\mathcal{A}}$), and make use of ":" to denote tensor slicing (e.g., $\mathbf{A}_{:j:} \in \mathbb{R}^{I_1 \times I_3}$ is obtained by selecting the j-th matrix slice of $\boldsymbol{\mathcal{A}}$ along the second dimension).

Matrix and tensor operations notation. Furthermore, we denote with $\odot$ the Hadamard (or element-wise product) of tensors having the same dimensions, and we denote with $\circ$ the outer products of vectors, i.e., given $\mathbf{u} \in \mathbb{R}^M, \mathbf{v} \in \mathbb{R}^N$ we have that their outer product $\mathbf{A} = \mathbf{u} \circ \mathbf{v} \in \mathbb{R}^{M \times N}$ is defined such that $a_{ij} = u_i v_j$ for all $(i, j) \in [M] \times [N]$. We denote with $||$ the concatenation operator over vectors, i.e., $\mathbf{u} \,||\, \mathbf{v} = [u_1, \ldots, u_M, v_1, \ldots, v_N]^\top \in \mathbb{R}^{M+N}$. We use $\otimes$ to express the Kronecker product between vectors, i.e., $\mathbf{u} \otimes \mathbf{v} \in \mathbb{R}^{MN}$ is the *row-wise* flattening of $\mathbf{u} \circ \mathbf{v}$ into an MN-dimensional vector. Finally, we use $\times_n$ to denote the tensor-matrix dot product along the n-th dimension, i.e., given a tensor $\boldsymbol{\mathcal{T}} \in \mathbb{R}^{I_1 \times \cdots \times I_d}$ and a matrix $\mathbf{A} \in \mathbb{R}^{J \times I_n}$, $n \in [d]$, then we have that $\boldsymbol{\mathcal{T}} \times_n \mathbf{A} \in \mathbb{R}^{I_1 \times \cdots \times I_{n-1} \times J \times I_{n+1} \cdots \times I_d}$ is defined in element-wise notation as $(\boldsymbol{\mathcal{T}} \times_n \mathbf{A})_{i_1 \cdots i_{n-1}\, j\, i_{n+1} \cdots i_d} = \sum_{i_n=1}^{I_n} t_{i_1 \cdots i_d} a_{j i_n}$, with $j \in [J]$.

2.1 Shallow Tensor Factorizations are Shallow Circuits

Tucker factorization. Tensor factorizations *approximate* high-dimensional tensors by a collection of lower-dimensional ones. Formally, given a tensor $\boldsymbol{\mathcal{T}} \in \mathbb{R}^{I_1 \times \cdots \times I_d}$, whose size grows exponentially with respect to the dimensions d, we seek a low-rank factorization for it (Kroonenberg, 2007). Many popular tensor factorization methods, such as the *canonical polyadic* decomposition (CP) (Carroll & Chang, 1970), *RESCAL* (Nickel et al., 2011), and the *higher-order singular value decomposition* (HOSVD) (De Lathauwer et al., 2000) are all particular cases of the *Tucker* factorization (Tucker, 1964; 1966). For this reason, our treatment of tensor factorizations will focus on Tucker first, and its hierarchical formulation (Grasedyck, 2010) later. Our results will generalize to special cases such as CP, RESCAL and HOSVD.

Definition 1 (Tucker factorization (Tucker, 1964))**.** Let $\boldsymbol{\mathcal{T}} \in \mathbb{R}^{I_1 \times \cdots \times I_d}$ be a d-dimensional tensor. The multilinear rank-$(R_1, \ldots, R_d)$ *Tucker factorization* of $\boldsymbol{\mathcal{T}}$ factorizes it as a *core tensor* multiplied by a matrix along each dimension, i.e.,

$$\boldsymbol{\mathcal{T}} \approx \boldsymbol{\mathcal{W}} \times_1 \mathbf{V}^{(1)} \times_2 \mathbf{V}^{(2)} \ldots \times_d \mathbf{V}^{(d)} \tag{1}$$

where $\boldsymbol{\mathcal{W}} \in \mathbb{R}^{R_1 \times \cdots \times R_d}$ is the core tensor, $\mathbf{V}^{(j)} \in \mathbb{R}^{I_j \times R_j}$ with $j \in [d]$ are the *factor matrices*, and $\approx$ denotes the approximation of the tensor on the left-hand side given by the right-hand side factorization. The above equation can be rewritten in element-wise notation as

$$t_{i_1 \cdots i_d} \approx \sum_{r_1=1}^{R_1} \cdots \sum_{r_d=1}^{R_d} w_{r_1 \cdots r_d}\, v^{(1)}_{i_1 r_1} \cdots v^{(d)}_{i_d r_d}. \tag{2}$$

Focusing on the element-wise notation, we can view the factorization of $\boldsymbol{\mathcal{T}}$ as a function c over d discrete variables $\mathbf{X} = \{X_j\}_{j=1}^d$, each having domain $\mathsf{dom}(X_j) = [I_j]$, such that $t_{\mathbf{x}} \approx c(\mathbf{x})$ for any assignment $\mathbf{x} = \langle i_1, \ldots, i_d \rangle$ to variables $\mathbf{X}$. In other words, each assignment to $\mathbf{X}$ is mapped to one scalar tensor entry, whose value is computed by c. Eq. (2) highlights that such a tensor factorization encodes a polynomial defined over the factor matrix values associated to assignments to variables $\mathbf{X}$ (Kolda, 2006). Therefore, we can represent the factorization encoded in c as a *circuit*, i.e., a computational graph consisting of sums and products as atomic operators, formally defined next.

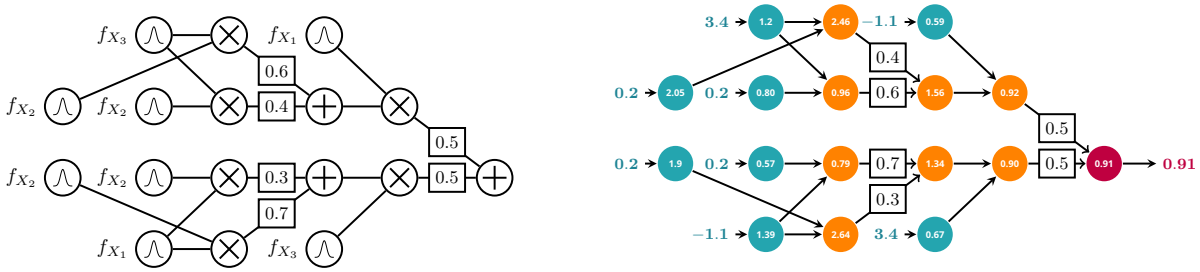

Figure 1: **Example of a circuit (left) and its evaluation (right)** for a circuit encoding the joint density over three continuous random variables X_1, X_2, X_3. We denote input units with $\bigwedge$ as they are univariate Gaussian distributions and label them with their scopes (left) while later on we will draw generic input units with an empty circle. To compute the joint density for $p(X_1 = -1.1, X_2 = 0.2, X_3 = 3.4)$, one has to first evaluate the Gaussian densities at the inputs (blue) and propagate the computed values. These densities are then multiplied across product units $\bigotimes$ and then passed through sums $\bigoplus$ (both in orange), whose parameters are here explicitly drawn in boxes. We will omit drawing the sum units weights in other pictures to avoid clutter. The value of $p(X_1 = -1.1, X_2 = 0.2, X_3 = 3.4) = 0.91$ is obtained by collecting the output of the last unit (in purple). See Section 3 for more circuits encoding distributions.

Definition 2 (Circuit (Choi et al., 2020; Vergari et al., 2021))**.** A *circuit* c is a parameterized directed acyclic computational graph[1] over variables $\mathbf{X}$ encoding a function $c(\mathbf{X})$, and comprising three kinds of computational units: *input*, *product*, and *sum* units. Each product or sum unit n receives the outputs of other units as inputs, denoted with the set $\mathsf{in}(n)$. Each unit n encodes a function c_n defined as: (i) $f_n(\mathsf{sc}(n))$ if n is an input unit, where f_n is a function over variables $\mathsf{sc}(n) \subseteq \mathbf{X}$, called its *scope*, (ii) $\prod_{j \in \mathsf{in}(n)} c_j(\mathsf{sc}(j))$ if n is a product unit, and (iii) $\sum_{j \in \mathsf{in}(n)} w_j c_j(\mathsf{sc}(j))$ if n is a sum unit, with $w_j \in \mathbb{R}$ denoting the weighted sum parameters. The scope of a product or sum unit n is the union of the scopes of its inputs, i.e., $\mathsf{sc}(n) = \bigcup_{j \in \mathsf{in}(n)} \mathsf{sc}(j)$. The size of a circuit c, denoted as $|c|$, is the number of edges between the computational units.

Circuits can be understood as multilinear polynomials with exponentially many terms, but compactly encoded in a deep computational graph of polynomial size (Darwiche, 2003; Zhao et al., 2016; Choi et al., 2020). From this perspective, it is possible to intuit how they are related to, but also different from, tensor factorizations. In fact, while also the latter encode compact multilinear operators (Eq. (2)), the indeterminates of the circuit polynomials can be more than just entries of matrices as per Def. 2, e.g., potentially non-linear input functions. For example, a circuit can encode the joint density over a collection of continuous random variables, and input functions f_n could encode Gaussian densities (Fig. 1). See also Opportunity 4 for a discussion on the many ways to encode input units in circuits.

Evaluating the function c encoded in a circuit is done by traversing its computational graph in the usual *feedforward* way – inputs before outputs, see Fig. 1. Furthermore, the circuit definition we provided can be more general than tensor factorizations as it can represent *sparse* computational graphs, i.e., where units are irregularly connected. As we will argue later, this does not need to be the case. Circuits can be, in fact, designed to be locally-dense as it is common in many modern implementations (Section 4). Locally-dense architectures are also how tensor factorizations will look like, when turned into circuits, as we demonstrate in the following constructive proposition for a general Tucker factorization (Def. 1).

Proposition 1 (Tucker as a circuit)**.** Let $\boldsymbol{\mathcal{T}} \in \mathbb{R}^{I_1 \times \cdots \times I_d}$ be a tensor being decomposed via a multilinear rank-$(R_1, \ldots, R_d)$ Tucker factorization, as in Eq. (1). Then, there exists a circuit c over variables $\mathbf{X} = \{X_j\}_{j=1}^d$ with $\mathsf{dom}(X_j) = [I_j]$, $j \in [d]$ computing the same factorization. Moreover, we have that $|c| \in \mathcal{O}(d \prod_{j=1}^d R_j)$.

Appendix A.1 details our proof construction and Fig. 2 illustrates it for the Tucker factorization of a three dimensional tensor. In a nutshell, we build a *shallow* circuit c over the same variables that, when evaluated,

[1] In our figures, the direction of the circuit edges is always assumed to be from input to output units, but it is not graphically showed to avoid clutter.

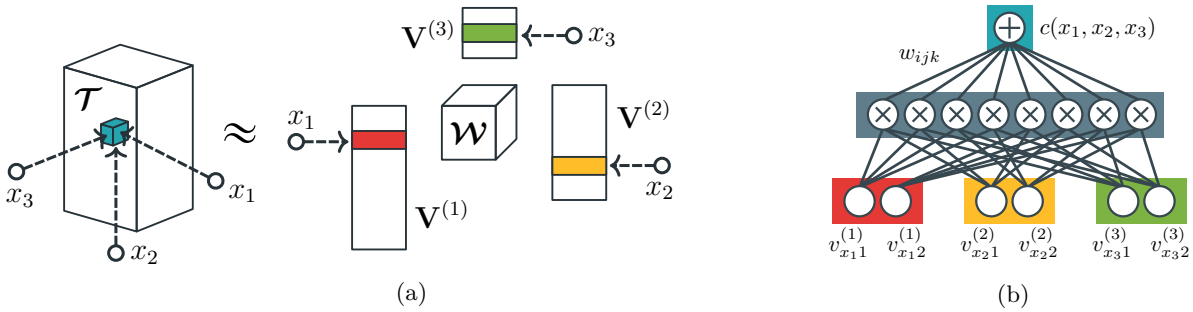

Figure 2: **Tucker tensor factorizations are circuits.** Given a tensor $\mathcal{T} \in \mathbb{R}^{I_1 \times I_2 \times I_3}$ and its multilinear rank-$(2, 2, 2)$ Tucker factorization $\mathcal{T} \approx \mathcal{W} \times_1 \mathbf{V}^{(1)} \times_2 \mathbf{V}^{(2)} \times_3 \mathbf{V}^{(3)}$ (a), we can encode it as a circuit c whose evaluation corresponds to computing an entry of the decomposed tensor, i.e., $t_{x_1 x_2 x_3} \approx c(x_1, x_2, x_3)$ for any entry index (x_1, x_2, x_3) (b). The directionality of the circuit connections goes from input units to output units, but it is not showed to avoid clutter. The sum unit is parameterized by the entries w_{ijk} of the core tensor $\mathcal{W}$, while the input units are parameterized by the factor matrices $\mathbf{V}^{(1)}, \mathbf{V}^{(2)}, \mathbf{V}^{(3)}$. For instance, evaluating the two input units depending on the index x_1 (b, in red) translates to indexing the x_1-th row of $\mathbf{V}^{(1)}$, i.e., $\mathbf{v}_{x_1:} = [v^{(1)}_{x_1 1} \;\; v^{(1)}_{x_1 2}]^\top$ (a, in red).

outputs the reconstructed tensor entry for a set of coordinates, i.e., it encodes Eq. (2). Its input functions f_n, in fact, map variable states to *embeddings*, i.e., the real values contained in the matrices obtained from the Tucker factorization, see Fig. 1. Note that one can easily particularize our construction to obtain circuits corresponding to other factorizations such as CP, RECAL and HOSVD.

As a concrete example of our construction, consider the following. Let $\mathcal{T} \in \mathbb{R}^{3 \times 3 \times 3}$ be a three-dimensional tensor defined as

$$\mathcal{T} = \left(\begin{pmatrix} -1.68 & 4.02 & -1.84 \\ 0.63 & \mathbf{-1.50} & 0.68 \\ 0.25 & -0.59 & 0.27 \end{pmatrix}, \begin{pmatrix} 16.83 & -40.24 & 18.36 \\ -6.27 & 14.99 & -6.84 \\ -2.48 & 5.918 & -2.7 \end{pmatrix}, \begin{pmatrix} 21.88 & -52.31 & 23.87 \\ -8.15 & 19.49 & -8.89 \\ -3.22 & 7.69, & -3.51 \end{pmatrix} \right) \tag{3}$$

and whose multilinear rank-$(2, 2, 2)$ Tucker decomposition is given by a tensor $\mathcal{W} \in \mathbb{R}^{2 \times 2 \times 2}$ whose entries are all 0.5 and by matrices

$$\mathbf{V}^{(1)} = \begin{pmatrix} \mathbf{0.1} & \mathbf{0.2} \\ -2.0 & -1.0 \\ 1.5 & -5.4 \end{pmatrix}, \quad \mathbf{V}^{(2)} = \begin{pmatrix} 1.1 & 9.1 \\ \mathbf{-3.3} & \mathbf{-0.5} \\ 0.7 & -2.2 \end{pmatrix}, \quad \mathbf{V}^{(3)} = \begin{pmatrix} -2 & 0.9 \\ \mathbf{0.23} & \mathbf{2.4} \\ -1.4 & 0.2 \end{pmatrix}. \tag{4}$$

Then, we can build a circuit c with the same structure as the one in Fig. 2, equipping its input units with embeddings taken from $\mathbf{V}^{(1)}$, $\mathbf{V}^{(2)}$ or $\mathbf{V}^{(3)}$, depending on their scope, and by setting the sum unit parameters to be the vector $\mathbf{w} \in \mathbb{R}^8$ obtained by vectorizing the tensor $\mathcal{W}$ and therefore having values $= (0.5, \ldots, 0.5)$. Now, to compute the approximate value of the $t_{1,2,2}$ entry in $\mathcal{T}$, we can just evaluate the circuit c in a feedforward way—evaluating inputs before outputs—to compute $c(1, 2, 2)$. This would yield the following computation:

$$\mathbf{w}^\top \left(\begin{pmatrix} \mathbf{0.1} & \mathbf{0.2} \end{pmatrix}^\top \otimes \begin{pmatrix} \mathbf{-3.3} & \mathbf{-0.5} \end{pmatrix}^\top \otimes \begin{pmatrix} \mathbf{0.23} & \mathbf{2.4} \end{pmatrix}^\top \right) \approx \mathbf{-1.4991}. \tag{5}$$

Note how the color-coded blocks inside the brackets correspond to the outputs of the input functions in the circuits (Fig. 2), and how the vector outer products ($\otimes$) realize the product units in c while the dot product with $\mathbf{w}$ is encoded in the final sum unit. We invite the reader to play with this example and try to recover other entries in the tensor, until they are comfortable with the translation of a tensor factorization into our circuit format. Furthermore, since circuits can represent factorizations, they inherit the same non-uniqueness issue commonly arising in many tensor factorization methods (e.g., Tucker). That is, the tensor factorization encoded by a circuit is not unique: one can change the circuit parameters while still encoding the same function. Finally, we remark that the multilinear-rank of the factorization now translates into the

number of the input units in the circuit representation. Later, for hierarchical factorizations turned into deep circuits (Section 2.2) ranks will turn into the number of units located at different depths as well.

Representing tensor factorizations as computational graphs of this kind will offer a number of opportunities for extending the former model class, in which case we will highlight them in boxes throughout the paper. At the same time, we can better understand why these factorizations already support the tractable computation of certain quantities of interest, e.g., the computation of integrals, information theoretic measures or maximization (Vergari et al., 2021). This can be done in a systematic way in the framework of circuits, that maps these computations to the presence of certain structural properties of the computational graph, precisely defining sufficient (and sometimes necessary) conditions for tractability. We start by defining *smoothness* and *decomposability*, two structural properties of circuits that allow to tractably compute summations over exponentially many variable assignments, which are often intractable to compute for other models.

Definition 3 (Unit-wise smoothness and decomposability (Darwiche & Marquis, 2002))**.** A circuit is *smooth* if for every sum unit n, its input units depend all on the same variables, i.e., $\forall i, j \in \mathsf{in}(n) \colon \mathsf{sc}(i) = \mathsf{sc}(j)$. A circuit is *decomposable* if for every product unit n, its input units depend on mutually disjoint sets of variables, i.e., $\forall i, j \; i \neq j \colon \mathsf{sc}(i) \cap \mathsf{sc}(j) = \varnothing$.

For a smooth and decomposable circuit one can exactly compute summations of the form $\sum_{\mathbf{z} \in \mathsf{dom}(\mathbf{Z})} c(\mathbf{y}, \mathbf{z})$, where $\mathbf{Z} \subseteq \mathbf{X}$, $\mathbf{Y} = \mathbf{X} \backslash \mathbf{Z}$, called *marginals*, in a single feedforward pass of its computational graphs (Choi et al., 2020). See also our discussion in Section 3 for more use cases of smoothness and decomposability. It is easy to verify that a Tucker tensor factorization represented as a circuit (e.g., Fig. 2) is both smooth and decomposable, and hence inherits tractable marginalization. In addition, under this light, one can understand the expressiveness of these factorizations, for multilinear polynomials expressiveness is usually characterized in terms of circuits with these structural properties (Shpilka & Yehudayoff, 2010; Martens & Medabalimi, 2014; de Colnet & Mengel, 2021).

Where do circuits and tensor factorizations come from? Now that we have established a first link between tensor factorizations and circuits, as the former can be rewritten as computational graphs with structural properties in the language of the latter, we also point out a first difference in how the two communities obtain and approach these objects. Tensor factorizations arise from the need of compressing a *given* high-dimensional tensor, which is usually *explicitly* represented (if not on memory, on disk). A factorization is then retrieved as the output of an optimization problem, e.g., find the factors that minimize a certain reconstruction loss (Sidiropoulos et al., 2017; Cichocki et al., 2007). In contrast, modern circuits are *learned from data*. While this can be done both in a supervised and unsupervised way, the latter is more common as circuits are learned to encode a probability distribution. Such a distribution can be thought as an *implicit* tensor that is never observed, but from which we sampled data points. Section 3 formalizes this and the circuit learning problem. Even if reconstructing tensors is generally done differently than learning circuit from data, *once a factorization is given, by looking at it as a circuit, we can open up new opportunities to use it and exploit it*. We highlight them as boxes in the following sections. Next, we discuss how the framework of circuits also generalizes hierarchical (or deeper) tensor factorizations, which will also provide the entry point of our pipeline for *learning* both circuits and tensor factorizations (Section 4).

2.2 Hierarchical Tensor Factorizations are Deep Circuits

Tensor factorizations can be stacked together to form a *deep* or *hierarchical* factorization that can be much more space-efficient (i.e., of much lower rank) than its *shallow* materialization. For instance, Grasedyck (2010) proposed *hierarchical Tucker*, which stacks many low-rank Tucker factorizations according to a fixed hierarchical partitioning of tensor dimensions. Cohen et al. (2015) showed that in most cases equivalent or even approximate shallow factorizations would instead require an exponential rank with respect to the number of dimensions. Similar theoretical results have been also shown for circuits, i.e., deep circuits can be exponentially smaller than shallow circuits, where the size of a circuit is the number of unit connections (Delalleau & Bengio, 2011; Martens & Medabalimi, 2014; Jaini et al., 2018b).

In this section, we first introduce the hierarchical Tucker factorization, show that it is an instance of a deep circuit, and later use this connection to describe modern tensorized circuit representations (Section 4). To do

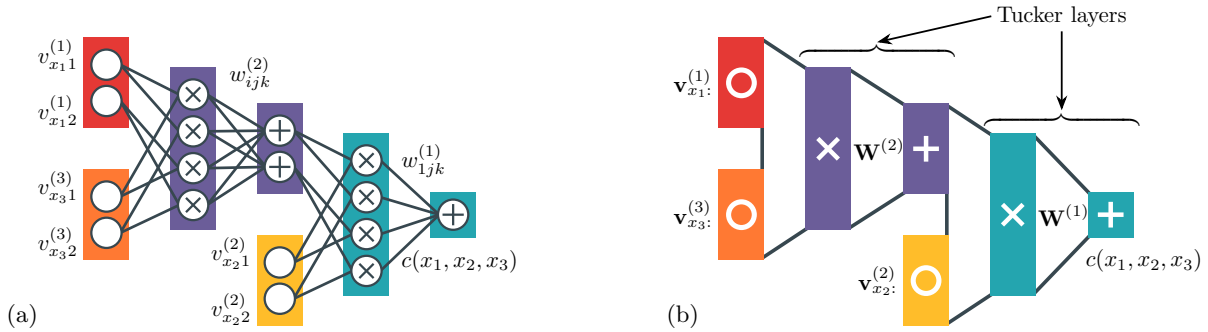

Figure 3: **Hierarchical Tucker factorizations are deep (tensorized) circuits** as shown here with the circuit representation of the hierarchical Tucker factorization of a three dimensional tensor (a), which is obtained by stacking two Tucker factorizations according to the RG in Fig. 4. Evaluating the circuit from left to right for some entry (x_1, x_2, x_3) computes the corresponding tensor entry. In (b) we show the equivalent tensorized architecture (Def. 7) obtained by grouping units into layers, according to the graphical convention introduced in Def. 7. Input layers map indices into rows of factor matrices, while products layers compute Kronecker products of their inputs, and sum units compute a matrix-vector product. The core tensors $\boldsymbol{\mathcal{W}}^{(2)} \in \mathbb{R}^{2\times2\times2}, \boldsymbol{\mathcal{W}}^{(1)} \in \mathbb{R}^{1\times2\times2}$ that parameterize the sum units in (a) are reshaped into matrices $\mathbf{W}^{(2)} \in \mathbb{R}^{2\times4}, \mathbf{W}^{(1)} \in \mathbb{R}^{1\times4}$ in (b). In Section 4 we will refer to the composition of Kronecker product and sum layers simply as *Tucker layer*, as showed in (b).

so, we borrow a tool from the circuit literature: a hierarchical partitioning of the scope of a circuit (Vergari et al., 2021), aka *region graph* (RG) (Dennis & Ventura, 2012). A RG is a bipartite graph whose nodes are either sets of variables, i.e., the dimensions of the tensor to decompose, or indicate how to partition such sets.

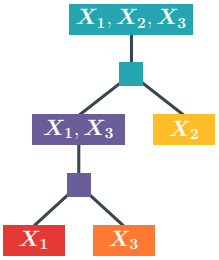

Figure 4: A tree RG.

Definition 4 (Region graph (Dennis & Ventura, 2012))**.** Given a set of variables $\mathbf{X}$, a *region graph* $\mathcal{R}$ is a bipartite and rooted directed acyclic graph (DAG) whose nodes are either *regions*, denoting subsets of $\mathbf{X}$, or *partitions*, specifying how a region is partitioned into other regions. The root is the region node $\mathbf{X}$.

Without loss of generality, we assume binary RGs, i.e., each region is partitioned into two others, as shown in Fig. 4.[2] Next, we define the hierarchical variant of Tucker.

Definition 5 (Hierarchical Tucker factorization)**.** Let $\boldsymbol{\mathcal{T}} \in \mathbb{R}^{I_1\times\cdots\times I_d}$ be a d-dimensional tensor, and let $\mathbf{X}$ be the region root of a tree-shaped binary RG $\mathcal{R}$ whose leaves have exactly one variable, where $\mathsf{dom}(X_j) = [I_j]$ for all $X_j \in \mathbf{X}$. The *hierarchical Tucker factorization* of $\boldsymbol{\mathcal{T}}$ is given by recursively applying Tucker factorizations according to the partitioning of indices induced by $\mathcal{R}$. There are three cases:

- First, for every leaf region $\mathbf{Z} = \{X_j\}$ in $\mathcal{R}$, we define $u^{(\mathbf{Z})}_{x_j r}$ to be an alias of the (x_j, r)-th entry of the factor matrix $\mathbf{V}^{(j)} \in \mathbb{R}^{I_j\times R_{\mathbf{Z}}}$ associated to $\mathbf{Z}$.
- Next, for every non-leaf region $\mathbf{Y} \subseteq \mathbf{X}$ partitioned into $(\mathbf{Z}_1, \mathbf{Z}_2)$ in $\mathcal{R}$, i.e., $\mathbf{Y} = \mathbf{Z}_1 \cup \mathbf{Z}_2$ with $\mathbf{Y} = \{Y_j\}_{j=1}^{l}$, $\mathbf{Z}_1 = \{Z_{1,j}\}_{j=1}^{m}$, $\mathbf{Z}_2 = \{Z_{2,j}\}_{j=1}^{n}$, we recursively define the Tucker factorization associated to $\mathbf{Y}$ as

$$u^{(\mathbf{Y})}_{y_1\cdots y_l s} \approx \sum_{r_1=1}^{R_{\mathbf{Z}_1}} \sum_{r_2=1}^{R_{\mathbf{Z}_2}} w^{(\mathbf{Y})}_{s\, r_1 r_2}\, u^{(\mathbf{Z}_1)}_{z_{1,1}\cdots z_{1,m} r_1}\, u^{(\mathbf{Z}_2)}_{z_{2,1}\cdots z_{2,n} r_2} \qquad \text{with } s \in [R_{\mathbf{Y}}], \tag{6}$$

  where $(R_{\mathbf{Y}}, R_{\mathbf{Z}_1}, R_{\mathbf{Z}_2})$ denotes the multilinear rank of the Tucker factorization. Moreover, $\boldsymbol{\mathcal{W}}^{(\mathbf{Y})} \in \mathbb{R}^{R_{\mathbf{Y}}\times R_{\mathbf{Z}_1}\times R_{\mathbf{Z}_2}}$ is the corresponding core tensor, and $\mathbf{y} = \langle y_1, \ldots, y_l\rangle$, $\mathbf{z}_1 = \langle z_{1,1}, \ldots, z_{1,m}\rangle$, $\mathbf{z}_2 = \langle z_{2,1}, \ldots, z_{2,m}\rangle$ are assignments to variables $\mathbf{Y}, \mathbf{Z}_1, \mathbf{Z}_2$, respectively.

[2]Similarly to our graphical notation of circuits (Def. 2), we remove the directionality of node connections from the figures and assume that edges are oriented from region nodes of more variables towards regions of fewer variables.

- Finally, in the case of the root region $\mathbf{Y} = \mathbf{X}$ in the recursive rule in Eq. (6), we define $R_{\mathbf{Y}} = 1$ and $u^{(\mathbf{Y})}_{x_1 x_2 \cdots x_d 1}$ in Eq. (6) becomes an alias of the entry $t_{x_1 x_2 \cdots x_d}$ of $\boldsymbol{\mathcal{T}}$.

We provide an example of a hierarchical Tucker factorization, as to show an application of the recursive Tucker factorization shown in Eq. (6). Given $\boldsymbol{\mathcal{T}} \in \mathbb{R}^{I_1 \times I_2 \times I_3}$ a a three-dimensional tensor, we factorize it via hierarchical Tucker according to the RG shown in Fig. 4. Since the RG in Fig. 4 has two partitionings, we recursively perform two Tucker factorizations (as in Eq. (6)), and choose $(R_{\{X_1,X_2,X_3\}}, R_{\{X_2\}}, R_{\{X_1,X_3\}})$ and $(R_{\{X_1,X_3\}}, R_{\{X_1\}}, R_{\{X_3\}})$ as the respective multilinear ranks, i.e., each entry of $\boldsymbol{\mathcal{T}}$ is approximated as

$$t^{\{X_1,X_2,X_3\}}_{x_1 x_2 x_3} \approx \sum_{r_1=1}^{R_{\{X_2\}}} \sum_{r_2=1}^{R_{\{X_1,X_3\}}} w^{\{X_1,X_2,X_3\}}_{1 r_1 r_2} \; v^{\{X_2\}}_{x_2\, r_1} \; u^{\{X_1,X_3\}}_{x_1 x_3\, r_2},$$

where $\boldsymbol{\mathcal{W}} \in \mathbb{R}^{1 \times R_{\{X_2\}} \times R_{\{X_1,X_3\}}}$ is the core tensor of the first Tucker factorization, $\mathbf{V}^{\{X_2\}} \in \mathbb{R}^{I_2 \times R_{\{X_2\}}}$ is the factor matrix associated to $\{X_2\}$, and $\boldsymbol{\mathcal{U}}^{\{X_1,X_3\}} \in \mathbb{R}^{I_1 \times I_3 \times R_{\{X_1,X_3\}}}$ consists of $R_{\{X_1,X_3\}}$ matrices of shape $I_1 \times I_3$ being factorized according to the second Tucker factorization,[3] i.e.,

$$u^{\{X_1,X_3\}}_{x_1 x_3\, r_2} = \sum_{r_3=1}^{R_{\{X_1\}}} \sum_{r_4=1}^{R_{\{X_3\}}} w^{\{X_1,X_3\}}_{r_2 r_3 r_4} \; v^{\{X_1\}}_{x_1\, r_3} \; v^{\{X_3\}}_{x_3\, r_4},$$

where $\mathbf{W}^{\{X_1,X_3\}} \in \mathbb{R}^{R_{\{X_1,X_3\}} \times R_{\{X_1\}} \times R_{\{X_3\}}}$, $\mathbf{V}^{\{X_1\}} \in \mathbb{R}^{I_1 \times R_{\{X_1\}}}$, and $\mathbf{V}^{\{X_3\}} \in \mathbb{R}^{I_3 \times R_{\{X_3\}}}$.

Following this recursive definition of a hierarchical Tucker factorization, we now build an equivalent circuit c encoding the same factorization, i.e., $t_{\mathbf{x}} \approx c(\mathbf{x})$, by stacking weighted sum and product units together as to construct a *deep* circuit. In the following constructive proposition we present this construction.

Proposition 2 (Hierarchical Tucker as a deep circuit)**.** Let $\boldsymbol{\mathcal{T}} \in \mathbb{R}^{I_1 \times \cdots \times I_d}$ be a tensor being decomposed using hierarchical Tucker factorization according to a RG $\mathcal{R}$. Then, there exists a circuit c over variables $\mathbf{X} = \{X_j\}_{j=1}^{d}$ with $\mathsf{dom}(X_j) = [I_j]$, computing the same factorization. Furthermore, given $\{\mathbf{Y}^{(i)}\}_{i=1}^{m} \subset 2^{\mathbf{X}}$ the set of all non-leaf region nodes $\mathbf{Y}^{(i)} \subseteq \mathbf{X}$ being factorized into $(\mathbf{Z}_1^{(i)}, \mathbf{Z}_2^{(i)})$ in $\mathcal{R}$, with corresponding Tucker factorization multilinear rank $(R_{\mathbf{Y}^{(i)}}, R_{\mathbf{Z}_1^{(i)}}, R_{\mathbf{Z}_2^{(i)}})$, we have that $|c| \in \mathcal{O}\left(\sum_{i=1}^{m} R_{\mathbf{Y}^{(i)}} R_{\mathbf{Z}_1^{(i)}} R_{\mathbf{Z}_2^{(i)}}\right)$.

Appendix A.2 shows the construction, also illustrated in Fig. 3a for a hierarchical Tucker factorization based on the RG showed in Fig. 4. In the very same way one can extend any tensor factorization to be hierarchical, one can represent such a construction as a circuit. However, in the circuit literature we found many architectures that are not limited to RGs that are trees nor to those having univariate input regions.

Opportunity 1. A wider choice of factorization structures

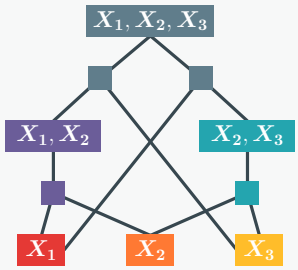

Figure 5: Region nodes can be shared between partitionings in a DAG RG.

Def. 4 allows for arbitrary DAGs and arbitrarily scoped-regions, while hierarchical tensor factorizations are usually presented in terms of RGs with a tree structure having region leaves containing *exactly one variable* (e.g., the RG in Fig. 4), which are sometimes called *dimension trees* or *mode cluster trees* (Grasedyck, 2010) in the tensor factorization community, and often *vtree* in circuit literature (Pipatsrisawat & Darwiche, 2008; Kisa et al., 2014; Wedenig et al., 2024a). More intricate RG structures can increase the expressiveness as well as flexibility in building deep circuits/hierarchical factorizations. Intuitively, we can share factor matrices among multiple factorizations, and therefore reduce the number of model parameters, making a more space-efficient implementation possible. See Peharz et al. (2020c;a) for more details. We provide an example of such a RG in Fig. 10 and Fig. 5 here on the left.

[3] The Tucker factorization of a three-dimensional tensor into only two factor matrices implicitly assumes the identity matrix as third factor, and it is also called *Tucker2 factorization* (Tucker, 1966; Kolda & Bader, 2009).

The reader can check that this RG encodes the hierarchical scope partitioning of the decomposable circuit in figure Fig. 1. Fig. 9 then illustrates a fragment of this RG and shows how tensor factorizations conforming to it can be constructed as circuits in Section 4. The circuit literature provides several ways to build RGs that are suitable for certain data modalities (e.g., image, sequence, tabular data), which can also be learned from data. Section 4.1 provides an overview of such techniques.

Imposing a particular factorization structure by means of a RG, and picking a particular parameterization for each region in it (as it will be discussed in Section 4), represents one way to encode novel hierarchical factorizations that do not correspond to existing ones. Fig. 6 shows some examples. There, we represent circuits in a layer-wise formalism as described later in Section 2.3.

Note that instantiating tensor factorizations from RGs defined as above preserve decomposability, and that circuits built from RGs in the literature are typically also smooth (Def. 3). Hierarchical Tucker and its variants are also smooth and decomposable and therefore support the tractable computation of a number of (probabilistic) inference tasks (Section 3). These hierarchical factorizations (and the corresponding deep circuits) that follow a tree-shaped RG with univariate leaves satisfy an additional structural property, called *structured-decomposability*. Structured decomposability enables the tractable computation of harder operations for which smoothness and decomposability are not enough. For instance, squaring particular tensor factorizations formalized in the graphical language of tensor networks, known as the Born rule in physics (Feynman, 1987; Glasser et al., 2019) (see also Section 2.4). We define structured decomposability below.

Definition 6 (Structured decomposability (Pipatsrisawat & Darwiche, 2008))**.** A circuit is *structured decomposable* if (1) it is smooth and decomposable, and (2) any pair of product units n, m having the same scope decompose their scope at their input units in the same way.

We can check that hierarchical Tucker yields a structured decomposable circuit easily, as it is obtained by stacking Tucker factorizations (which are computed by decomposable circuits) based on a tree RG, which in turn synchronizes all product units to decompose in the same way. We emphasize that eliciting the few structural properties that can explain the tractable computation of many different quantities of interest can help save effort aimed at (re)discovering and (re)engineering algorithms for specific hierarchical factorizations.

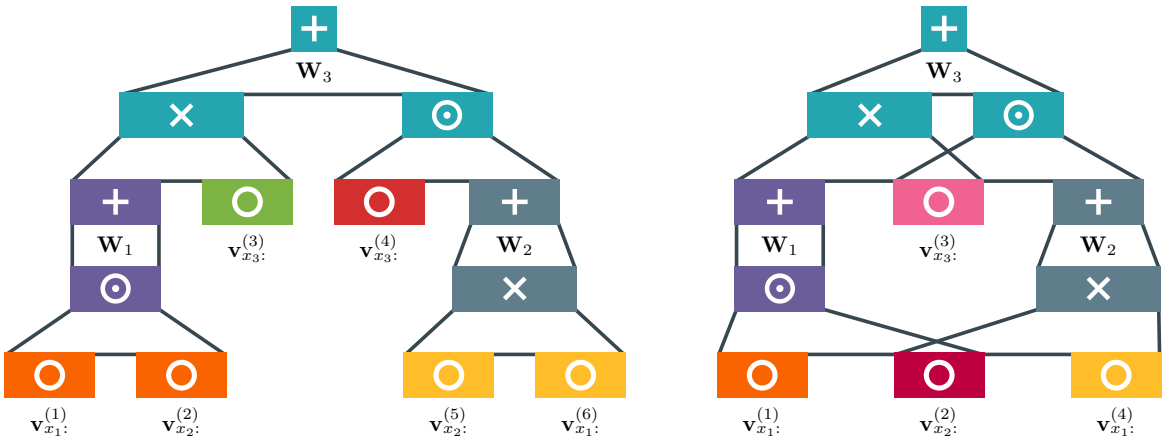

Figure 6: **Tensorized circuits can encode novel hierarchical multilinear factorizations by mixing different structures and layers.** Section 2.3 and Fig. 7 formalize and illustrate our tensorized circuit formalism, respectively. **The figure on the left** shows a tensorized circuit over variables $\mathbf{X} = \{X_1, X_2, X_3\}$ encoding an allowed multilinear factorization of a three-dimensional tensor (as it is smooth and decomposable, see Def. 8). Note that each input layer has its own factor matrix $\mathbf{V}^{(j)}$ with $j \in [6]$, and the architecture consists of a mix of Hadamard, Kronecker and sum inner layers. Overall, this tensorized circuit do not map to a known hierarchical factorization. **The figure on the right** shows a similar tensorized circuit, where the factor matrices $\mathbf{V}^{(2)}$ and $\mathbf{V}^{(3)}$ are instead shared while still encoding an allowed multilinear factorization.

Opportunity 2. Efficient Compositional Operations over Factorizations

Given one or more tensor factorizations appearing as operands in a computation of interest, how can we automatically devise a tractable algorithm for it without having to materialize the exponentially large tensor operands? The circuit literature holds the answer and offers other structural properties that can unlock the tractable computation of many complex inference scenarios, in a *reusable* fashion. E.g., when two deep circuits conform to the same tree RG, they are said to be *compatible* (Vergari et al., 2021). Given two hierarchical tensor factorizations p and q over $\mathbf{X}$, if they are compatible one can compute general expectations of the form

$$\sum_{\mathbf{x}} p(\mathbf{x})q(\mathbf{x}) \tag{expectations}$$

in closed form in time $\mathcal{O}(|p||q|)$, where $|p|$ and $|q|$ are the size of the corresponding circuits encoding such factorizations. On the other hand, maximization problems as in maximum-a-posteriori inference

$$\max_{\mathbf{y}} p(\mathbf{y}, \mathbf{E} = \mathbf{e}) \tag{MAP inference}$$

where $\mathbf{e}$ is the *evidence* assignment to variables $\mathbf{E} \subset \mathbf{X}$, and $\mathbf{y}$ is the assignment to the remaining variables $\mathbf{Y} = \mathbf{X} \backslash \mathbf{E}$ for which we want to maximize p, can be solved exactly and efficiently if p is a decomposable circuit that supports an additional property, *determinism* (Darwiche, 2009). In a nutshell, sum units in a deterministic circuit receive inputs from functions with disjoint support (see Choi et al. (2020) for details). While determinism is a consolidated property in the circuit literature, it is off the radar for (hierarchical) tensor factorizations. Furthermore, the circuit literature provides a systematic way to quickly devise the tractability conditions for a given mathematical expression that involves sums, products, powers, exponentials and logarithms, and therefore automatically distill corresponding tractable algorithms (Vergari et al., 2021). For example, if one wants to compute the Rényi's α-divergence between two factorizations p and q over variables $\mathbf{X}$, for $\alpha \in \mathbb{N}$, defined as

$$(1-\alpha)^{-1} \log \sum_{\mathbf{x}} p^{\alpha}(\mathbf{x}) q^{1-\alpha}(\mathbf{x}), \tag{α-divergence}$$

then this can be done quickly if p and q can be represented as smooth, decomposable and compatible circuits and q is also deterministic. Vergari et al. (2021) shows how to automatically distill the tractable computation of more information-theoretic quantities.

2.3 Representing Circuits in a Tensorized Formalism

Representing (hierarchical) tensor factorization as (deep) circuits highlights how circuit units can be naturally grouped together by type and scope into *layers*, as hinted already in Fig. 2. This perspective presents a new opportunity: defining and representing certain circuit structures as *tensorized computational graphs*. While circuits in the literature are defined in terms of scalar computational units, sum, product and inputs and single connections (Def. 2), many successful implementations of circuits nowadays already group units into tensors (Vergari et al., 2019a; Peharz et al., 2020c;a; Liu & Van den Broeck, 2021b; Loconte et al., 2024a) with the goal of speeding up computation by using the acceleration provided by GPUs. Following these ideas, we now provide a general tensorized circuit definition that offers a *modular* way to build overparameterized circuit architectures. This will allow us to design a single learning pipeline that subsumes many existing architectures (Section 4), and also suggest a way to create novel ones by mixing and reusing small "blocks".

Definition 7 (Tensorized circuit)**.** A *tensorized circuit* c is a computational graph composed of three kinds of layers: *input*, *product* and *sum*. Each layer $\boldsymbol{\ell}$ consists of computational units defined over the same scope $\mathsf{sc}(\boldsymbol{\ell})$. Every non-input layer receives the output vectors of other layers as inputs, denoted with the set $\mathsf{in}(\boldsymbol{\ell})$. The three kinds of layers are defined as follows:

- Each input layer $\boldsymbol{\ell}$ has scope $\mathbf{Y} \subseteq \mathbf{X}$ and computes a vector function $f \colon \mathsf{dom}(\mathbf{Y}) \to \mathbb{R}^K$.
- Each product layer $\boldsymbol{\ell}$ computes either an Hadamard product $(\bigodot_{\boldsymbol{\ell}_j \in \mathsf{in}(\boldsymbol{\ell})} \boldsymbol{\ell}_j)$ or Kronecker product $(\bigotimes_{\boldsymbol{\ell}_j \in \mathsf{in}(\boldsymbol{\ell})} \boldsymbol{\ell}_j)$ over the vectors it receives from its input layers $\boldsymbol{\ell}_j$.

- A sum layer with S sum units computes the matrix-vector product $\mathbf{W}(\,||_{\boldsymbol{\ell}_j \in \mathsf{in}(\boldsymbol{\ell})} \boldsymbol{\ell}_j(\mathsf{sc}(\boldsymbol{\ell}_j))$, where $||$ denotes vector concatenation and $\mathbf{W} \in \mathbb{R}^{S \times K}$, $K > 0$ are the sum layer parameters.

Note that if a sum layer $\boldsymbol{\ell}$ receives only one input vector, i.e., $|\mathsf{in}(\boldsymbol{\ell})| = 1$, then it simply computes $\mathbf{W}\boldsymbol{\ell}_1(\mathsf{sc}(\boldsymbol{\ell}_1))$. Furthermore, we retrieve the previous scalar unit-wise definition by setting K, the size of each layer, to 1. The above four types of layers constitute the basic "Lego blocks" that we will later use to create more sophisticated layers (Section 4.3, Section 5) and reproduce all modern circuit architectures (Table 1).

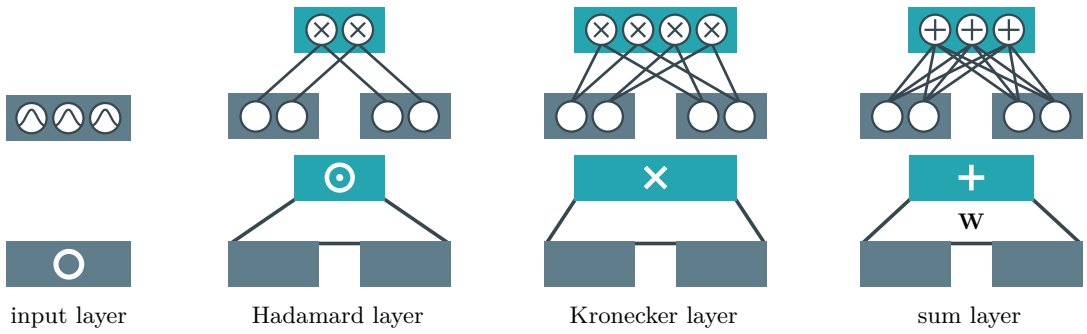

Figure 7: **Tensorized "Lego blocks".** In the rest of the figures we will abstract away from individual connections between units (as we did so far, and as we do in the top row illustrations) and represent layers as (colored) blocks (bottom row). Input layers are the only layers that do not have any other layer as input, i.e., they take a variables assignment and output a vector computed by a function f. Hadamard and Kronecker product layers receive inputs from at least two other layers (represented in gray), and compute the Hadamard and Kronecker products of their inputs, respectively. A sum layer parameterized by a weight matrix $\mathbf{W}$ concatenates its input layers into a single vector, and then multiplies it by $\mathbf{W}$.

As a first example on how this definition can help to abstract away from details in circuit architectures, see Fig. 3. There, sum and Kronecker product layers are used to stack two Tucker tensor factorizations to represent a hierarchical one. We provide in Section 4 a systematic way to stack different layers and build a deep circuit in this way. We can now easily extend the unit-wise definition of structural properties in Def. 3 to this layer-wise representation, by defining the scope of each layer.

Definition 8 (Layer-wise smoothness and decomposability)**.** A tensorized circuit over variables $\mathbf{X}$ is *smooth* if for every sum layer $\boldsymbol{\ell}$, its inputs depend all on the same variables, i.e., $\forall \boldsymbol{\ell}_i, \boldsymbol{\ell}_j \in \mathsf{in}(\boldsymbol{\ell}) : \mathsf{sc}(\boldsymbol{\ell}_i) = \mathsf{sc}(\boldsymbol{\ell}_j)$, where $\mathsf{sc}(\boldsymbol{\ell}) \subseteq \mathbf{X}$ is the scope of layer $\boldsymbol{\ell}$, i.e., the scope of the units in $\boldsymbol{\ell}$. It is *decomposable* if for every product layer $\boldsymbol{\ell}$ in it, its inputs depend on disjoint sets of variables, i.e., $\forall \boldsymbol{\ell}_i, \boldsymbol{\ell}_j \in \mathsf{in}(\boldsymbol{\ell}), i \neq j : \mathsf{sc}(\boldsymbol{\ell}_i) \cap \mathsf{sc}(\boldsymbol{\ell}_j) = \varnothing$.

Note that by assuming that every layer is composed by units sharing the same scope, and by using the three layers defined in Def. 7, we obtain tensorized circuits that are smooth and decomposable *by design*. Furthermore, if the RG of a deep circuit is a tree, then the tensorized circuit will be structured-decomposable (Def. 6) as well. It is possible to quickly read these properties out of the graphical representation of hierarchical Tucker as a tensorized circuit in Fig. 3b. Next, we use this layered abstraction to bridge to the popular *tensor networks*, and show how they can be naturally encoded as deep circuits.

2.4 Tensor Networks as Deep Circuits

Tensor networks (TNs) are often the preferred way to represent hierarchical tensor factorizations in fields such as physics and quantum computing (Markov & Shi, 2008; Schollwoeck, 2010). TNs come with a graphical language – Penrose notation – to encode tensor dot products in a compact graphical formalism (also called *tensor contractions*). See Orús (2013) for a review. Perhaps, the most popular TN factorization is the matrix-product state (MPS) (Pérez-García et al., 2007), also called tensor-train factorization (TT) (Oseledets, 2011; Glasser et al., 2019; Novikov et al., 2021). For instance, given a tensor $\boldsymbol{\mathcal{T}} \in \mathbb{R}^{I_1 \times \cdots \times I_d}$, its

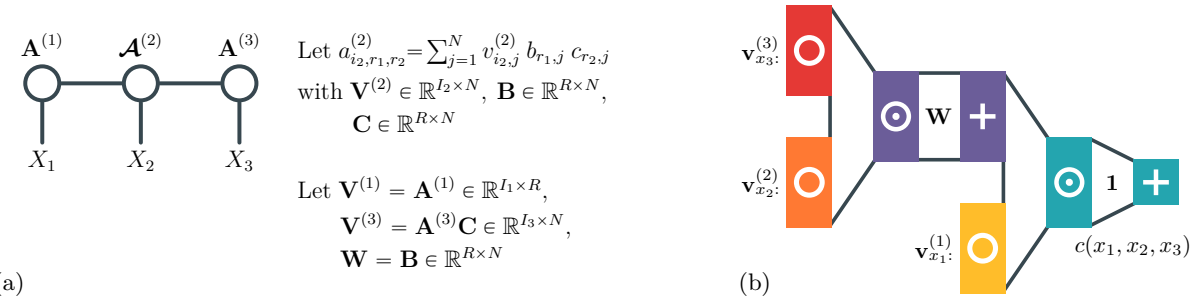

Figure 8: **A MPS/TT represented as a deep tensorized circuit** with Hadamard product layers (b). To obtain the parameters of the circuit, the tensor $\boldsymbol{\mathcal{A}}^{(2)}$ in the MPS/TT (a, showed in Penrose graphical notation) is firstly factorized into matrices $\mathbf{V}^{(2)}, \mathbf{B}, \mathbf{C}$ through a CANDECOMP/PARAFAC decomposition (Carroll & Chang, 1970). Then, $\mathbf{V}^{(1)}, \mathbf{V}^{(3)}, \mathbf{W}$ are obtained as in the figure (a). See Loconte et al. (2024a) for the detailed circuit construction. In (b) we denote with $\mathbf{1}$ a row-matrix whose entries are all ones.

rank-R MPS/TT factorization is defined in element-wise notation as

$$t_{i_1 \cdots i_d} \approx \sum_{r_1=1}^{R} \sum_{r_2=1}^{R} \cdots \sum_{r_{d-1}=1}^{R} a^{(1)}_{i_1,r_1} a^{(2)}_{i_2,r_1,r_2} \cdots a^{(d-1)}_{i_{d-1},r_{d-2},r_{d-1}} a^{(d)}_{i_{d-1},r_{d-1}} \tag{7}$$

where $\mathbf{A}^{(1)} \in \mathbb{R}^{I_1 \times R}$, $\mathbf{A}^{(d)} \in \mathbb{R}^{I_d \times R}$, and $\boldsymbol{\mathcal{A}}^{(j)} \in \mathbb{R}^{I_j \times R \times R}$ with $1 < j < d$. That is, an MPS factorization decomposes $\boldsymbol{\mathcal{T}}$ into the complete contraction of a chain of smaller tensors $\mathbf{A}^{(1)}$, $\mathbf{A}^{(d)}$, and $\{\boldsymbol{\mathcal{A}}^{(j)}\}_{j=2}^{d-1}$. Fig. 8a shows an example of a MPS/TT represented in Penrose graphical notation, i.e., where nodes denote the tensors $\mathbf{A}^{(1)}, \boldsymbol{\mathcal{A}}^{(2)}, \ldots, \boldsymbol{\mathcal{A}}^{(d-1)}, \mathbf{A}^{(d)}$, edges denote summations over shared indices, and $X_1, \ldots, X_d$ denote the tensor indices whose assignment yield the corresponding tensor entry. Loconte et al. (2024a) showed how an MPS can be represented as deep tensorized circuits by encoding summations and products in Eq. (7) into sum and (Hadamard) product layers, respectively.

Proposition 3 (MPS as deep tensorized circuits (Loconte et al., 2024a))**.** Let $\boldsymbol{\mathcal{T}} \in \mathbb{R}^{I_1 \times \cdots \times I_d}$ be a tensor being decomposed via a rank R matrix-product state (MPS) factorization. Then, there exists a structured decomposable tensorized circuit c over variables $\mathbf{X} = \{X_j\}_{j=1}^{d}$ with $\mathsf{dom}(X_j) = [I_j], j \in [d]$ computing the same factorization, i.e., $t_{\mathbf{x}} \approx c(\mathbf{x})$ for all entries $\mathbf{x}$. In addition, we have that $|c| \in \mathcal{O}(dN^2)$ with $N \leqslant \min\{R^2, R \max\{I_1, \ldots, I_d\}\}$.

In Fig. 8 we show a tensorized circuit representing a MPS/TT over variables $\mathbf{X} = \{X_1, X_2, X_3\}$, and, as detailed in the proof of Proposition 3 in Loconte et al. (2024a), the parameters of its input and dense layers are obtained by decomposing the tensors $\{\boldsymbol{\mathcal{A}}^{(j)}\}_{j=2}^{d-1}$ of the MPS/TT. Similarly to the tensorized circuit representation of hierarchical Tucker (Proposition 2), Proposition 3 yields a tensorized circuit that is structured decomposable (Def. 6). Structured-decomposability is the crucial property in MPS/TTs that allows to perform certain operations over them tractably, for instance squaring them as to recover a *Born machine* – a probabilistic model devised to simulate quantum many-body systems in physics (Orús, 2013; Glasser et al., 2019). Understanding this enables practitioners to design alternative Born machine architectures that are not limited to a sequence of tensor operations as encoded in a "linear" RG, without having to prove the tractability of the square operation over these architectures from scratch (Shi et al., 2005). This is one of the opportunities we highlighted for hierarchical tensor factorizations once represented as circuits (Opportunity 1 and Opportunity 2). Further opportunities will be presented in the next section and directly translates to TNs as well as classical tensor factorizations.

Next steps. Until now, we discussed the generic case of decomposing a real-valued tensor. On the other hand, tensor factorizations that are tailored for non-negative data (e.g. images), called *non-negative tensor factorizations*, factorize tensors into non-negative factors that can be interpreted much more easily (Cichocki & Phan, 2009). In Section 3, we connect non-negative tensor factorizations methods to the literature of circuits for probabilistic modeling, which allows us to interpret them as deep latent-variable models.

In addition, by bridging non-negative tensor factorizations and their representation as (deep) circuits, we showcase a number of future research opportunities related to both parameterizing tensor factorizations and performing probabilistic inference with them.

3 From Non-negative Factorizations to Circuits for Probabilistic modeling

Much attention has been posed in machine learning on circuit representations for tractable *probabilistic* modeling, i.e., for modeling probability distributions that support tractable inference. Circuits built with such a purpose are usually called *probabilistic circuits* (PCs) (Vergari et al., 2019b; Choi et al., 2020). In this section, we connect non-negative tensor factorizations and PCs, showing a number of research opportunities for the tensor factorization community within the probabilistic machine learning panorama.

First, we bridge non-negative (hierarchical) tensor factorizations with the discrete latent variable interpretation of (deep) PCs, showing examples of available algorithms for linear-time probabilistic inference that exploit this interpretation (not only marginals, as discussed in the previous section, but also sampling). Second, we show how the rich literature on PCs provides several compact parameterization techniques that can yield non-linear factorizations. At the same time, we leverage optimization tricks from the non-negative tensor literature to learn PCs. Finally, we connect with the literature of infinite-dimensional tensor factorizations showing their relationship with PCs encoding probability density functions, as well as with PCs equipped with infinite-dimensional sum units. We start by describing how to represent a probability distribution over finitely-discrete random variables as a tensor factorization.

Let $p(\mathbf{X})$ be a probability mass function (PMF) over finitely-discrete random variables $\mathbf{X} = \{X_j\}_{j=1}^d$, where each $X_j \in \mathbf{X}$ takes values in $\mathsf{dom}(X_j) = [I_j]$. Then, the simplest representation of $p(\mathbf{X})$ is that of a *probability tensor* $\boldsymbol{\mathcal{T}} \in \mathbb{R}_+^{I_1 \times \cdots \times I_d}$ such that every entry encodes the probability of a joint configuration of $\mathbf{X}$, i.e., $t_{x_1 \cdots x_d} = p(x_1, \ldots, x_d)$ for any $\mathbf{x} = \langle x_1, \ldots, x_d \rangle \in \mathsf{dom}(\mathbf{X})$. Clearly, this representation is inefficient, as it scales exponentially in space with respect to the number of variables d. A natural way to compactly model $p(\mathbf{X})$ is via a non-negative tensor factorization, e.g., the non-negative version of Tucker (Kim & Choi, 2007), where the factor matrices $\{\mathbf{V}^{(j)}\}_{j=1}^d$ and the core tensor $\boldsymbol{\mathcal{W}}$ showed in Eq. (2) are restricted to have non-negative entries only. By trivially specializing Proposition 2, we can encode the non-negative hierarchical Tucker factorization (Vendrow et al., 2021) in a circuit c that outputs non-negative values, also called a PC.

Definition 9 (Probabilistic circuit (Choi et al., 2020))**.** A *probabilistic circuit* (PC) over variables $\mathbf{X}$ is a circuit encoding a function $c(\mathbf{X})$ that is non-negative for all assignments to $\mathbf{X}$, i.e., $\forall \mathbf{x} \in \mathsf{dom}(\mathbf{X}) \colon c(\mathbf{x}) \geqslant 0$.

A sufficient condition to ensure a circuit is a PC is constraining both the parameters of sum units and the outputs of input units to be non-negative, resulting in a circuit that is called *monotonic* (Shpilka & Yehudayoff, 2010).[4] For instance, the circuit encoding a non-negative hierarchical Tucker factorization that we mentioned above is a monotonic PC, as its sum unit weights (i.e., the entries of the core tensor $\boldsymbol{\mathcal{W}}$) and the outputs of its input units (i.e., the entries of the factor matrices $\{\mathbf{V}^{(j)}\}_{j=1}^d$) are restricted to be non-negative. Smoothness and decomposability in circuits allow for the tractable computation of summation and integrals (Section 2.1), which translates into exactly computing any marginal or conditional distribution for a PC with these structural properties (Vergari et al., 2019b). However, these PCs are not just probabilistic models that allow to tractably evaluate probabilistic queries over $p(\mathbf{x})$, they are also *generative models* from which it is possible to sample exactly.

3.1 Non-negative tensor factorizations as generative models

As non-negative factorizations—such as non-negative hierarchical Tucker—are smooth and (structured) decomposable PCs (Defs. 3 and 6), they inherit the ability of PCs to perform tractable inference and to generate new data points, i.e., certain configurations of the variables they are defined on. To the best of our knowledge, this treatment of tensor factorizations as generative models has gone unnoticed so far. We discuss it in the following, showing how one can devise (faster) sampling algorithms for these representations.

[4] Non-monotonic PCs – circuits allowing for negative parameters but still guaranteeing non-negative outputs – are possible, see e.g., Loconte et al. (2024a).

First, we review the simplest way to sample from a non-negative factorization. Consider a non-negative (hierarchical) Tucker factorization (Def. 5) encoding $p(\mathbf{X})$ and modeled as tensorized monotonic PC c. We can sample a data point $\mathbf{x} = \langle x_1, \ldots, x_d \rangle$ from $p(\mathbf{X})$ by autoregressively sampling one variable at a time, conditioned to the previously sampled variable assignments. That is, we can first marginalize all variables except X_1, and then sample from the distribution $p(X_1)$, i.e., $x_1 \sim p(X_1)$. This can be done in time $\mathcal{O}(|c|)$, as c is both smooth and decomposable (Def. 3, Def. 8). Then, for all $d > 1$, we condition w.r.t. to the assignments to variables $\{X_i\}_{i=1}^{d-1}$ and sample X_d, i.e., $x_d \sim p(X_d \mid X_1, \ldots, X_{d-1})$. This "naive" sampling procedure requires worst-case time $\mathcal{O}(d|c|)$, where $|c|$ is the circuit size (see Def. 2). This can be inefficient in case of large d. However, for smooth and decomposable circuits, we can sample in $\mathcal{O}(|c|)$ only, by interpreting them as discrete *latent variable models* (Peharz et al., 2017; Vergari et al., 2018).

Opportunity 3. Tensor factorizations as discrete latent variable models

Each sum unit n in a smooth PC can be thought as a *mixture model* computing:

$$c_n(\mathbf{X}) = \sum_{i=1}^{K} w_{n,i}\, c_{n,i}(\mathbf{X}), \quad \text{where} \quad \sum_{i=1}^{K} w_{n,i} = 1, \quad w_{n,i} > 0, \tag{8}$$

i.e., a convex combination of the its K inputs, each one representing a distribution. At the same time, this can be interpreted as summing out a discrete latent variable Z_n that has K different states,

$$p_n(\mathbf{X}) = \sum_{i=1}^{K} p(Z_n = i)\, p_{n,i}(\mathbf{X} \mid Z_n = i)$$

where the non-negative weights $w_{n,i}$ are the marginal probabilities of this latent variable. As such, the whole circuit, and hence the corresponding non-negative tensor factorization, can be seen as a *hierarchical latent variable model* (Peharz et al., 2016; Choi et al., 2011), with as many discrete latent variables as the number of sum units. Therefore, as for any mixture model, to sample $\mathbf{x}$ we can first sample the latent variables, and then sample the mixture components. In practice, this sampling procedure can be done efficiently by performing a backward traversal of the circuit computational graph (Vergari et al., 2019a; Dang et al., 2022a). We provide this algorithm for tensorized circuits in Algorithm C.1, which sample a batch of N data points in parallel and discuss it in Appendix C. Other efficient probabilistic inference tasks can be "imported" from the circuit literature for smooth and decomposable PCs. See Vergari et al. (2021) for more details.

3.2 How to parameterize probability tensor factorizations?

Circuits and tensor factorizations are the output of two different optimization problems that however share some common challenges. Understanding them can open new opportunities for both communities. In application scenarios of (non-negative) tensor factorizations, the main task is to compress or reconstruct a given tensor, which is generally explicitly represented in memory. Hence, the parameters of the factorization are optimized as to minimize a reconstruction loss (Cichocki et al., 2007). In contrast, modern PCs are *learned from data*. That is, one is given a dataset of N datapoints $\{\mathbf{x}^{(i)}\}_{i=1}^{N}$ that are assumed to be drawn i.i.d. from and *unknown* distribution $p(\mathbf{X})$ (Bishop & Nasrabadi, 2006). The probability tensor that encodes $p(\mathbf{X})$ is therefore implicit and cannot be fully materialized, as the probability distribution is unknown, but also because of its possible exponential—or even infinite—size.

As learning in PCs often reduces to an optimization problem, i.e., maximizing the data (log-)likelihood (Peharz et al., 2016), enforcing the non-negativity of the circuit needs to be done using one or more *reparameterizations*, i.e., mapping real-valued parameters to the non-negative sum unit weights. This is necessary as the sum unit weights of a monotonic PC need to form a convex combination to yield a valid distribution (as shown in Eq. (8)). For instance, we can squash the K parameters $\boldsymbol{\theta} \in \mathbb{R}^K$ associated to a sum unit with K inputs through a softmax function

$$\mathbf{w} = \mathsf{softmax}(\boldsymbol{\theta}), \qquad \boldsymbol{\theta} \in \mathbb{R}^K. \tag{9}$$

The usage of such reparameterization combined with input functions encoding probability distributions delivers a PC whose normalization constant is 1, as the probabilities of all variable assignments sum up to

one, which is direct consequence of having the weights of each sum unit summing up to one. For a tensorized circuit, such a reparameterization would act row-wise on the parameter matrix associated to every sum layer.

Luckily, if the circuit is smooth and decomposable (Def. 3), we can still compute its normalization constant exactly and efficiently even if sum weights are not normalized (Peharz et al., 2015). This allows us to use alternative ways to reparameterize a monotonic PC c, even if its reparameterization delivers an unnormalized distribution, i.e., a distribution not integrating to 1. In fact, we can still recover a valid distribution $p(\mathbf{X})$ efficiently via normalization, i.e., $p(\mathbf{X}) = c(\mathbf{X})/Z$ with $Z = \sum_{\mathbf{x} \in \mathsf{dom}(\mathbf{X})} c(\mathbf{x})$ being the normalization constant. For instance, we can enforce each single sum unit parameter θ to be non-negative via exponentiation

$$w = \exp(\theta), \qquad \theta \in \mathbb{R}. \tag{10}$$

In this paper, we introduce a third way, a simpler implementation trick that we borrow from the literature on gradient-based optimization for non-negative tensor factorizations (Cichocki et al., 2007): projecting the parameters of all sum units in the positive orthant after every optimization step, i.e.,

$$w = \max(\epsilon, \theta), \qquad \theta \in \mathbb{R},\ \epsilon > 0 \tag{11}$$

where ϵ is a small threshold close to zero and max is applied element-wise. Each reparameterization can yield a different loss landscape and lead to different solution during optimization. In our experiments (Section 6), we found this third reparameterization to be the most effective to learn monotonic PCs.

When it comes to input units in monotonic PCs, they need to model *valid distributions*. Common parameterizations can include simple PMFs (or densities, see Section 3.4) such as Bernoulli or Categorical distributions, or even other probabilistic models as long as they can be tractably marginalized. This yields a set of possible parameterizations that go beyond the simple mappings from indices to matrix entries, as usually used in tensor factorizations (Proposition 1 and Fig. 2).

Opportunity 4. A wide range of possible parameterizations

Estimating a PMF $p(\mathbf{X})$ via a probabilistic model is another way to perform an implicit tensor compression. If this model is a circuit, then this compression exactly maps to a non-negative hierarchical tensor factorization but over a number of *basis functions*, which are the circuit input units. These input units (thus also input layers in our tensorized formalism) can encode more memory efficient and more expressive functions than indicator functions. For instance, one can use Binomial distributions instead of categoricals as to drastically reduce the number of parameters of the factorizations (Peharz et al., 2020c). In the case of infinite-dimensional probability tensors (see Section 3.4 below), discrete variables with infinite support can instead be modeled by using Poisson distributions (Molina et al., 2017) or generative models as input layers, such as normalizing flows (Papamakarios et al., 2021; Sidheekh et al., 2023), variational auto-encoders (Tan & Peharz, 2019), or also non-linear functions that can be integrated efficiently, e.g., splines (Novikov et al., 2021; Loconte et al., 2024a). Parameterizing input units in this way yields a tensor factorization that uses *non-linearities*. Along this direction, in the circuit literature parameters of sum layers have been directly parameterized by neural networks (Shao et al., 2020; 2022; Gala et al., 2024a). These non-linear cases have only been explored very recently in the matrix and tensor factorization literature (Leplat et al., 2023; Awari et al., 2024).

3.3 Reliable Neuro-symbolic integration

A prominent use case for tractable inference with PCs is in safety-critical applications, when it is necessary to enforce *hard constraints* over the predictions of *neural* classifiers (Ahmed et al., 2022; van Krieken et al., 2024). These constraints can be expressed as logical formulas over symbols extracted by a perceptual component (the classifier). For example, the safety rule that a self-driving car has to stop in front of a pedestrian or a traffic light (Marconato et al., 2024b;a) can be written as a propositional logical formula $\phi : (\mathrm{P} \vee \mathrm{R} \implies \mathrm{S})$, where P, R and S are Boolean variables representing that a Pedestrian and a Red-light have been detected in the video stream of the car and the action to Stop has to be taken. Circuits are especially suitable for

this neuro-symbolic integration scenario (De Raedt et al., 2019) because they can represent both probability distributions and logical formulas. These two representations can be used in a single classifier to guarantee that the predictions that will violate the given constraint will always have 0 probability. More formally, we can implement such a classifier, mapping inputs $\mathbf{x}$ to outputs $\mathbf{y}$ that have to satisfy a constraint ϕ, in this way (Ahmed et al., 2022):

$$p(\mathbf{y} \mid \mathbf{x}) \propto q(\mathbf{y} \mid \mathbf{x}) \mathbb{1}\{\mathbf{y} \models \phi\} \tag{12}$$

where $q(\mathbf{y} \mid \mathbf{x})$ is a conditional distribution encoded in a circuit that can be parameterized by a neural network (see Opportunity 4) and $\mathbb{1}\{\mathbf{y} \models \phi\}$ is an indicator function that is 1 when the predictions $\mathbf{y}$ satisfy ($\models$) the constraint ϕ. For instance, $\mathbf{y}$ is a Boolean assignment to variables P, R, S in our self-driving car example, and $\mathbb{1}\{\mathbf{y} \models \phi\}$ is 1 iff substituting $\mathbf{y}$ to variables in ϕ yields "true" ($\top$). This indicator function can be compactly represented as a circuit made of sum and product units through a process called *knowledge compilation* (Darwiche & Marquis, 2002; Chavira & Darwiche, 2008; Choi et al., 2013).[5] If both the probability distribution q and the indicator function for the constraint ϕ are compatible circuits (Opportunity 2), one can efficiently multiply them and renormalize by computing the partition function (Vergari et al., 2021), which equals the probability that the hard constraint ϕ holds given $\mathbf{x}$, i.e.,

$$\sum\nolimits_{\mathbf{y}} q(\mathbf{y} \mid \mathbf{x}) \mathbb{1}\{\mathbf{y} \models \phi\} = \mathbb{E}_{\mathbf{y} \sim q(\mathbf{y} \mid \mathbf{x})} \left[\mathbb{1}\{\mathbf{y} \models \phi\}\right] = p(\phi = \top \mid \mathbf{x}) \tag{13}$$

also called the *weighted model count* (Chavira & Darwiche, 2008; van Krieken et al., 2024) which is the crucial quantity to compute when combining logical and probabilistic reasoning (Darwiche, 2009; Zeng et al., 2020). This possible integration, as far as we can tell, is off the radar of the tensor factorizations community.

Opportunity 5. Structured sparsity via logical constraints

Circuits encoding logical formulas are generally very sparse, nonetheless, they still represent a (sparse) factorization of a tensor, in this case a Boolean one. Analogously to the probability tensor described at the beginning of Section 3, this Boolean tensor would encode the logical formula as an exponentially large table of zeros and ones. Multiplying a probability tensor compactly encoded as circuit q as in Eq. (12) with this compact representation of a Boolean tensor equals to a structured form of *masking*: all the invalid (according to the logical constraint ϕ) entries in the probability tensor are forcefully set to zero, thus making such entries not predictable. A possible opportunity is therefore to connect with the vast literature of knowledge compilation (Darwiche & Marquis, 2002; Choi et al., 2013; Oztok & Darwiche, 2017) to impose structured sparsity to tensor factorizations.
Possible applications include neuro-symbolic integration for graph data (Loconte et al., 2023) as well as representing rankings and user preferences (Choi et al., 2015), scaling cryptographic attacks (Wedenig et al., 2024b), enforcing constraints over the output of LLMs (Zhang et al., 2023) and promoting their self-consistency (Calanzone et al., 2024).

3.4 Infinite-Dimensional Probability Tensors and Continuous Factorizations

Until now, we discussed circuits representing a (hierarchical) factorization of a tensor having finite dimensions, i.e., where the number of entries in every dimension is finite. That is, these circuits are defined over a set of discrete variables, each having a finite number of states. In this section, we focus on factorizations of tensors that can have dimensions having an infinite (and possibly uncountable) number of entries or *quasi-tensors* (Townsend & Trefethen, 2015). Analogously to the symmetry between (hierarchical) tensor factorizations and circuits (Section 2) we show that quasi-tensors can be represented as circuits defined over at least one variable having infinite (and possibly uncountable) domain. Furthermore, by connecting with a very recent class of circuits equipped with integral units, we point out at opportunities regarding the parameterization of infinite-rank (hierarchical) tensor factorizations, i.e., factorizations whose rank is not necessarily finite. We ground these ideas to the problem of modeling a probability density function (PDF).

[5] Note that arbitrary ANDs and ORs in a logical formula do not directly correspond to products and sums in our circuit language. It is necessary to *compile* the formula in a new representation that contains ANDs over sub-formulas with disjoints scopes – corresponding to decomposable products – and XORs – corresponding to deterministic sum units, and pushes negation towards the input functions (Darwiche & Marquis, 2002).

Formally, let $p(\mathbf{X})$ be a PDF over continuous variables $\mathbf{X} = \{X_j\}_{j=1}^d$, where each $X_j \in \mathbf{X}$ takes values in $\mathsf{dom}(X_j) = \mathbb{R}$. Then, $p(\mathbf{X})$ can be represented as an infinite-dimensional probability tensor $\boldsymbol{\mathcal{T}}$ such that $t(x_1, \ldots, x_d) = p(x_1, \ldots, x_d)$ for any $\mathbf{x} \in \mathsf{dom}(\mathbf{X})$. Infinite-dimensional tensors such as $p(\mathbf{X})$ can be decomposed into a finite number of sums and products of factor matrices that live in Hilbert spaces of generic functions. For instance, we can re-adapt the Tucker factorization showed in Def. 1 as a different factorization method where, instead of having factor matrices $\mathbf{V}^{(j)} \in \mathbb{R}^{I_j \times R_j}$ for all j, we encode a vector of R_j functions $\mathcal{F}^{(j)} = \{f_{r_j}^{(j)} \colon \mathsf{dom}(X_j) \to \mathbb{R}\}_{r_j=1}^{R_j}$. That is, we factorize $\boldsymbol{\mathcal{T}}$ as

$$t(x_1, \ldots, x_d) \approx \sum_{r_1=1}^{R_1} \cdots \sum_{r_d=1}^{R_d} w_{r_1 \cdots r_d} f_{r_1}^{(1)}(x_1) \cdots f_{r_d}^{(d)}(x_d). \tag{14}$$

Here, we have $\boldsymbol{\mathcal{W}} \in \mathbb{R}^{R_1 \times \cdots \times R_d}$. Then, one can trivially modify Proposition 1 such that this Tucker factorization of $p(\mathbf{X})$ can be represented as a PC of the same size where the input units over variable X_j now encode the functions in $\mathcal{F}^{(j)}$. Similarly, one can retrieve PCs encoding mixed probability distributions over discrete *and* continuous variables (Molina et al., 2018), thus encoding factorizations of a quasi-tensor. In the same way, one can easily re-adapt hierarchical Tucker to factorize $p(\mathbf{X})$, thus yielding an equivalent deeper circuits over continuous variables.

Note that, while Eq. (14) is a factorization of an infinite-dimensional tensor, it is still a *finite* factorization. That is, the ranks $R_1, \ldots, R_d$ are finite, and therefore the circuit representing the same factorization has a sum unit having $R_1 \cdots R_d$ inputs (see Fig. 2). Very recent works have proposed to augment the circuit definition (Def. 2) with *integral units* which, roughly speaking, encode a sum over an infinite and uncountable number of inputs (Gala et al., 2024a;b). We can consider such PCs as encoding continuous factorizations of a probability tensor, which can be though of as infinite-rank factorizations. For instance, consider the problem of factorizing a finite-dimensional tensor $\boldsymbol{\mathcal{T}} \in \mathbb{R}^{I_1 \times \cdots \times I_d}$. Instead of considering a finitely-dimensional core tensor $\boldsymbol{\mathcal{W}} \in \mathbb{R}^{R_1 \times \cdots \times R_d}$ in Tucker (Eq. (2)), we can use a function $\omega \colon \mathsf{dom}(\mathbf{Z}) \to \mathbb{R}$ over continuous variables $\mathbf{Z} = \{Z_i\}_{i=1}^d$, where each Z_i has domain $\mathsf{dom}(Z_j) = \mathbb{R}$. Similarly, we replace each factor matrix $\mathbf{V}^{(j)} \in \mathbb{R}^{I_j \times R}$ with a vector of I_j functions $\{f_{i_j}^{(j)} \colon \mathsf{dom}(Z_j) \to \mathbb{R}\}_{i_j=1}^{I_j}$, for all j. By doing so and since $\mathbf{Z}$ consists of continuous variables, we are in practice replacing the summations in Eq. (2) with a multivariate integral over $\mathbf{Z}$. That is, we factorize $\boldsymbol{\mathcal{T}}$ as

$$t_{x_1 \cdots x_d} \approx \int_{\mathsf{dom}(\mathbf{Z})} \omega(z_1, \ldots, z_d) \; f_{x_1}^{(1)}(z_1) \cdots f_{x_d}^{(d)}(z_d) \; \mathrm{d}\mathbf{z}. \tag{15}$$

Similarly, one can retrieve hierarchical versions of such continuous tensor factorizations, with applications for probabilistic modeling (Gala et al., 2024b). In the case of the integral in Eq. (15) being intractable to compute, quadrature rules can be applied as to approximate it. See Gala et al. (2024a) for the details.

Opportunity 6. More factorizations of alternative representations of distributions

Instead of explicitly encoding $p(\mathbf{X})$ by modeling its PMF or PDF one can instead encode its *probability generating function*, *characteristic function* or its *cumulative density function*. Circuits have been used to compactly represent these alternative representations of distributions. For instance, Yu et al. (2023) proposed to build circuits that encode characteristic functions to represent and learn distribution over mixed discrete and continuous data domains. These characteristic circuits have also found application in causal probabilistic inference (Poonia et al., 2024). Similarly to the correspondence between circuits and tensor factorizations shown in the previous sections, a characteristic circuit can be seen as a hierarchical factorization of a tensor encoding a characteristic function, i.e., a factorization of a tensor with complex entries that however still implicitly encodes a probability distribution.

In the next section, we present a generic pipeline that can be used to build both finite-dimensional and infinite-dimensional hierarchical probability tensor factorizations as deep tensorized PCs (Def. 7).

Table 1: **De-structuring circuit and tensor factorization architectures, and their implementations, into simpler design choices** conforming to our pipeline: which region graphs (Section 4.1) and sum-product layers to use (Section 4.3), and whether to apply folding (Section 4.4). New designs are possible by mix & matching these existing base ingredients. Furthermore, we propose new region graphs that deliver more efficient tensorized circuit: QG, QT-2 and QT-4. By leveraging tensor factorizations of the weights of folded circuits, we propose two new sum-product layers: CP, CP^{S} and CP^{XS}. Check mark ✓ means that even if the original implementation of HCLTs does not implement folding as we describe it here, they achieve similar parallelism by custom CUDA kernels. In Appendix B we present a detailed discussion on the design choices of our pipeline that are implicitly made in each PC architecture.

PC Architecture	Region Graph	Sum-Product Layer	Fold
Poon&Domingos (Poon & Domingos, 2011)	PD	$\text{CP}^{\top}$	✗
RAT-SPN (Peharz et al., 2020c)	RND	Tucker	✗
EiNet (Peharz et al., 2020a)	$\{$ RND, PD $\}$	Tucker	✓
HCLT (Liu & Van den Broeck, 2021b)	CL	$\text{CP}^{\top}$	✓
HMM/$\text{MPS}_{\mathbb{R}\geqslant 0}$ (Glasser et al., 2019)	LT	$\text{CP}^{\top}$	✗
BM (Han et al., 2018)	LT	$\text{CP}^{\top}$	✗
TTDE (Novikov et al., 2021)	LT	$\text{CP}^{\top}$	✗
NPC^2 (Loconte et al., 2024a)	$\{$ LT, RND $\}$	$\{$ $\text{CP}^{\top}$, Tucker $\}$	✓
TTN (Cheng et al., 2019)	QT-2	Tucker	✗
Mix & Match (our pipeline)	$\left\{ \begin{array}{l} \text{RND, PD, LT,} \\ \text{CL, QG, QT-2, QT-4} \end{array} \right\}$	$\times$ $\left\{ \begin{array}{l} \{ \text{Tucker, CP, CP}^{\top} \} \cup \\ \{ \text{CP}^{\text{S}}, \text{CP}^{\text{XS}} \mid \textsc{Fold} \checkmark \} \end{array} \right.$	$\times$ $\{$ ✗, ✓ $\}$

4 How to Build and Scale Circuits: A Tensorized Perspective

We now have all the necessary background to start exploiting the connections between (hierarchical) tensor factorizations and (deep) circuits. In particular, in this section, we will show how we can understand and unify many—apparently different—ways to build circuits (and other factorizations) in a single pipeline leveraging tensor factorizations as modular abstractions. By doing so, we can "disentangle" what are the key ingredients to build and effectively learn overparameterized circuits, i.e., circuits with a very large number of parameters (Table 1).

Fig. 9 summarizes our pipeline: **i)** first, one builds a RG structure to enforce the necessary structural properties (Section 4.1), then, **ii)** populates such a template by introducing units and grouping them into layers (Section 4.2), following the many possible tensor factorizations abstractions (Section 4.3), optionally, **iii)** these layers can be "folded", i.e., stacked together to exploit GPU parallelism (Section 4.4). Finally, the circuit parameters can be optimized by gradient descent or expectation maximization (Peharz et al., 2016; Zhao et al., 2016).

4.1 Building and Learning Region Graphs

The first step of our pipeline is to construct a RG (Def. 4). It specifies a hierarchical partitioning of the input variables according to which we build deep circuit architectures. In particular, PCs that are built out of RGs satisfying crucial structural properties such as smoothness and decomposability by design (and structured-decomposability if the RG is a tree and has univariate leaves, see Section 2.2), which in turn guarantee tractable inference for many queries of interest (Section 2). RGs are explicitly used to build PCs in some papers (Peharz et al., 2020c;a), but as we show next, they can be implicitly found in many other PC and tensor factorization architectures. We also introduce a novel way to quickly build RGs for images that are dataset-agnostic but exploit of the structure of pixels.

Linear tree RGs (LT). A simple way to instantiate a RG is by building partitionings that factorize one variable at a time. That is, given π a ordering over variables $\mathbf{X}$, each i-th partition node factorizes its scope $\{X_{\pi(1)}, \ldots, X_{\pi(i)}\}$ into regions $\{X_{\pi(1)}, \ldots, X_{\pi(i-1)}\}$ and $\{X_{\pi(i)}\}$. We call the resulting RG a linear tree (LT)

RG, and show an example for it in case of three variables in Fig. 4. The ordering of the variables can be the lexicographical one or depending on additional information such as time when modeling sequence data. This sequential RG is the one adopted by chain-like tensor network factorizations, such as MPS, TTs or BMs (Pérez-García et al., 2007; Oseledets, 2011), as well as hidden Markov models (HMMs) when represented as PCs (Rabiner & Juang, 1986; Liu et al., 2023a).

Randomized tree RGs (RND). A slightly more sophisticated way to build a RG is to construct a tree that is balanced. This can be done in a dataset-agnostic way by randomly partitioning variables recursively. That is, the root region $\mathbf{X}$ is recursively partitioned by randomly splitting variables in approximately even subsets, until no further partitionings are possible. This approach, which we label with RND, has been introduced to build *randomized-and-tensorized sum-product networks* (RAT-SPNs) (Peharz et al., 2020c). A similar approach has been described by Di Mauro et al. (2017; 2021), with the difference that some randomly-chosen subsets of the data are also taken into account when parameterizing the circuit, thus entangling the construction of the RG with the circuit parameterization.

Poon-Domingos construction (PD). One can devise other RG algorithms that are tailored for specific data modalities, but that are still dataset-agnostic. In the case of images where variables are associated to pixel values, Poon & Domingos (2011) proposed to split them as to form a deep hierarchy of patches, by recursively performing horizontal and vertical cuts. However, the main drawback of this approach, labeled PD, is that it generally yields very deep circuit architectures that are hard to optimize (Section 6), as it considers *all* the possible ways to recursively split an image into patches whose number grows fast with respect to the image size. The PD RG has been extensively used in the circuit literature, e.g., for architectures like EiNets (Peharz et al., 2020a).

Novel RGs for image data: quad graphs (QG) and trees (QT). We want to devise RGs that are dataset-agnostic but still aware of the pixel structure as PD, while at the same time not falling prey of the same optimization issues. Therefore, we propose a much simpler way to construct image-tailored RGs that delivers smaller circuits that can achieve better performances, even when compared to RGs learned from data (see Section 6). Algorithm D.1 in the Appendix details our construction. Similarly to PD, it builds a RG by recursively splitting image patches of approximately the same size, but differently from PD it only splits them into four parts (a one vertical and horizontal cut) sharing the newly created patches. We call such RG *quad-graph* (QG). Fig. 10 shows an example of a QG RG for a 3x3 image.

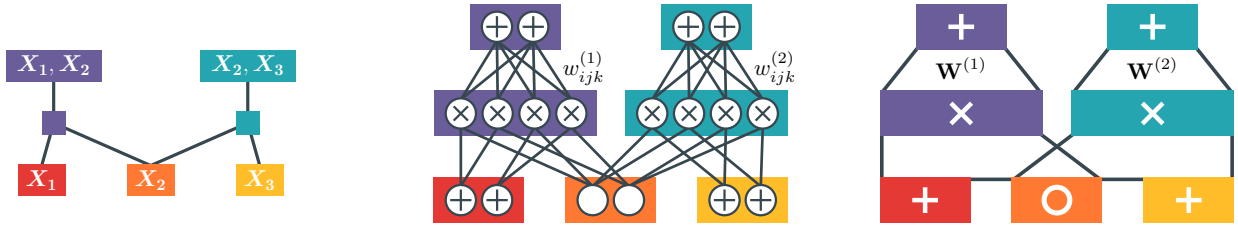

(**i**) Build a region graph.

(**ii**) Overparameterize & tensorize.

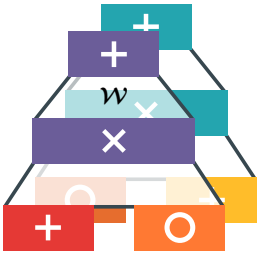

(**iii**) Folding.

Figure 9: **Our pipeline for building overparameterized circuits.** Given a (fragment of) region graph (i), we overparameterize it with sum, product and input units. In this case, the connections between sum and product units encode a Tucker factorization (e.g., as in Fig. 2). Then, we tensorize it by grouping units into layers (ii). In the final folding step, we can fuse together those layers that can be evaluated in parallel (iii). To do so, we stack the parameter matrices $\mathbf{W}^{(1)}, \mathbf{W}^{(2)}$ into a tensor $\mathcal{W}$.

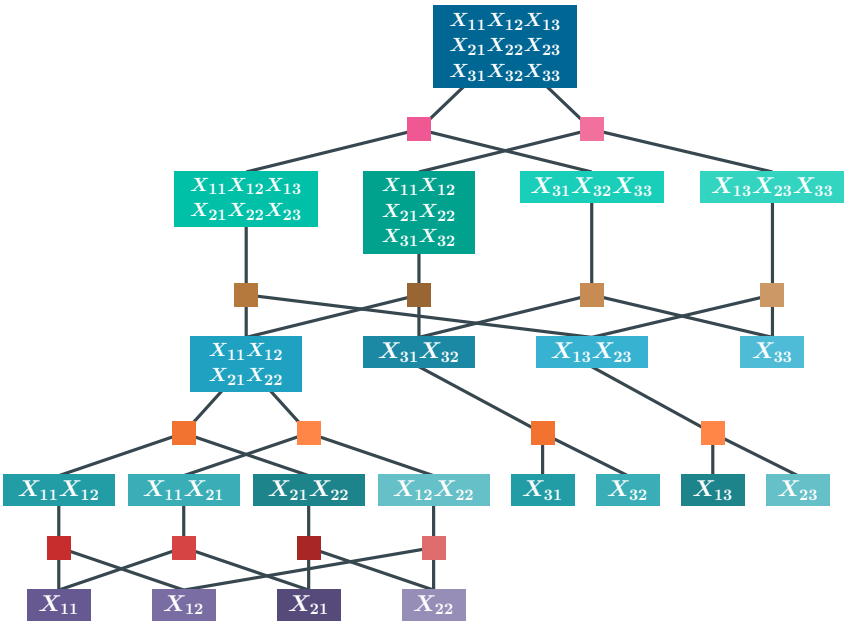

Figure 10: **The quad graph (QG)**. We illustrate the quad graph RG delivered by Algorithm D.1 passing $H = 3$, $W = 3$ and isTree = False as input arguments. The region graph is *unbalanced* as the image size (3×3) is not a power of 2. Differently from our quad trees (QTs), QGs have regions partitioned in more than a single way (e.g., the root region node), and regions can be shared among partitions. For example, in a QT, the top region could only be partitioned in a single way into two or four subregions, respectively called QT-2 and QT-4 region graphs.

Alternatively, one can obtain a tree RG by splitting the patches both horizontally and vertically, but without sharing patches. We call such tree RG *quad-tree* (QT). Since regions of such RGs are associated to image patches, we can choose to partition them in different ways. In particular, we will denote with QT-2 a QT whose regions are partitioned in two parts (bottom and top parts of the patch), and with QT-4 a QT whose regions are partitioned into four parts (following a quadrant division partitioning). With QT-2 we retrieve tensor factorizations tailored for image-data used in prior work (Cheng et al., 2019).

Learning RGs from data. The approaches discussed so far do not depend on the training data. To exploit the data in the construction of RGs, one can test the statistical independence of subset of features inside a region node $\mathbf{Y} \subseteq \mathbf{X}$. This is the approach used in the seminal LearnSPN algorithm (Gens & Domingos, 2013), later extended in many other works (Molina et al., 2018; Di Mauro et al., 2019). All these variants never mention a RG, but one is built implicitly by performing these statistical test and by introducing regions that are associated to a different "chunk" of data obtained by clustering (Vergari et al., 2015). Alternatively, one can split regions according to some heuristics over the data that result in region nodes being shared (Jaini et al., 2018a). The same idea is at the base of the Chow-Liu algorithm to learn the tree-shaped PGM that better approximates the data likelihood (Chow & Liu, 1968b). The Chow-Liu algorithm (CL) can be used to implicitly build a RG as well, as done in many structure learning variants (Vergari et al., 2015; Rahman et al., 2014; Choi et al., 2011). A more recent approach that leverages this idea and that generally yields state-of-the-art performance first learns the Chow-Liu tree, then treats it as a latent tree model (Choi et al., 2011) that is finally compiled into a PC (Liu & Van den Broeck, 2021b). The construction of this *hidden* Chow-Liu *tree* (HCLT) exactly follows the steps in our pipeline, once one disentangles the role of the RG from the rest.

The construction of other PC and tensor factorization architectures mentioned so far (i.e., RAT-SPNs, EiNets, MPSs, BMs, etc) also follows the same pattern, and can be easily categorized in our pipeline (Table 1). They not only differ in terms of the RGs they are built from, but also on the kind of the chosen sum and product layers. In the next section, we provide a generic algorithm that builds a tensorized circuit architecture from a given RG, given a selection of sum and product layers encoding tensor factorizations.

4.2 Overparameterize & Tensorize Circuits

Given a RG, the simplest way to build a circuit is to associate a single input distribution unit per leaf region, a single sum per inner region, and an single product unit per partition, and then connect them following the RG structure. This would deliver a smooth and (structured-)decomposable circuit that is

Algorithm 1 $\mathsf{overparamAndTensorize}(\mathcal{R}, \mathcal{F}, K)$

Input: a RG $\mathcal{R}$ over variables $\mathbf{X}$, the sum layers width K, and the type of input functions $\mathcal{F}$.
Output: A tensorized circuit c over $\mathbf{X}$.

1: $\mathcal{L} \leftarrow \mathsf{emptyMap}$ ▷ From regions to layers
2: **for each** region $\mathbf{Y} \in \mathsf{postOrderTraversal}(\mathcal{R})$ **do**
3: **if** $\mathbf{Y}$ is partitioned into $\{(\mathbf{Z}_1^{(i)}, \mathbf{Z}_2^{(i)})\}_{i=1}^N$ **then**
4: $\Lambda \leftarrow \varnothing$
5: $C \leftarrow 1$ **if** $\mathbf{Y} = \mathbf{X}$ **else** K
6: **for** $i = 1$ **to** N **do**
7: $\boldsymbol{\ell} \leftarrow \mathsf{SumProdLayer}(\mathcal{L}[\mathbf{Z}_1^{(i)}], \mathcal{L}[\mathbf{Z}_2^{(i)}], C, K)$
8: $\Lambda \leftarrow \Lambda \cup \{\boldsymbol{\ell}\}$
9: $\mathcal{L}[\mathbf{Y}] \leftarrow \mathsf{pop}(\Lambda)$ **if** $|\Lambda|{=}1$ **else** $\mathsf{SumLayer}(\Lambda)$
10: **else** ▷ $\mathbf{Y}$ is a leaf region in $\mathcal{R}$
11: $\mathcal{L}[\mathbf{Y}] \leftarrow \mathsf{InputLayer}(\mathbf{Y}, K, \mathcal{F})$
12: **return** A circuit having $\mathcal{L}[\mathbf{X}]$ as output layer

Algorithm 2 $\mathsf{SumProdLayer}(\boldsymbol{\ell}_1, \boldsymbol{\ell}_2, C, K)$

Input: Layers $\boldsymbol{\ell}_1, \boldsymbol{\ell}_2$ with width K and output width C.
Output: A composition of sum & product layers.

1: **procedure** ($\mathsf{parameterizeTucker}$)
2: Let $\mathbf{W} \in \mathbb{R}^{C \times K^2}$ be the sum layer parameters
3: **return** $\boldsymbol{\ell}$ computing $\mathbf{W}\,(\boldsymbol{\ell}_1(\mathbf{Z}_1) \otimes \boldsymbol{\ell}_2(\mathbf{Z}_2))$
4: **procedure** ($\mathsf{parameterizeCP}$)
5: Let $\mathbf{Q}^{(1)}, \mathbf{Q}^{(2)} \in \mathbb{R}^{C \times K}$ be the parameters
6: **return** $\boldsymbol{\ell}$ computing $(\mathbf{Q}^{(1)}\boldsymbol{\ell}_1(\mathbf{Z}_1)) \odot (\mathbf{Q}^{(2)}\boldsymbol{\ell}_2(\mathbf{Z}_2))$

Algorithm 3 $\mathsf{SumLayer}(\{\boldsymbol{\ell}_i\}_{i=1}^N)$

Input: Input layers $\{\boldsymbol{\ell}_i\}_{i=1}^N$ having scope $\mathbf{Y}$ and width K, with $N > 1$. **Output:** A sum layer.

1: Let $\mathbf{W} \in \mathbb{R}^{K \times (NK)}$ be the sum layer parameters
2: **return** $\boldsymbol{\ell}$ computing $\mathbf{W}(\,||_{i=1}^N \boldsymbol{\ell}_i(\mathbf{Y}))$

sparsely connected, and it is in fact the strategy that the many structure learning algorithms discussed in the previous section were implicitly using (Gens & Domingos, 2013; Vergari et al., 2015; Molina et al., 2018). We can adapt this strategy to the "deep learning recipe", and output instead an *overparameterized* circuit that is locally densely-connected. With overparameterization we refer to the process of "populating" a RG with not one but many sum, product and input units of the same scope. The resulting tensorized computational graph (Def. 7) has many more learnable parameters and lends itself to be parallelized on GPU, as we can vectorize computational units sharing the same scope as to form dense layers. Algorithm 1 details the overparameterization and tensorization process. The algorithm takes as input: a RG $\mathcal{R}$, the type of input functions $\mathcal{F}$ (e.g., Gaussians), and the number of sum units K which governs the expressiveness of the circuit, or equivalently the rank of the factorization.[6] Furthermore, we can customize the choice of input layers as well as how to stack sum and product layers together, yielding many ways to build circuits with different degrees of efficiency and expressiveness.

Constructing input layers. The first step of Algorithm 1 consists of associating input units to leaf regions, i.e., regions that are not further decomposed. Leaf regions are often univariate, i.e., of the form $\mathbf{Y} = \{X_j\}$ for some variable $X_j \in \mathbf{X}$. For each leaf region over a variable X_j we introduce K input units, each computing a function $f_i \colon \mathsf{dom}(X_j) \to \mathbb{R}$. To guarantee the non-negativity of the output in monotonic PCs, f_i are often chosen to be non-negative, e.g., by choosing them to be probability mass or density functions (Choi et al., 2020). However, one can possibly choose f_i from a much wider set of expressive function families, e.g., polynomial splines (de Boor, 1971; Loconte et al., 2024a), neural networks (Shao et al., 2020; Correia et al., 2023; Gala et al., 2024a;b) and normalizing flows (Sidheekh et al., 2023). See also Opportunity 4. Then, the input units can be tensorized by effectively replacing them with an input layer $\boldsymbol{\ell} \colon \mathsf{dom}(X_j) \to \mathbb{R}^K$ such that $\boldsymbol{\ell}(X_j)_i = f_i(X_j)$ with $i \in [K]$ can be computed in parallel (L11 in Algorithm 1). Next, sum and product layers are built and connected according to the variables partitioning specified in the given RG.

4.3 Abstracting sum and product layers into modules

Alongside input layers, we introduced the other atomic "Lego blocks" for tensorized circuits in Def. 7: sum layers, Hadamard and Kronecker product layers. In the following, we will use these blocks to create *composite* layers that will act as further abstractions that can be seamlessly plugged in Algorithm 1. These composite layers include: ***Tucker*** (Fig. 11), ***CP*** (Fig. 15) and $\boldsymbol{CP}^{\top}$ (Fig. 16) layers. Each of these layers encodes a local factorization and stacks and connects internal sum and product units in a different way as to increase expressiveness or efficiency.

[6] As in a (hierarchical) Tucker factorization, we can select d different numbers of units, one for each layer, thus encoding a $K_1, \ldots, K_d$-rank factorization. For simplicity, we assume that $K_1 = K_2 = \ldots = K_d$.

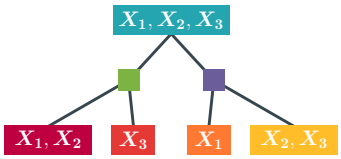

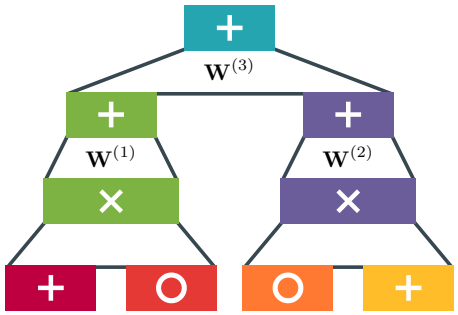

Figure 12: **A region node split into two partitionings** $(\{X_1, X_2\}, \{X_3\})$ and $(\{X_1\}, \{X_2, X_3\})$ of $\{X_1, X_2, X_3\}$ (above) is overparameterized using Tucker layers having parameters $\mathbf{W}^{(1)}, \mathbf{W}^{(2)} \in \mathbb{R}^{K \times K^2}$, and with an additional sum layer parameterized by $\mathbf{W}^{(3)} \in \mathbb{R}^{S \times (2K)}$, for some $S > 0$ (right).

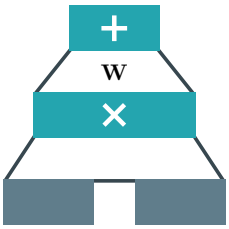

Figure 11: Tucker layer

Note that given our semantics for tensorized layers, stacking these composite abstractions by applying Algorithm 1 over a RG will always output a tensorized circuit that is smooth and (structured-)decomposable (Def. 8).

We start by considering composite layers that adopt the connectivity of computational units in the Tucker factorization, as showed in Fig. 2. This is a pattern introduced in architectures such as RAT-SPNs (Peharz et al., 2020c) and EiNets (Peharz et al., 2020a). There, a region node over $\mathbf{Y} \subseteq \mathbf{X}$ and partitioned into $(\mathbf{Z}_1, \mathbf{Z}_2)$ is parameterized as a layer $\boldsymbol{\ell}$ that is a composition of a Kronecker product layer followed by a sum layer, i.e., computing

$$\boldsymbol{\ell}(\mathbf{Y}) = \mathbf{W}\left(\boldsymbol{\ell}_1(\mathbf{Z}_1) \otimes \boldsymbol{\ell}_2(\mathbf{Z}_2)\right) \tag{Tucker-layer}$$

where $\mathbf{W} \in \mathbb{R}^{K \times K^2}$ is the parameter matrix for a given number of units K, and $\boldsymbol{\ell}_1, \boldsymbol{\ell}_2$ are its input layers (in grey in Fig. 11), each computing a K-dimensional vector obtained via overparameterization and tensorization of region nodes over $\mathbf{Z}_1, \mathbf{Z}_2$, respectively. Algorithm 2 composes sum and product layers as to construct Eq. (Tucker-layer), and it is called to overparameterize the circuit (see L6-8 in Algorithm 1). However, note that the flexibility provided by Algorithm 1 allows us to define other possible parameterizations in Algorithm 2, without changing the rest of the algorithm.

Overparameterizing multiple partitionings, the Mixing layer case. Some RGs can have multiple partitionings for a same region, as shown in Fig. 12. More formally, given a region node $\mathbf{Y} \subseteq \mathbf{X}$, we can split it into $N > 1$ different partitioning, i.e., $\{(\mathbf{Z}_1^{(i)}, \mathbf{Z}_2^{(i)})\}_{i=1}^N$, with $\mathbf{Y} = \mathbf{Z}_1^{(i)} \cup \mathbf{Z}_2^{(i)}$ for every i. This is the case of the PD RG used in EiNets (Peharz et al., 2020a), and the proposed QG (see Section 4.1 and Fig. 10). We illustrate an example of such RG in Fig. 12. The design adopted in EiNets to overparameterize them is to build an *apparently* special layer called *mixing layer* by Peharz et al. (2020a) computing

$$\boldsymbol{\ell}(\mathbf{Y}) = \sum_{i=1}^{N} \mathbf{w}_{i:} \odot \boldsymbol{\ell}_i(\mathbf{Y}) \tag{Mixing-layer}$$

where $\mathbf{W} \in \mathbb{R}^{N \times K}$ denote the parameter matrix of $\boldsymbol{\ell}$, and each $\boldsymbol{\ell}_i$ is a layer that outputs a K-dimensional vector. However, we observe that Eq. (Mixing-layer) can be computed by a simple sum layer that already conforms to our Def. 7. In fact, Eq. (Mixing-layer) can be rewritten as $\boldsymbol{\ell}(\mathbf{Y}) = \mathbf{W}'(\|_{i=1}^{N} \boldsymbol{\ell}_i(\mathbf{Y}))$, where $\mathbf{W}' \in \mathbb{R}^{K \times (NK)}$ is the parameter matrix obtained by concatenating N diagonal matrices $\{\mathbf{W}'_i\}_{i=1}^N$ along the columns, with $\mathbf{W}'_i \in \mathbb{R}^{K \times K}$ for $i \in [K]$. This observation demystifies the need of treating mixing layers as yet another type of layers, which happens to be the case in current EiNets implementations (Peharz et al., 2020a; Braun, 2021). Algorithm 3 specifies the construction of the generalization of the mixing layer as a single sum layer (used in L9 of Algorithm 1). Section 4.3 illustrates the overparameterization and tensorization of a region being decomposed in more than one partitioning. Note that from our perspective it becomes clear that such a sum layer does not necessarily increase the expressiveness, i.e., at the scalar unit level one could merge connected sum units as a single sum unit. For this reason, in Section 6 we experiment with mixing layers whose parameter entries are fixed during learning.[7]

[7] And we found that empirically this speeds up learning and does improve performances a bit.

4.4 Folding to Further Accelerate Learning and Inference

The final and optional step of our proposed pipeline (Fig. 9) consists of stacking together the layers that share the same functional form as to increase GPU parallelism. We name this step *folding*. Note that folding is only a syntactic transformation of the circuit, i.e., it does not change the encoded function and hence it preserves its expressiveness. This simple syntactic "rewriting" of a circuit can however significantly impact learning and inference performance. In fact, folding is the core ingredient of the additional speed-up introduced by EiNets (Peharz et al., 2020a) with respect to the same non-folded circuit architectures such as RAT-SPNs (Peharz et al., 2020c) which share with EiNets the other architecture details, e.g., the use of Tucker layers (see Table 1). As such, the difference in performance that is usually reported when treating RAT-SPNs and EiNets as two different PC model classes (see e.g., Liu et al. (2023a)) must depend on other factors, such as the choice of the RG or a discrepancy in other hyperparameters used to learn these models, e.g., the chosen optimizer. By disentangling these aspects in our pipeline, we can design experiments that truly highlight which factors are responsible for increased performance (see Section 6).

Folding layers. To retrieve the folded representation of the Tucker layer (Eq. (Tucker-layer)), we need to stack the parameter matrices along a newly-introduced dimension, which we call *the fold dimension*. Then, we can compute products accordingly to such extra dimension. For instance, given a set $\{\boldsymbol{\ell}^{(n)}\}_{n=1}^{F}$ of Tucker layers having scopes $\{\mathbf{Y}^{(n)}\}_{n=1}^{F}$, respectively, we evaluate them *in parallel with a single folded layer* $\boldsymbol{\ell}$ computing a $F \times K$ matrix and defined as

$$\boldsymbol{\ell}\left(\bigcup_{n=1}^{F}\mathbf{Y}^{(n)}\right)_{n:} = \mathbf{W}_{n::}\left[\boldsymbol{\ell}_1\left(\bigcup_{n=1}^{F}\mathbf{Z}_1^{(n)}\right)_{n:} \otimes \boldsymbol{\ell}_2\left(\bigcup_{n=1}^{F}\mathbf{Z}_2^{(n)}\right)_{n:}\right] \qquad \text{with } n \in [F] \qquad \text{(Tucker-folded)}$$

where $\boldsymbol{\ell}_1$ (resp. $\boldsymbol{\ell}_2$) denotes a folded layer computing the F left (resp. right) inputs to $\boldsymbol{\ell}^{(n)}$, each defined over variables $\mathbf{Z}_1^{(n)}$ (resp. $\mathbf{Z}_2^{(n)}$), and each $\mathbf{W}_{n::} \in \mathbb{R}^{K \times K^2}$ is the parameter matrix of $\boldsymbol{\ell}^{(n)}$. In other words, $\mathbf{W}_{n::}$ is the n-th slice along the first dimension of a tensor $\boldsymbol{\mathcal{W}} \in \mathbb{R}^{F \times K \times K^2}$ obtained by stacking together the parameter matrices of each Tucker layer. Since the same region node can possibly take part in multiple partitionings of other region nodes (e.g., see Fig. 9**i**), we might have folded inputs $\boldsymbol{\ell}_1, \boldsymbol{\ell}_2$ computing the same outputs. We illustrate an example of this in Fig. 9**iii**, which shows the folding of two Tucker sum-product layers sharing one input. In Appendix F, we report a pytorch snippet implementing a folded Tucker layer with an einsum operation. For this reason, while folding provides considerable speed-up when evaluating a tensorized circuit, it might come at the cost of increased memory usage depending on the chosen RG.

How to choose the layers to fold? It remains to decide how to choose the layers to fold together. The simplest way is traversing the tensorized circuit top-down (i.e., from the outputs towards the inputs) and to fold layers located at the same depth in the computational graph. However, note that we can also fold layers at different depth. For example, all input layers can be folded together if they encode the same input functional for all variables. This is the approach adopted in EiNets (Peharz et al., 2020a) and the one that will be used in all our experiments and benchmarks (see Section 6). However, note that this is not regarded as the optimal way to fold layers, and different ways of choosing the layers to fold might bring additional speed-up and memory savings when tailored for specific architectures. While we do not investigate different ways of folding layers other than the one mentioned above, the disentanglement of the folding and overparameterization steps (Section 4.2) in our proposed pipeline will foster future work to rely on the wide literature on parallelizing generic computational graphs (Shah et al., 2023).

5 Compressing Circuits and Sharing Parameters via Tensor Decompositions

In this section, we exploit again the literature of tensor factorizations to improve the design and learning of circuit architectures. We start by observing that as the parameters in circuit layers in our pipeline are stored in large tensors (see e.g., Eqs. (Tucker-layer) and (Tucker-folded)) they *can in principle be factorized again*. And since factorizations are circuits (Proposition 1), in the end we obtain several variants of circuit architectures and layers, some of which are new and offer an interesting trade-off between speed and accuracy (Section 5.2), while others are implicitly being used in the construction of existing circuits and tensor

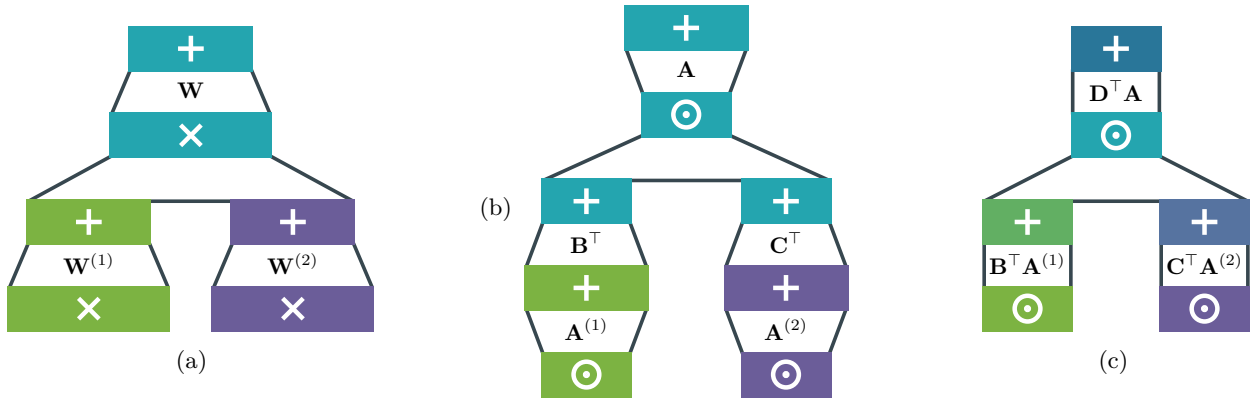

Figure 14: **Compressing Tucker layers into CP layers.** Given a (fragment of) tensorized circuit equipped with Tucker layers (a), we compress it by computing a CP factorization for each parameter matrix $\mathbf{W}^{(1)}$, $\mathbf{W}^{(2)}$, and $\mathbf{W}$. By doing so, we recover a different parameterization given by the factor matrices of the CP factorizations, and the product layers now compute a Hadamard product of their inputs (b). Finally, we can simplify the circuit by *collapsing* consecutive sum layers (c). The circuit structure showed in (a) is typical of RAT-SPNs and EiNets architectures, while the one in (c) captures the connectivity in HCLTs, MPS/TTs, BMs and more (Table 1), since it interleaves Hadamard product and sum layers (e.g., see MPS/TT in Fig. 8).

factorizations (Table 1). Again, we start from Tucker layers, with the aim of *compressing* a deep circuit using them, i.e., approximating it by using less parameters.

5.1 Compressing Tucker layers

Although expressive, Tucker layers in circuits require learning and storing K^3 parameters, encoded in the matrix $\mathbf{W} \in \mathbb{R}^{K \times K^2}$ in Eq. (Tucker-layer), which can be reshaped as the three dimensional tensor $\boldsymbol{\mathcal{W}} \in \mathbb{R}^{K \times K \times K}$. More in general, by relaxing the assumption of binary RGs made so far, a Tucker layer taking N input layers will be parameterized by K^{N+1} parameters. To retrieve a more space efficient parameterization of a Tucker layer, we propose to compress its parameter tensor $\boldsymbol{\mathcal{W}}$ via a rank-R *canonical polyadic* (CP) factorization, which we define below.

Definition 10 (CP factorization (Carroll & Chang, 1970))**.** Let $\boldsymbol{\mathcal{T}} \in \mathbb{R}^{I_1 \times \cdots \times I_d}$ be a d-dimensional tensor. The rank-R *canonical polyadic* (CP) of $\boldsymbol{\mathcal{T}}$ factorizes it as a sum of R rank-1 tensors, i.e.,

$$\boldsymbol{\mathcal{T}} \approx \sum_{r=1}^{R} \mathbf{v}_{:r}^{(1)} \circ \cdots \circ \mathbf{v}_{:r}^{(d)} \qquad \text{or in element-wise notation} \qquad t_{i_1 \cdots i_d} \approx \sum_{r=1}^{R} v_{i_1 r}^{(1)} \cdots v_{i_d r}^{(d)} \tag{16}$$

where $\mathbf{V}^{(j)} \in \mathbb{R}^{I_j \times R}$ with $j \in [d]$ are factor matrices.

Note that a CP factorization can be represented as a circuit as it is a special case of the Tucker factorization (Proposition 1). With this in mind, we proceed by decomposing the $\boldsymbol{\mathcal{W}} \in \mathbb{R}^{K \times K \times K}$ parameter tensor of a Tucker layer via a rank-R CP factorization such that $R \ll K$, i.e.,

$$\boldsymbol{\mathcal{W}} \approx \sum_{r=1}^{R} \mathbf{a}_{:r} \circ \mathbf{b}_{:r} \circ \mathbf{c}_{:r} \qquad \text{or in element-wise notation} \qquad w_{ijk} \approx \sum_{r=1}^{R} a_{ir} b_{jr} c_{kr} \tag{17}$$

where $\mathbf{A}, \mathbf{B}, \mathbf{C} \in \mathbb{R}^{K \times R}$ are newly-introduced parameter matrices. This new parameterization requires only $3KR$ parameters and unlocks a faster evaluation of Tucker layers. That is, we can rewrite the function computed by a Tucker layer $\boldsymbol{\ell}$ in element-wise notation as

$$\boldsymbol{\ell}(\mathbf{Y}) = \mathbf{A}\left[\left(\mathbf{B}^\top \boldsymbol{\ell}_1(\mathbf{Z}_1)\right) \odot \left(\mathbf{C}^\top \boldsymbol{\ell}_2(\mathbf{Z}_2)\right)\right] \tag{18}$$

where $\boldsymbol{\ell}_1, \boldsymbol{\ell}_2$ are input layers to $\boldsymbol{\ell}$ having width K and scopes $\mathbf{Z}_1, \mathbf{Z}_2$, respectively.

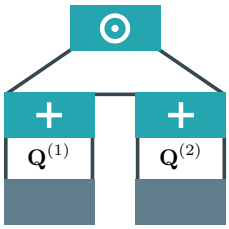

Figure 15: CP layer.

Therefore, evaluating a compressed Tucker layer that has undergone the CP factorization requires time $\mathcal{O}(KR)$ (Eq. (18)), rather than $\mathcal{O}(K^3)$ (Eq. (Tucker-layer)). On top of this, we observe that if we use a CP factorization to all Tucker layers in a PC, we will obtain a circuit in which sum and product layers are not alternated anymore. For example, starting from the Tucker layers in Fig. 14a, we would obtain a new architecture where product layers can be followed by two sum layers, as in Fig. 14b, e.g., one parameterized by $\mathbf{A}^{(1)} \in \mathbb{R}^{K \times R}$ feeding another sum layer parameterized by $\mathbf{B}^\top \in \mathbb{R}^{R \times K}$. As we can always rewrite any composition of consecutive sum layers with a single sum layer parameterized by a product of matrices (e.g., by $\mathbf{B}^\top \mathbf{A}^{(1)} \in \mathbb{R}^{R \times R}$), we can *collapse* the adjacent sum layers as to obtain the simplified architecture in Fig. 14c. More formally, under such observation and by assuming that $\boldsymbol{\ell}_1, \boldsymbol{\ell}_2$ are also Tucker layers being decomposed, we can rewrite Eq. (18) as

$$\boldsymbol{\ell}(\mathbf{Y}) = \left(\mathbf{Q}^{(1)} \boldsymbol{\ell}_1(\mathbf{Z}_1)\right) \odot \left(\mathbf{Q}^{(2)} \boldsymbol{\ell}_2(\mathbf{Z}_2)\right) \tag{CP-layer}$$

where $\mathbf{Q}^{(1)}, \mathbf{Q}^{(2)} \in \mathbb{R}^{R \times R}$ are parameter matrices of sum layers, such that $\mathbf{Q}^{(1)} = \mathbf{B}^\top \mathbf{A}^{(1)}$, $\mathbf{Q}^{(2)} = \mathbf{C}^\top \mathbf{A}^{(2)}$. That is, we reduced the overall width of each layer from K to the smaller R while still approximately computing a Tucker layer, by assuming that $\boldsymbol{\mathcal{W}}$ was originally low-rank. From now on, we will refer to Eq. (CP-layer) as CP layer. This is a new compositional abstraction we can use instead of Tucker layers in Algorithm 2 to build tensorized circuits out of a RG. For monotonic PCs, one can still recover the Tucker layer factorization above by replacing the CP factorization (Eq. (17)) with its non-negative version (Cichocki & Phan, 2009), which ensures the factors $\mathbf{A}, \mathbf{B}, \mathbf{C}$ and hence $\mathbf{Q}^{(1)}, \mathbf{Q}^{(2)}$ to be non-negative matrices. Furthermore, a folded version of Eq. (CP-layer) can be obtained similarly to the one for Eq. (Tucker-layer) (see Section 4.4).

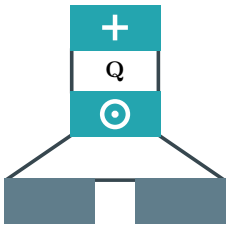

Figure 16: $\text{CP}^\top$ layer.

Finally, we introduce another type of layer which is very similar to the CP-layer above except that the Hadamard product is performed before the vector-matrix multiplication. We denote this sum-product layer as $\text{CP}^\top$, spelled *CP-transpose* or *CP-T*. Formally, a $\text{CP}^\top$ layer $\boldsymbol{\ell}$ computes

$$\boldsymbol{\ell}(\mathbf{Y}) = \mathbf{Q}\left(\boldsymbol{\ell}_1(\mathbf{Z}_1) \odot \boldsymbol{\ell}_2(\mathbf{Z}_2)\right), \tag{$\text{CP}^\top$-layer}$$

where $\mathbf{Q} \in \mathbb{R}^{R \times R}$. The main difference between using CP and $\text{CP}^\top$ layers is when these are applied on top of input layers, as there might be a slight difference in expressiveness. For instance, the product of two mixtures of Gaussians is different from a mixture of the product of two Gaussians.

Architectures such as HCLTs are latent tree models (Choi et al., 2011) and as such they can be rewritten as tensorized circuits using $\text{CP}^\top$ layers (Table 1) plus one additional sum layer, as illustrated in Fig. 18. More specifically, since HCLTs are monotonic circuits, we can interpret each of the parameter matrices $\mathbf{Q} \in \mathbb{R}_+^{R \times R}$ in Eq. ($\text{CP}^\top$-layer) as conditional probability tables[8] of the form $p(Z_i \mid Z_j)$ with latent variables Z_i, Z_j attached to the latent tree model the HCLT is compiled from (as we mentioned in Section 4.1). In other words, the difference between these tensorized circuit architectures and others such as EiNets or RAT-SPNs translates to simply a CP factorization of parameters if one fixes the same RG. In Appendix B we show that the same line of thought can be applied to the many tensorized PC architectures that have been developed so far. That is, Appendix B further details how the tensorized PC architectures reported in Table 1 can be understood and built within our pipeline, by specifying which RG and sum and product layer composition to use (Tucker, CP or $\text{CP}^\top$), and whether to fold the computational graph or not. Next, we show how we can further exploit tensor factorizations as to build and compress *folded* tensorized circuit architectures.

5.2 Parameter Sharing by Tensor Factorizations

We now focus on the problem of sharing parameters across layers in a tensorized PC. Again, we will exploit tensor factorizations for this task. Consider a tensorized PC built out of a RG as per our pipeline (Section 4.2). It is reasonable to assume that layers located at the same depth of the RG could store similar structure in

[8]The term $\text{CP}^\top$ is indeed a pun on the term conditional probability tables (CPTs) in the Bayesian network terminology.

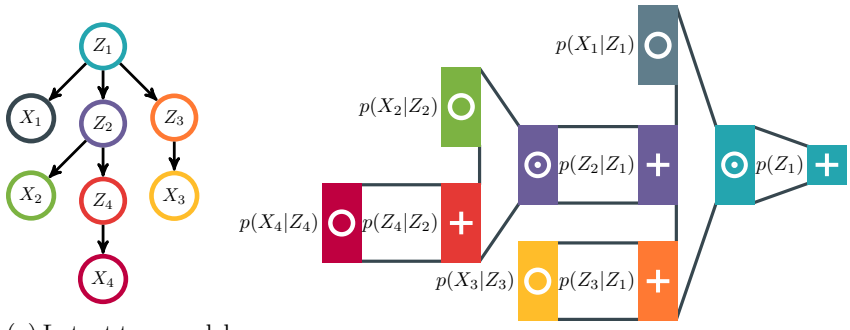

(a) Latent tree model

(b) Tensorized PC

Figure 18: **PGMs can be compiled as tensorized PCs.** We show how the PGM in (a), a latent tree model (LTM), with latent variables Z_i and observable variables X_i, can be compiled in the tensorized PC over $\mathbf{X}$ in (b) using input, dense, and $\text{CP}^\top$ layers parameterized by the conditional probability tables of the LTM, following the compilation algorithm proposed by Liu & Van den Broeck (2021b).

their parameter tensors. For example, two distinct layers having adjacent pixel patches of the same size as scope may apply a similar transformation to their respective inputs, because we can assume the distributions of the two pixel patches to be quite similar. If the RG is a perfectly balanced binary tree, folding the resulting circuit translates to folding layers located at the same depth in the computational graph, i.e., layers that are likely to share the same structure in parameter space. This motivates us to implement parameter sharing as a factorization across layers being folded.

Specifically, we start by compressing a folded Tucker layer (Eq. (Tucker-folded)) and to retrieve a new layer that implements the aforementioned parameter sharing, we again decompose its parameter tensor via a CP factorization (Def. 10). This time, we will have to decompose $\boldsymbol{\mathcal{W}} \in \mathbb{R}^{F\times K\times K\times K}$, i.e., the 4-dimensional tensor obtained by reshaping of the parameter tensor of a folded Tucker layer $\boldsymbol{\ell}$, where F indicates the folding dimension. By applying a rank-R CP factorization such that $R \ll K$, we obtain that

$$\boldsymbol{\mathcal{W}} \approx \sum_{r=1}^{R} \mathbf{d}_{:r} \circ \mathbf{a}_{:r} \circ \mathbf{b}_{:r} \circ \mathbf{c}_{:r} \qquad \text{or in element-wise notation} \qquad w_{nijk} \approx \sum_{r=1}^{R} d_{nr} a_{ir} b_{jr} c_{kr} \tag{19}$$

where $\mathbf{A}, \mathbf{B}, \mathbf{C} \in \mathbb{R}^{K\times R}$ and $\mathbf{D} \in \mathbb{R}^{F\times R}$. Note that $\mathbf{A}, \mathbf{B}, \mathbf{C}$ are independent of the fold dimension and are effectively shared among folds. By decomposing the parameter tensor in Eq. (Tucker-folded) as in Eq. (19) and by collapsing sum layers as done for the Tucker layer above, we can rewrite Eq. (Tucker-folded) as

$$\boldsymbol{\ell}\left(\bigcup_{n=1}^{F} \mathbf{Y}^{(n)}\right)_{n:} = \mathbf{d}_{n:} \odot \left(\mathbf{Q}^{(1)}\boldsymbol{\ell}_1\left(\bigcup_{n=1}^{F} \mathbf{Z}_1^{(n)}\right)_{n:}\right) \odot \left(\mathbf{Q}^{(2)}\boldsymbol{\ell}_2\left(\bigcup_{n=1}^{F} \mathbf{Z}_2^{(n)}\right)_{n:}\right) \qquad n \in [F] \qquad (\text{CP}^{\text{S}}\text{-layer})$$

where $\mathbf{Q}^{(1)}, \mathbf{Q}^{(2)} \in \mathbb{R}^{R\times R}$ do not depend on the fold dimension, and $\mathbf{D} \in \mathbb{R}^{F\times R}$. However, we can go further in sharing parameters and drop the fold-dependent parameter matrix $\mathbf{D}$ from Eq. (CP^{S}-layer), hence effectively fixing it to be a matrix of ones. The reason is that its contribution can be "absorbed" by the matrices associated to the following sum layers (i.e., similarly to the "collapse" of consecutive sum layers shown in Fig. 14). We will refer to this layer as CP^{XS}. Our experiments (Section 6) support this conjecture: as we experiment with both CP^{S} and CP^{XS}, we find they achieve comparable performances for distribution estimation. These two new composite layers are a nice addition to the circuit literature, and possible inspiration to further layer designs.

Opportunity 7. Many new layer and circuit architectures

So far we introduced Tucker, CP, $\text{CP}^\top$, CP^{S} and CP^{XS} as possible composite layers for circuits and tensor factorizations. We provide pytorch snippet for such layers in Appendix F. However, one is not limited to this list and can design new ones: as long as they are compositions of the same building blocks outlined in Def. 7, they can be seamlessly plugged into Algorithm 1 as to construct new tensor factorizations represented as tensorized circuits.

Our experiments (Section 6) show the combination of RG and layer choices can have a significant impact on the resulting performances of the chosen architecture (may it be time and memory requirements or accuracy as distribution estimators), hence justifying further exploring the design space of PC architectures. Lastly, we remark that one is not limited to pick the same composite layer for each node in a RG, according to Algorithm 1. From the point of view of tensor factorizations, this would result in a peculiar "Frankenstein" hierarchical tensor factorization that mixes different local factorizations. We have previously shown in Fig. 6 an example of such a hierarchical tensor factorization. From a ML perspective, determining which layer structure to select for each RG node can be cast as a *neural architecture search* task (Ren et al., 2021).

Table 2: **Distribution estimation results.** We report the test-set bpd of our best architectures, QT-CP-512 and QG-CP-512, and compare them against HCLT (Liu & Van den Broeck, 2021b), RAT-SPN (Peharz et al., 2020c), SparsePC (Dang et al., 2022a), IDF (Hoogeboom et al., 2019), BitSwap (Kingma et al., 2019), BBans (Townsend et al., 2019) and McBits (Ruan et al., 2021). SparsePC is a structure learning algorithm for PCs that iteratively finetunes both structure and parameters of a trained PC and can potentially be applied as a post-processing step to the PCs we are learning with our pipeline. HCLT results are taken from (Gala et al., 2024a). Dataset CelebA* is preprocessed using the lossless YCoCg transform.

	QT-CP-512	QG-CP-512	HCLT (CL-CP)	RAT (RND-Tucker)	Sp-PC	IDF	BitS	BBans	McB
Mnist	1.17	1.17	1.21	1.67	1.14	1.90	1.27	1.39	1.98
F-mnist	3.38	3.32	3.34	4.29	3.27	3.47	3.28	3.66	3.72
Emn-mn	1.70	1.64	1.70	2.56	1.52	2.07	1.88	2.04	2.19
Emn-le	1.70	1.62	1.75	2.73	1.58	1.95	1.84	2.26	3.12
Emn-ba	1.73	1.66	1.78	2.78	1.60	2.15	1.96	2.23	2.88
Emn-by	1.54	1.47	1.73	2.72	1.54	1.98	1.87	2.23	3.14
	QT-CP-256	QG-CP-128							
CelebA	5.33	5.33							
CelebA*	5.24	5.20							

6 Empirical Evaluation: Which RG and Layers to use?

Destructuring modern PC architectures (as well as tensor factorizations) into our pipeline (Fig. 9) allows us to create new tensorized architectures by simply following a mix & match approach (Table 1). At the same time, it helps us understand what really matters between different model classes from the point of views of expressiveness, speed of inference and easiness of optimization. We can now in fact easily disentangle key ingredients such as the role of RGs and the choice of composite layers in modern circuit architectures, and pinpoint which is responsible for a boost in performance. For example, HCLTs have been considered as one of the best performing circuit model architectures in recent benchmarks (Liu et al., 2022; 2023a), but until now it has not been clear why they were outperforming other architectures such as RAT-SPNs and EiNets. Within our framework, we can try to answer that question by answering more precise questions: *is it the effect of their RG that is learned from data (Section 4.1)*?, *the use of their composite sum-product layer parameterization (Section 5.1)?* or *are other hyperparameter choices the culprit*? (spoiler: it is going to be the use of CP layers).

Specifically, in this section we are interested in answering the following three research questions following a rigorous empirical investigation. **RQ1)** What are the computational resources needed (time and GPU memory) at test and training time for some of the many tensorized architectures we can now build? **RQ2)** What is the impact of the choice of RG and composite sum-product layer on the performance of tensorized circuits trained as distribution estimators? **RQ3)** Can we retain (most of) the performances of pre-trained tensorized PCs using Tucker layers if we factorize these into CP layers as illustrated in Fig. 14a → Fig. 14b? Note that we are not asking what is the impact of folding (Section 4.4), as we already know the answer:

folding is essential for large-scale tensorized architectures. As such, throughout all experiments, we use folded tensorized circuits. *We emphasise that the aim of our experiments is not to reach state-of-the-art results in distribution estimation, but rather that of understanding the role of the ingredients of tensorized circuit architectures.* All experiments were run on a single NVIDIA RTX A6000 GPU with 48GB of memory.

A new circuit nomenclature. We remark that HCLT, EiNets, RAT-SPNs, and all the other acronyms in Table 1 do not denote different model *classes* but just different *architectures*. They are instances of the same model class: smooth and (structured-)decomposable circuits. In the following, we will denote a tensorized architecture as [RG]-[sum-product layer], possibly followed by K, the number of units used for overparameterizing layers as in Algorithm 1. Under this nomenclature, RAT-SPNs and EiNets will both be encoded as RND-Tucker when they are both build with a random RG. When they are built with a Poon&Domingos RG, they will instead be referred to as PD-Tucker, meanwhile HCLTs will become CL-CP.

Task & Datasets. We will mainly evaluate our architectures by performing distribution estimation on image datasets. We use the MNIST-family, which includes 6 datasets of gray-scale 28x28 images—MNIST (LeCun et al., 2010), FASHIONMNIST (Xiao et al., 2017), and EMNIST with its 4 splits (Cohen et al., 2017)—and the CelebA dataset down-scaled at 64x64 (Liu et al., 2015), which we explore in two versions: one with RGB pixels and the other with pixels preprocessed by the lossless YCoCg color-coding (Malvar & Sullivan, 2003), as recent results suggested that such a transform can greatly lower bpds.[9] Furthermore, we perform experiments on tabular data with continuous variables. In particular, we will evaluate different tensorized layers by performing density estimation on 5 UCI datasets, as they are typically used to evaluate normalizing flows (Papamakarios et al., 2017). We report the statistics of the UCI dataset in Table E.5.

Parameter optimization. We train circuits to estimate the probability distribution that is assumed to have generated the images, considering each pixel as a random variable. As such, the input units in the circuit represent Categorical distributions having 256 values. For RGB images, we associate three Categorical distribution units per pixel (one per color channel). Instead, for the 5 UCI datasets (Table E.5), we use input units representing univariate Gaussian distributions, and we learn both the means and the standard deviations. We perform maximum likelihood by stochastic gradient ascent, i.e., want to maximize the following objective

$$\mathcal{L}(\mathcal{B}, c) = \sum_{\mathbf{x} \in \mathcal{B}} \log(c(\mathbf{x})) - \log(Z), \tag{20}$$

where $Z = \sum_{\mathbf{x}} c(\mathbf{x})$ is the partition function of the PC c[10], and $\mathcal{B}$ a batch of training data. After some preliminary experiments, we found that optimizing PCs with Adam (Kingma & Ba, 2015) using a learning rate of 10^{-2} delivered, on average, the best performing models for the datasets we considered. We also settled to reparameterize the circuit sum parameters via clamping and setting $\epsilon = 10^{-19}$ (Eq. (11)) after each optimization step as to keep them non-negative, as it was giving the best learning dynamics among all possible reparameterizations (Section 3.2). In the following, we will summarize our findings when answering RQ1-3, while distilling recommendations for practitioners on how to build and learn circuits.

RQ1) Benchmarking time & space for different tensorized architectures. For these experiments, we consider the following RGs: PD, as commonly used in architectures such as RAT-SPNs and EiNets, and the two novel light-weight and data-agostic RGs we introduced in Section 4.1, QTs [11] and QGs . We do not consider RND as it is usually just a balanced binary tree (Peharz et al., 2020c), and as such would yield the same time and memory performance of a QT. For the same reason we do not consider CL as they are tree RGs that end up being quasi-balanced after being rooted.[12] For layers, we consider Tucker (Eq. (Tucker-layer)), CP (Eq. (CP-layer)), CP^{S} (Eq. (CP^{S}-layer)) and CP^{XS} (Section 5.2).

[9] We take this evidence from Liu et al. (2023a;b), which use however a lossy variant of the YCoCg transform that unfortunately artificially inflates likelihoods. As such, their bpds for PCs are not directly comparable with ours, nor with the other deep generative models in their tables. We confirmed this issue in their evaluation protocol via personal communication.

[10] After training, one can efficiently "embed" the normalization constant in the parameters of a PC, effectively renormalizing them (and thus yielding a partition function Z equal to 1), as detailed in Peharz et al. (2015).

[11] Throughout our experiments, we will refer to QT-4 simply as QT.

[12] The root is chosen to be the barycenter of the graph to increase parallelism (Dang et al., 2021; 2022c).

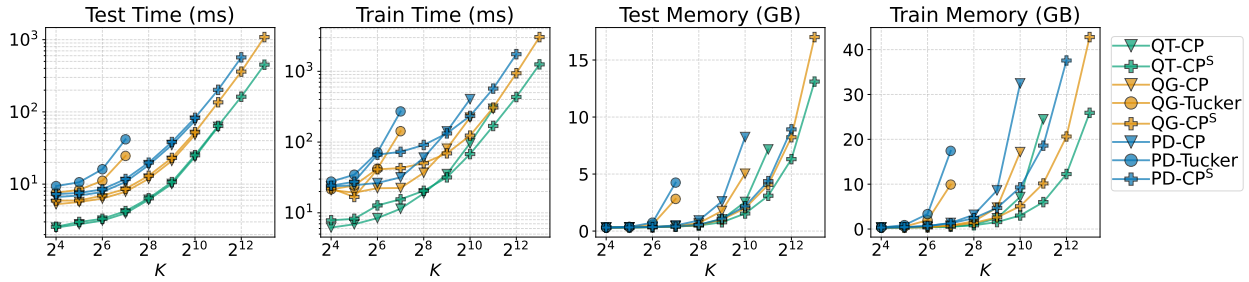

Figure 19: **Benchmarking the role of RGs and composite layers in tensorized circuits.** We report the average time (ms) and GPU memory usage (GiBs) to process a batch of 128 samples from MNIST for different tensorized architectures—listed in the legend on the right—at different values of K (x-axis). The stats are reported for both test and training scenarios, where for training one has to expect additional overhead from performing gradient ascent.

In Fig. 19, we report the average time and GPU memory peak required to process a batch of data from MNIST for several tensorized PC architectures built by mix & matching different RGs and type of sum-product layers mentioned above, when possible on our GPU budget. For each architecture, we vary the model size by varying K, the number of units for each layer, in $\{16, 32, 64, 128, 256, 512, 1024, 2048, 4096, 8192\}$. We observe that the QT and QG region graphs deliver more scalable architectures than those based on the commonly used PD which is consistently slower and uses more memory. At the same time, one can see that CP and CP^S layers scale more gracefully: CP can accommodate $K = 2^{10}$ with QT as a RG and CP^S even larger values of K, up to 2^{13} with QG as well. Doing this is instead computationally impractical for Tucker layers on our GPUs, which allow only for $K = 128$ at most. We underline that this is expected as models using Tucker layers have more parameters than those using CP layers for the same model size K. This also explain why the architecture QT-Tucker is missing: QTs iteratively split images in 4 parts (Algorithm D.2) and therefore appling Tucker layers would require $\mathcal{O}(K^4)$ parameters for such architectures, which is unfeasible even for $K = 16$ on our GPUs.

We emphasise that non-folded versions of these architectures, e.g. RAT-SPNs (Peharz et al., 2020c), can be orders of magnitude slower, therefore hindering both learning and deployment in practice. In Fig. E.1 in the Appendix, we show the results of the same benchmark reported in Fig. 19 but for the CelebA dataset, which is more challenging because it is equivalent to perform distribution estimation on a much higher dimensional space ($12,288 = 64 \times 64 \times 3$ instead of $784 = 28 \times 28 \times 1$).[13]. From this additional experiment, we can conclude that even in higher dimensions the scaling behavior of RGs and layers is the same. Finally, in Fig. E.3, we zoom on a comparison between CP^S and CP^XS. There, we show that for the same choice of RG and K, CP^S and CP^XS layers require the same time/space resources as expected, with CP^XS only being slightly faster at training-time.

Takeaway 1.

QT and QG should be preferred to PD as RGs if we want to scale circuits, with the former being the most scalable than the latter. Layer-wise, CP layers scale, as expected, to larger values of K than Tucker layers and for even larger layers parameter sharing (CP^S, CP^XS) is recommended.

RQ2) Accuracy as distribution estimators. We now test our tensorized PCs as distribution estimators and we consider our mixed&matched architecture from RQ1. For each architecture, we vary the model size by varying K, the number of units for each layer, in $\{16, 32, 64, 128, 256, 512\}$ for the MNIST family and up to 256 for CelebA. To assess the effect of learning RGs from data, we compare against HCLTs ($\text{CL-CP}^\top$ in our nomenclature) as reported in (Dang et al., 2022a). We use a batch size of 256, and train for at most 200

[13]Note that for our RQ1, all image datasets with the same resolutions would yield the very same results. So the fact we pick as a grey-scale dataset MNIST and not F-MNIST is not really important.

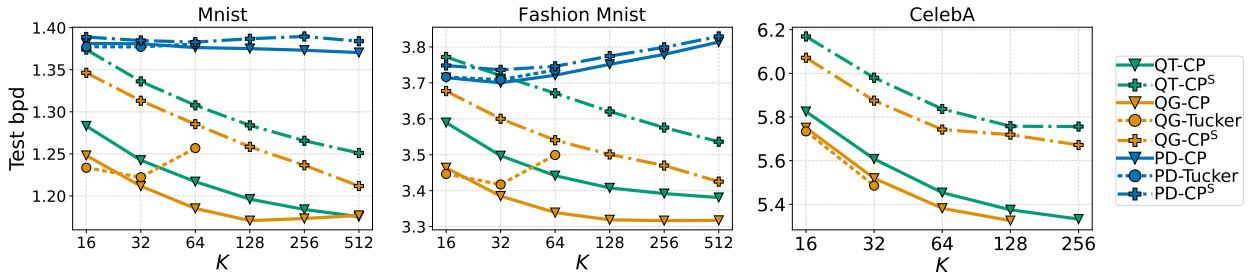

Figure 20: **Overparameterizing tensorized architectures delivers better performing models when using QTs and QGs, but not when using PDs.** We report the test-set bpd (y-axis) at different values of K (x-axis) for MNIST (left), FASHIONMNIST (middle) and CELEBA (right) averaged over 5 runs for different tensorized architectures, which we report in the legend on the right. We keep the mixing layers in QG- and PD-based models fixed and normalized. We use a batch size of 256.

epochs stopping training if the validation log-likelihood does not improve after 5 epochs. We use the average test-set bits-per-dimension (bpd) as the evalutation criterion, i.e. $\texttt{bpd}(\mathcal{D}, c) = -\mathcal{L}(\mathcal{D}, c)/(d \cdot \log 2)$, where d is the number of features in dataset $\mathcal{D}$ and $\mathcal{L}$ is defined as in Eq. (20).

In Fig. 20 we report the average test-set bpd on MNIST, FASHIONMNIST and CELEBA. An immediate visible pattern emerges when comparing the architectures w.r.t. the choice of RG: Both QT- and QG-based architectures outperform those based on PD, and also manage to scale to larger datasets like CELEBA. On average, the best performing architectures are those built out of QGs. This is expected as such RGs, different from QTs, allow different partitionings for a same region (and therefore require the usage of mixing layers as discussed in Eq. (Mixing-layer)). The PD region graphs, despite being DAG-shaped as QGs, deliver underperforming tensorized architectures, suggesting that bigger models, while carrying more expressively, are harder to train, a behavior also noted by Liu et al. (2023a). This is particularly evident looking at the trend of PD-based architectures on FASHIONMNIST.

In Table 2, we compare our best performing architectures, with other state-of-the-art probabilistic models even outside the circuit literature. Our architectures deliver close-to state-of-the-art results, outperforming some VAE- and flow-based models. When compared with RGs learned from data, as it is the case for HCLT, we note that our simpler, data-agnostic alternatives, QTs and QGs, perform equally well or better. Using them instead of the a CL RG saves the quadratic cost needed to learn the corresponding Chow-Liu tree (Dang et al., 2021).

As for the choice of type of sum-product layer, Tucker and CP layers deliver very similar performance on PD. We conjecture that this is due to PD being harder to train in general, as for other RGs the trend changes. In fact, with QT and QG, we observe that Tucker delivers the best bpds for the smallest values for K. Scaling it to larger Ks is impractical however. CP and variants not only scale better (see RQ1 and Fig. 19), but are able to deliver the best bpds for larger K. As expected, CP consistently outperforms CP^{S} having more learnable parameters. However, if one has to privilege time over accuracy, CP^{S} can be a useful alternative. Finally, we report results for CP^{XS} layers and learnable mixing layers in Appendix E, along with the results showed in Fig. 20 in tabular form. We confirm that CP^{S} and CP^{XS} layers are equivalently accurate and that one does *not* have to learn mixing layer parameters in tensorized PCs with DAG-shaped RGs Section 4.3. All these conclusions carry over also to a larger image dataset such as CELEBA, using or not the lossless YCoCg color-coding.

Density estimation on tabular datasets. Finally, we perform density estimation experiments on UCI datasets (Table E.5), and compare the results achieved by tensorized PCs constructed by our pipeline by parameterizing a RND RG (Section 4.1) with either CP or Tucker layers. To give context to our results, we show the average test log-likelihoods achieved by normalizing flow models (Papamakarios et al., 2021) that are often evaluated on UCI datasets: MADE (Germain et al., 2015), RealNVP (Dinh et al., 2017), MAF (Papamakarios et al., 2017) and NSF (Durkan et al., 2019). As additional baselines, we show results of other

Table 3: **Tucker layers are harder to scale than CP layers on high-dimensional UCI datasets.** We show the best average test log-likelihoods achieved by normalizing flow models (top) and tensorized PCs that can be instantiated from our pipeline (bottom). See main text for their description. Tensorized PCs obtained by parameterizing random binary tree RGs (Section 4.1) with CP (RND-CP) perform better on higher-dimensional datasets Hepmass and MiniBooNE than those with Tucker layers (RND-Tucker), while the latter have an advantage on lower-dimensional datasets such as Power and Gas. For RND-CP and RND-Tucker, we report the layer width (K) of the best performing model as a subscript of the log-likelihoods. Fig. E.5 shows training and test log-likelihoods achieved by varying the layer width K. Details in Appendix E.1.

	Power	Gas	Hepmass	M.BooNE	BSDS300
MADE (Germain et al., 2015)	-3.08	3.56	-20.98	-15.59	148.85
RealNVP (Dinh et al., 2017)	0.17	8.33	-18.71	-13.84	153.28
MAF (Papamakarios et al., 2017)	0.24	10.08	-17.73	-12.24	154.93
NSF (Durkan et al., 2019)	0.66	13.09	-14.01	-9.22	157.31
Gaussian	-7.74	-3.58	-27.93	-37.24	96.67
EiNet-LRS (Sidheekh et al., 2023, RND-Tucker)	0.36	4.79	-22.46	-34.21	—
TTDE Novikov et al. (2021, LT-CP$^\top$)	0.46	8.93	-21.34	-28.77	143.30
RND-CP	0.28_{256}	5.01_{256}	-22.52_{64}	-30.69_{128}	120.82_{64}
RND-Tucker	0.52_{64}	8.41_{256}	-23.47_{32}	-31.30_{8}	119.09_{64}

PCs supporting tractable marginalization: a single multivariate Gaussian, Einsum networks (Peharz et al., 2020a) with input layers encoding flows (EiNet-LRS) (Sidheekh et al., 2023), and TTDE (Novikov et al., 2021). We emphasize that both EiNet-LRS and TTDE can be built using our pipeline and characterized with our nomenclature, the former as RND RGs parameterized by Tucker layers, and the latter as LT RGs parameterized by CP$^\top$layers (Table 1). Table 3 shows that CP layers to deliver better performances than Tucker layers on high-dimensional UCI datasets and therefore in the case of deeper tensorized PCs. On the other hand, Tucker layers outperform CP layers on the lower-dimensional UCI datasets. We believe this is due the parameters of Tucker layers being more difficult to train and scale, similarly to our observation for Mnist and FashionMnist in the case of QG RGs in Fig. 20. We further detail in Appendix E.1 the experimental setting, and show in Fig. E.5 the results achieved by varying the layer width K.

Takeaway 2.

In the case of image datasets, our recommendation for a go-to architecture is QG-CP-K, with the largest possible K one can squeeze in their GPU memory. If computational resources are not enough, one can trade-off accuracy with speed and use QT-{CP,CP^{S} }-K. As a general trend, the simpler the architecture the easier training and scaling are. This is also suggested by our results on UCI datasets, where the simpler CP layers can perform better for high-dimensional datasets than Tucker.

RQ3) Compressing circuits with Tucker layers. For our last research question, consider the problem when a trained circuit with Tucker layers is given, and we want to compress it into a smaller one using CP layers by using our compression pipeline as illustrated in Fig. 14a and Fig. 14b. With this in mind, we investigate the change in performance, if any, w.r.t. the number of tunable parameters. Specifically, for each folded Tucker layer (Eq. (Tucker-folded)) in the given circuit, parameterized with a tensor $\boldsymbol{\mathcal{W}}$ of shape $F \times K \times K \times K$ we compress each tensor slice $\boldsymbol{\mathcal{W}}_{f:::}$ by performing non-negative (NN) CP factorization via alternating least squares (Shashua & Hazan, 2005). This optimization eventually delivers a tensor $\boldsymbol{\mathcal{W}}'$ of shape $F \times 3 \times R \times K$ for a R-ranked factorization.

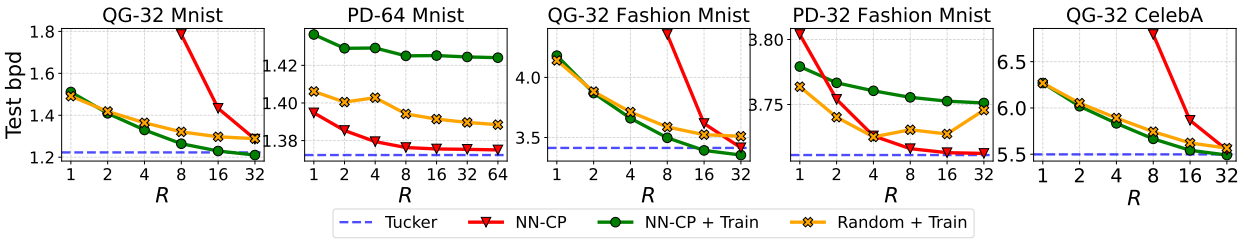

Figure 21: **Compressing Tucker layers into CP layers** (Fig. 14a → Fig. 14b) **can yield smaller and accurate models** as seen when we performing non-negative (NN) CP factorization via alternating least squares (Shashua & Hazan, 2005). In each plot, we report the bpd of a pre-trained Tucker-layered PC (dashed blue line), whose RG, size K and dataset on which it was trained on are detailed on the top. We report the bpd of several R-ranked NN-CP factorizations of such PCs (red curves), which we then use as initialization for further fine-tuning (green curves). Finally, we report the bpd of Tucker-compressed PCs (Fig. 14b) trained from a random initialization of their parameters (yellow curves).

We sketch the results of our investigation in Fig. 21. As expected, taking a pre-trained Tucker-layered PC (blue dashed line) and compressing its parameters via NN-CP factorization leads to a similar-performing model as the rank R of the approximation increases, as shown by the bpd trend of the red curves in Fig. 21. Interestingly, we observe a key difference between the two region graphs utilized. For tensorized PCs based on PD region graphs, even a rank 1 approximation (i.e. $R = 1$) leads to a relatively small bpd lose, while this is not the case for PCs built out of QGs. We conjecture that PD-based PCs have parameter tensors that are of much lower rank than QG-based PCs, and that very deep PCs learn low-rank parameter matrices.

Next, we investigate whether we can use these compressed models as an effective initialization scheme for smaller circuits, which we further train (fine-tune) to maximize the training data likelihood (Eq. (20)). Again, we see a different trend when comparing w.r.t. the region graph used, as shown by the bpds encoded as green curves in Fig. 21. Specifically, for PD-based PCs such fine-tuning leads to a quick overfitting already in the first optimization steps, leading to much higher bpds on test data. In contrast, fine-tuning QG-based PCs leads to models that consistently match or even outperform the original Tucker-based PCs (blue dashed line), i.e., we observe green curves consistently being below red curves and breaking the dashed blue lines.

As an additional baseline, we use the architecture of these compressed models (Fig. 14b) but train them from scratch: starting from a random initialization of its parameters. Fig. 21 illustrates that the NN-CP initialization can be better than a random one as it leads to better performing models when using QG RGs (yellow curves over green curves). This trend flips when using PD region graphs (yellow curves below green curves), again signaling that much information for these models could be stored in the RG more than in the parameters of the circuit. This, in turn, suggests that while new hierarchical factorizations with highly intricated RGs but very low-rank inner tensors are possible, they might be harder to learn effectively.

Takeaway 3.

Deep circuits encode distributions in highly-structured factorizations whose parameters can be effectively further compressed, e.g., by NN-CP factorizations. This yields a simple and effective procedure to distill a smaller tractable model from a larger one: compress each layer of the latter, then fine-tune the former by maximum-likelihood estimation.

7 Additional Related Work

In the previous sections, we surveyed and bridged the literature of circuit representations and tensor factorizations, and as such we have already reviewed several related works from both communities. Now, we discuss works that partially tried to establish this connection in the past, by trying to connect to probabilistic graphical models.

Tensor networks and PGMs. TNs (Orús, 2013) are widely used to model many-body systems in physics and quantum mechanics (Schollwoeck, 2010), and have been used to simulate quantum computations on classical hardware (Markov & Shi, 2008). They have been applied more recently for machine learning applications (Stoudenmire & Schwab, 2016; Han et al., 2018; Efthymiou et al., 2019; Bonnevie & Schmidt, 2021). As they essentially an alternative formalism for probabilistic graphical models over discrete variables (Koller & Friedman, 2009), people have started drawing connections between the two formalisms. For example, Bonnevie & Schmidt (2021) connects non-negative MPS/TTs to PGMs and offers routines for probabilistic reasoning. Similarly, Glasser et al. (2020) explores the same connection, but instead of drawing TNs as PGMs, they draw them as factor graphs (Kschischang et al., 2001).

Interestingly, these works are not aware of the latent variable interpretation of non-negative factorizations (Section 3.1) as they miss the connection through circuits. For the same reason, they are limited to autoregressive sampling (Opportunity 3). To the best of our knowledge, this latent-variable perspective has been (re)discovered only very recently in this concurrent work by Ghalamkari et al. (2024) who proposes the classical expectation-maximization (EM) algorithm to learn them. EM is a consolidated way to learn the parameters of circuits (Peharz et al., 2016; 2020a) by maximum likelihood.

Instead, by representing non-negative tensor factorizations as monotonic PCs, we effortlessly unlock the developed theory and algorithms required to perform complex probabilistic inference, with possible applications in lossless compression (Liu et al., 2022), neuro-symbolic AI with correctness guarantees (Ahmed et al., 2022) and constrained text generation (Zhang et al., 2023). Finally, results about the succinctness or expressive efficiency of these factorizations (Glasser et al., 2019) have been used recently to prove circuit lowerbounds (Loconte et al., 2024a;b).

Probabilistic circuits and PGMs. The modern formulation of PCs has been introduced for the first time in (Vergari et al., 2019b) as a unifying framework for several existing tractable probabilistic models (TPMs) including arithmetic circuits, (Darwiche, 2001), probabilistic decision graphs (Jaeger, 2004), and-or graphs (Marinescu & Dechter, 2009), cutset networks (Rahman et al., 2014), sum-product networks (Poon & Domingos, 2011) and more (Choi et al., 2020). The aim of PCs has been to abstract away from the different syntaxes and model formalisms of the above TPMs and focus on structural properties that enable tractable inference in each. Non-negative tensor factorizations and tensor networks have been underlooked in this effort so far. Several ways to compile discrete PGMs into PCs (or one of the above formalisms) have been devised in the past (Oztok & Darwiche, 2017; Shen et al., 2016; Choi et al., 2013). These compilation techniques yield sparse deterministic circuits, and only recently PCs have started to be represented first in code (Peharz et al., 2020c;a; Liu & Van den Broeck, 2021b) and then formally (Loconte et al., 2024a) as tensorized architectures. Perhaps this lack of tensorized compilation targets has hidden the connection between PCs and matrix and tensor factorizations. The closest connection we are aware of can be found in Jaini et al. (2018b): they bridge sum-product networks to hierarchical mixture models and HMMs and hint at a connection with tensorial mixture models (Sharir et al., 2017) a variant of hierarchical Tucker (Def. 5). Loconte et al. (2024a) formally reduced MPSs and BMs to circuits and started drawing a bridge with the literature on expressiveness of tensor factorizations (Glasser et al., 2019).

Matrix factorizations and circuit complexity results. Finding lower bounds to the rank of matrix factorizations can be used as a proxy to prove lower bounds to the size of circuits satisfying particular structural properties (de Colnet & Mengel, 2021). Proving an *exponential* (w.r.t. the number of variables) size lower bound for a class of circuits shows a limitation on which functions they can compute in polynomial time and number of parameters, thus allowing us to precisely separate circuit classes in terms of their expressiveness (Valiant, 1979; Martens & Medabalimi, 2014). Recently, lower bounding the non-negative rank (Gillis, 2020) and the square root rank (Fawzi et al., 2014; Lee & Wei, 2014) of matrices has been used to draw an expressiveness hierarchy of classes of PCs with negative real and complex-valued parameters for distribution estimation (Loconte et al., 2024a;b). Since circuits generalize many tensor network factorizations (see Section 2.4), showing size lower bounds for a class of circuits can be used to show size lower bounds for tensor networks *regardless of their structure*, e.g. as shown by Loconte et al. (2024b) in generalizing a known rank lower bound for real Born machines obtained by squaring a MPS/TT (Glasser et al., 2019).

8 Conclusion

In this paper, we laid the foundations to connect two communities in ML that developed independently but are sharing many research directions: circuits and tensor factorizations. Despite their apparently different syntax, the way they are usually presented, and the tasks in which they are commonly employed, these two formalisms significantly overlap in semantics and potential applications. We create this bridge between communities by first establishing a formal reduction of popular tensor factorizations to circuits in Section 2.

We hope this can propel research on how to design more and more scalable low-rank parameterization for probabilistic inference. To this end, we highlighted a number of possible future avenues for the matrix and tensor factorization communities that leverage the connection with circuits we established: designing hierarchical factorizations with non-tree structures (Opportunity 1); using the property-driven calculus that circuits offer to automatically derive tractable algorithms in a compositional way (Opportunity 2); treat non-negative (hierarchical) factorizations as deep latent variable models (Opportunity 3); devise factorizations over non-discrete and non-linear input spaces (Opportunity 4); embed logical constraints to realize neuro-symbolic systems that can reason with symbolic knowledge (Opportunity 5); devising alternative ways to compactly encode distributions, going beyond probability masses or densities (Opportunity 6); as well as devising flexible factorizations by changing only the structure of (some) layers in a circuit representation (Opportunity 7).

From the point of view of the circuit community, we leveraged this connection to systematize and demystify the construction of modern tensorized and overparameterized circuits (Section 4). We proposed a single pipeline that generalizes existing (tensor factorization and circuit) architectures and introduced a new nomenclature, based on the steps of our pipeline, to understand old but also new architectures that can be created by mixing & matching these steps (see Table 1). Our empirical analysis of popular ways to combine these ingredients highlights how lower-rank structures can be easier to learn and useful to compress higher-rank layers (Section 6). Finally, we distilled our findings in clear-cut recommendations (Takeaways 1 to 3) for practitioners that want to learn and scale circuits on high-dimensional data, and we hope this can foster future rigorous analysis.

Broader Impact Statement

This work is fundamental research in probabilistic modeling and reasoning and as such the algorithms and architectures discussed here can impact many possible downstream applications, in ways that go beyond our control. For example, circuits, or tensor factorizations, could be used in computer vision classifiers to amplify the bias already encoded in non-curated datasets or be used in safety-critical applications without eliciting valid safety requirements. Since it is hard to foresee all possible future misuses, we urge practitioners to pay attention to concrete problematic uses of our methodologies: use the time that tractable models save while performing inference to reflect on the direct impact your application can have.

References

Kareem Ahmed, Stefano Teso, Kai-Wei Chang, Guy Van den Broeck, and Antonio Vergari. Semantic probabilistic layers for neuro-symbolic learning. In *Advances in Neural Information Processing Systems 35 (NeurIPS)*, volume 35, pp. 29944–29959. Curran Associates, Inc., 2022.

Magda Amiridi, Nikos Kargas, and Nicholas D. Sidiropoulos. Low-rank characteristic tensor density estimation part i: Foundations. *IEEE Transactions on Signal Processing*, 70:2654–2668, 2022. doi: 10.1109/TSP.2022.3175608.

Atharva Awari, Harrison Nguyen, Samuel Wertz, Arnaud Vandaele, and Nicolas Gillis. Coordinate descent algorithm for nonlinear matrix decomposition with the relu function. *arXiv preprint*, 2024.

Ivana Balazevic, Carl Allen, and Timothy M. Hospedales. Tucker: Tensor factorization for knowledge graph completion. In *EMNLP-IJCNLP*, pp. 5184–5193. Association for Computational Linguistics, 2019.

Christopher M. Bishop and Nasser M. Nasrabadi. Pattern recognition and machine learning. *J. Electronic Imaging*, 16:049901, 2006.

Rasmus Bonnevie and Mikkel N. Schmidt. Matrix product states for inference in discrete probabilistic models. *Journal of Machine Learning Research*, 22:187:1–187:48, 2021.

Steven Braun. Simple-einet: An EinsumNetworks Implementation, 2021. URL https://github.com/braun-steven/simple-einet.

Diego Calanzone, Stefano Teso, and Antonio Vergari. Towards logically consistent language models via probabilistic reasoning. *arXiv preprint arXiv:2404.12843*, 2024.

J. Douglas Carroll and Jih-Jie Chang. Analysis of individual differences in multidimensional scaling via an n-way generalization of "eckart-young" decomposition. *Psychometrika*, 35:283–319, 1970.

Mark Chavira and Adnan Darwiche. On probabilistic inference by weighted model counting. *Artificial Intelligence.*, 172(6-7):772–799, 2008.

Song Cheng, Lei Wang, Tao Xiang, and Pan Zhang. Tree tensor networks for generative modeling. *Physical Review B*, 99(15):155131, 2019.

Arthur Choi, Doga Kisa, and Adnan Darwiche. Compiling probabilistic graphical models using sentential decision diagrams. In *Symbolic and Quantitative Approaches to Reasoning with Uncertainty: 12th European Conference, ECSQARU 2013, Utrecht, The Netherlands, July 8-10, 2013. Proceedings 12*, pp. 121–132. Springer, 2013.

Arthur Choi, Guy Van den Broeck, Adnan Darwiche, Qiang Yang, and Michael Wooldridge. Tractable learning for structured probability spaces: A case study in learning preference distributions. In *24th International Joint Conference on Artificial Intelligence (IJCAI)*, volume 2015, pp. 2861–2868. IJCAI, 2015.

Myung Jin Choi, Vincent YF Tan, Animashree Anandkumar, and Alan S Willsky. Learning latent tree graphical models. *Journal of Machine Learning Research*, 12:1771–1812, 2011.

YooJung Choi, Antonio Vergari, and Guy Van den Broeck. Probabilistic circuits: A unifying framework for tractable probabilistic modeling. Technical report, University of California, Los Angeles (UCLA), 2020.

C. K. Chow and C. N. Liu. Approximating discrete probability distributions with dependence trees. *IEEE Transactions on Information Theory*, 14(3):462–467, 1968a.

CKCN Chow and Cong Liu. Approximating discrete probability distributions with dependence trees. *IEEE transactions on Information Theory*, 14(3):462–467, 1968b.

Andrzej Cichocki and Anh Huy Phan. Fast local algorithms for large scale nonnegative matrix and tensor factorizations. *IEICE Trans. Fundam. Electron. Commun. Comput. Sci.*, 92-A(3):708–721, 2009.

Andrzej Cichocki, Rafal Zdunek, and Shun-ichi Amari. Nonnegative matrix and tensor factorization [lecture notes]. *IEEE signal processing magazine*, 25(1):142–145, 2007.

Gregory Cohen, Saeed Afshar, Jonathan Tapson, and André van Schaik. EMNIST: Extending MNIST to handwritten letters. In *IJCNN 2017*, pp. 2921–2926, 2017. doi: 10.1109/IJCNN.2017.7966217.

Nadav Cohen, Or Sharir, and Amnon Shashua. On the expressive power of deep learning: A tensor analysis. In *Annual Conference Computational Learning Theory*, 2015.

Alvaro H. C. Correia, Gennaro Gala, Erik Quaeghebeur, Cassio de Campos, and Robert Peharz. Continuous mixtures of tractable probabilistic models. In *The Thirty-Seventh AAAI Conference on Artificial Intelligence (AAAI-23)*, 2023.

Meihua Dang, Antonio Vergari, and Guy Van den Broeck. Strudel: A fast and accurate learner of structured-decomposable probabilistic circuits. *The International Journal of Approximate Reasoning (IJAR)*, 140: 92–115, 2021.

Meihua Dang, Anji Liu, and Guy Van den Broeck. Sparse probabilistic circuits via pruning and growing. *Advances in Neural Information Processing Systems (NeurIPS)*, 35:28374–28385, 2022a.

Meihua Dang, Anji Liu, Xinzhu Wei, Sriram Sankararaman, and Guy Van den Broeck. Tractable and expressive generative models of genetic variation data. In *Research in Computational Molecular Biology*, pp. 356–357, 2022b. doi: 10.1007/978-3-031-04749-7_26.

Meihua Dang, Antonio Vergari, and Guy Van den Broeck. Strudel: A fast and accurate learner of structured-decomposable probabilistic circuits. *International Journal of Approximate Reasoning*, 140:92–115, 2022c.

Adnan Darwiche. Decomposable negation normal form. *Journal of the ACM (JACM)*, 48:608–647, 2001.

Adnan Darwiche. A differential approach to inference in bayesian networks. *Journal of the ACM (JACM)*, 50(3):280–305, 2003.

Adnan Darwiche. *Modeling and Reasoning with Bayesian Networks.* Cambridge University Press, 2009.

Adnan Darwiche and Pierre Marquis. A knowledge compilation map. *Journal of Artificial Intelligence Research (JAIR)*, 17:229–264, 2002.

Carl de Boor. Subroutine package for calculating with B-splines. Technical report, Los Alamos National Lab. (LANL), 1971.

Alexis de Colnet and Stefan Mengel. A compilation of succinctness results for arithmetic circuits. In *18th International Conference on Principles of Knowledge Representation and Reasoning (KR)*, pp. 205–215, 2021.

Lieven De Lathauwer, Bart De Moor, and Joos Vandewalle. A multilinear singular value decomposition. *SIAM Journal on Matrix Analysis and Applications*, 21:1253–1278, 2000.

Luc De Raedt, Robin Manhaeve, Sebastijan Dumancic, Thomas Demeester, and Angelika Kimmig. Neuro-symbolic= neural+ logical+ probabilistic. In *NeSy@ IJCAI*, 2019.

Olivier Delalleau and Yoshua Bengio. Shallow vs. deep sum-product networks. *Advances in neural information processing systems*, 24, 2011.

Aaron W. Dennis and Dan Ventura. Learning the architecture of sum-product networks using clustering on variables. In *Advances in Neural Information Processing Systems 25 (NeurIPS)*, pp. 2033–2041. Curran Associates, Inc., 2012.

Nicola Di Mauro, Antonio Vergari, Teresa Maria Altomare Basile, and Floriana Esposito. Fast and accurate density estimation with extremely randomized cutset networks. In *ECML/PKDD*, 2017.

Nicola Di Mauro, Floriana Esposito, Fabrizio G. Ventola, and Antonio Vergari. Sum-product network structure learning by efficient product nodes discovery. *Intelligenza Artificiale*, 12:143–159, 2019.

Nicola Di Mauro, Gennaro Gala, Marco Iannotta, and Teresa M.A. Basile. Random probabilistic circuits. In *Proceedings of the Thirty-Seventh Conference on Uncertainty in Artificial Intelligence*, volume 161 of *Proceedings of Machine Learning Research*, pp. 1682–1691. PMLR, 27–30 Jul 2021.

Laurent Dinh, Jascha Sohl-Dickstein, and Samy Bengio. Density estimation using Real NVP. In *5th International Conference on Learning Representations (ICLR)*, 2017.

Conor Durkan, Artur Bekasov, Iain Murray, and George Papamakarios. Neural spline flows. In *Advances in Neural Information Processing Systems 32 (NeurIPS)*, pp. 7511–7522. Curran Associates, Inc., 2019.

Stavros Efthymiou, Jack D. Hidary, and Stefan Leichenauer. Tensor network for machine learning. *ArXiv*, abs/1906.06329, 2019.

Hamza Fawzi, João Gouveia, Pablo A. Parrilo, Richard Z. Robinson, and Rekha R. Thomas. Positive semidefinite rank. *Mathematical Programming*, 153:133–177, 2014.

Richard P. Feynman. Negative probability. In *Quantum Implications: Essays in Honour of David Bohm*, pp. 235–248. Methuen, 1987.

Gennaro Gala, Cassio de Campos, Robert Peharz, Antonio Vergari, and Erik Quaeghebeur. Probabilistic integral circuits. In *Proceedings of The 27th International Conference on Artificial Intelligence and Statistics*, volume 238 of *Proceedings of Machine Learning Research*, pp. 2143–2151. PMLR, 2024a.

Gennaro Gala, Cassio de Campos, Antonio Vergari, and Erik Quaeghebeur. Scaling continuous latent variable models as probabilistic integral circuits, 2024b.

Aryo Pradipta Gema, Dominik Grabarczyk, Wolf De Wulf, Piyush Borole, Javier Antonio Alfaro, Pasquale Minervini, Antonio Vergari, and Ajitha Rajan. Knowledge graph embeddings in the biomedical domain: Are they useful? a look at link prediction, rule learning, and downstream polypharmacy tasks. *arXiv preprint arXiv:2305.19979*, 2023.

Robert Gens and Pedro M. Domingos. Learning the structure of sum-product networks. In *International Conference on Machine Learning*, 2013.

Mathieu Germain, Karol Gregor, Iain Murray, and Hugo Larochelle. MADE: Masked autoencoder for distribution estimation. In *32nd International Conference on Machine Learning (ICML)*, pp. 881 – 889, 2015.

Kazu Ghalamkari, Jesper Løve Hinrich, and Morten Mørup. Non-negative tensor mixture learning for discrete density estimation. *arXiv preprint arXiv:2405.18220*, 2024.

Nicolas Gillis. *Nonnegative Matrix Factorization*. Society for Industrial and Applied Mathematics (SIAM), 2020.

Ivan Glasser, Ryan Sweke, Nicola Pancotti, Jens Eisert, and Ignacio Cirac. Expressive power of tensor-network factorizations for probabilistic modeling. In *Advances in Neural Information Processing Systems 32 (NeurIPS)*, pp. 1498–1510. Curran Associates, Inc., 2019.

Ivan Glasser, Nicola Pancotti, and J Ignacio Cirac. From probabilistic graphical models to generalized tensor networks for supervised learning. *IEEE Access*, 2020.

Lars Grasedyck. Hierarchical singular value decomposition of tensors. *SIAM journal on matrix analysis and applications*, 31(4):2029–2054, 2010.

Zhao-Yu Han, Jun Wang, Heng Fan, Lei Wang, and Pan Zhang. Unsupervised generative modeling using matrix product states. *Physical Review X*, 8:031012, Jul 2018.

John Hood and Aaron J. Schein. The ALℓ_0CORE tensor decomposition for sparse count data. In *Proceedings of The 27th International Conference on Artificial Intelligence and Statistics*, volume 238 of *Proceedings of Machine Learning Research*, pp. 4654–4662. PMLR, 02–04 May 2024.

Emiel Hoogeboom, Jorn W. T. Peters, Rianne van den Berg, and Max Welling. Integer discrete flows and lossless compression. In *NeurIPS*, pp. 12134–12144, 2019.

Edward J. Hu, Yelong Shen, Phillip Wallis, Zeyuan Allen-Zhu, Yuanzhi Li, Shean Wang, Lu Wang, and Weizhu Chen. Lora: Low-rank adaptation of large language models. In *The Tenth International Conference on Learning Representations, ICLR 2022, Virtual Event, April 25-29, 2022*. OpenReview.net, 2022.

Manfred Jaeger. Probabilistic decision graphs—combining verification and ai techniques for probabilistic inference. *International Journal of Uncertainty, Fuzziness and Knowledge-Based Systems*, 12(supp01): 19–42, 2004.

Priyank Jaini, Amur Ghose, and Pascal Poupart. Prometheus: Directly learning acyclic directed graph structures for sum-product networks. In *European Workshop on Probabilistic Graphical Models*, 2018a.

Priyank Jaini, Pascal Poupart, and Yaoliang Yu. Deep homogeneous mixture models: Representation, separation, and approximation. In S. Bengio, H. Wallach, H. Larochelle, K. Grauman, N. Cesa-Bianchi, and R. Garnett (eds.), *Advances in Neural Information Processing Systems (NeurIPS)*, volume 31. Curran Associates, Inc., 2018b.

Yong-Deok Kim and Seungjin Choi. Nonnegative tucker decomposition. In *CVPR*. IEEE Computer Society, 2007.

Diederik P. Kingma and Jimmy Ba. Adam: A method for stochastic optimization. In *3rd International Conference on Learning Representations (ICLR)*, 2015.

Friso Kingma, Pieter Abbeel, and Jonathan Ho. Bit-swap: Recursive bits-back coding for lossless compression with hierarchical latent variables. In *Proceedings of the 36th International Conference on Machine Learning*, volume 97 of *Proceedings of Machine Learning Research*, pp. 3408–3417, 2019.

Doga Gizem Kisa, Guy Van den Broeck, Arthur Choi, and Adnan Darwiche. Probabilistic sentential decision diagrams. In *International Conference on Principles of Knowledge Representation and Reasoning*, 2014.

Tamara G. Kolda. Multilinear operators for higher-order decompositions. Technical report, Sandia National Laboratories, 2006.

Tamara G. Kolda and Brett W. Bader. Tensor decompositions and applications. *Society of Industrial and Applied Mathematics (SIAM) Review*, 51(3):455–500, 2009.

Tamara G. Kolda, Brett W. Bader, and Joseph P. Kenny. Higher-order web link analysis using multilinear algebra. In *ICDM*, pp. 242–249. IEEE Computer Society, 2005.

Daphne. Koller and Nir Friedman. *Probabilistic Graphical Models: Principles and Techniques*. Adaptive computation and machine learning. MIT Press, 2009.

Pieter M. Kroonenberg. *Applied Multiway Data Analysis*. Wiley Interscience, 2007.

Frank R Kschischang, Brendan J Frey, and H-A Loeliger. Factor graphs and the sum-product algorithm. *IEEE Transactions on information theory*, 47(2):498–519, 2001.

Yann LeCun, Corinna Cortes, and CJ Burges. MNIST handwritten digit database. *ATT Labs [Online]. Available: http://yann.lecun.com/exdb/mnist*, 2, 2010.

Troy Lee and Zhaohui Wei. The square root rank of the correlation polytope is exponential. *ArXiv*, abs/1411.6712, 2014.

Valentin Leplat, Le Thi Khanh Hien, Akwum Onwunta, and Nicolas Gillis. Deep nonnegative matrix factorization with beta divergences. *arXiv preprint arXiv:2309.08249*, 2023.

Anji Liu and Guy Van den Broeck. HCLT reference implementation, 2021a. URL https://github.com/Tractables/ProbabilisticCircuits.jl.

Anji Liu and Guy Van den Broeck. Tractable regularization of probabilistic circuits. In *Advances in Neural Information Processing Systems 34 (NeurIPS)*, pp. 3558–3570. Curran Associates, Inc., 2021b.

Anji Liu, Stephan Mandt, and Guy Van den Broeck. Lossless compression with probabilistic circuits. In *International Conference on Learning Representations*, 2022.

Anji Liu, Honghua Zhang, and Guy Van den Broeck. Scaling up probabilistic circuits by latent variable distillation. In *The Eleventh International Conference on Learning Representations (ICLR)*, 2023a.

Xuejie Liu, Anji Liu, Guy Van den Broeck, and Yitao Liang. Understanding the distillation process from deep generative models to tractable probabilistic circuits. In *International Conference on Machine Learning*, pp. 21825–21838. PMLR, 2023b.

Ziwei Liu, Ping Luo, Xiaogang Wang, and Xiaoou Tang. Deep learning face attributes in the wild. In *Proceedings of International Conference on Computer Vision (ICCV)*, December 2015.

Lorenzo Loconte, Nicola Di Mauro, Robert Peharz, and Antonio Vergari. How to turn your knowledge graph embeddings into generative models via probabilistic circuits. In *Advances in Neural Information Processing Systems 37 (NeurIPS)*. Curran Associates, Inc., 2023.

Lorenzo Loconte, M. Sladek Aleksanteri, Stefan Mengel, Martin Trapp, Arno Solin, Nicolas Gillis, and Antonio Vergari. Subtractive mixture models via squaring: Representation and learning. In *The Twelfth International Conference on Learning Representations (ICLR)*, 2024a.

Lorenzo Loconte, Stefan Mengel, and Antonio Vergari. Sum of squares circuits, 2024b.

Xindian Ma, Peng Zhang, Shuai Zhang, Nan Duan, Yuexian Hou, Ming Zhou, and Dawei Song. A tensorized transformer for language modeling. In *NeurIPS*, pp. 2229–2239, 2019.

Henrique Malvar and Gary Sullivan. Ycocg-r: A color space with rgb reversibility and low dynamic range. *ISO/IEC JTC1/SC29/WG11 and ITU-T SG16 Q*, 6, 2003.

Emanuele Marconato, Samuele Bortolotti, Emile van Krieken, Antonio Vergari, Andrea Passerini, and Stefano Teso. Bears make neuro-symbolic models aware of their reasoning shortcuts. In *Uncertainty in Artificial Intelligence (UAI)*, 2024a.

Emanuele Marconato, Stefano Teso, Antonio Vergari, and Andrea Passerini. Not all neuro-symbolic concepts are created equal: Analysis and mitigation of reasoning shortcuts. *Advances in Neural Information Processing Systems*, 36, 2024b.

Antonio Mari, Gennaro Vessio, and Antonio Vergari. Unifying and understanding overparameterized circuit representations via low-rank tensor decompositions. In *6th Workshop on Tractable Probabilistic Modeling*, 2023.

Radu Marinescu and Rina Dechter. And/or branch-and-bound search for combinatorial optimization in graphical models. *Artificial Intelligence*, 173(16-17):1457–1491, 2009.

Igor L. Markov and Yaoyun Shi. Simulating quantum computation by contracting tensor networks. *SIAM Journal on Computing*, 38(3):963–981, 2008.

James Martens and Venkatesh Medabalimi. On the expressive efficiency of sum product networks. *arXiv preprint arXiv:1411.7717*, 2014.

Alejandro Molina, Sriraam Natarajan, and Kristian Kersting. Poisson sum-product networks: A deep architecture for tractable multivariate poisson distributions. In *AAAI Conference on Artificial Intelligence*, 2017.

Alejandro Molina, Antonio Vergari, Nicola Di Mauro, Sriraam Natarajan, Floriana Esposito, and Kristian Kersting. Mixed sum-product networks: A deep architecture for hybrid domains. In *AAAI Conference on Artificial Intelligence*, 2018.

Maximilian Nickel, Volker Tresp, and Hans-Peter Kriegel. A three-way model for collective learning on multi-relational data. In *ICML*, pp. 809–816. Omnipress, 2011.

Maximilian Nickel, Kevin Murphy, Volker Tresp, and Evgeniy Gabrilovich. A review of relational machine learning for knowledge graphs. *Proceedings of the IEEE*, 104(1):11–33, 2015.

Georgii S. Novikov, Maxim E. Panov, and Ivan V. Oseledets. Tensor-train density estimation. In *37th Conference on Uncertainty in Artificial Intelligence (UAI)*, volume 161 of *Proceedings of Machine Learning Research*, pp. 1321–1331. PMLR, 2021.

Román Orús. A practical introduction to tensor networks: Matrix product states and projected entangled pair states. *Annals of Physics*, 349:117–158, 2013.

Ivan. V. Oseledets. Tensor-train decomposition. *SIAM Journal on Scientific Computing*, 33:2295–2317, 2011.

Umut Oztok and Adnan Darwiche. On compiling dnnfs without determinism. *ArXiv*, abs/1709.07092, 2017.

Yannis Panagakis, Jean Kossaifi, Grigorios G. Chrysos, James Oldfield, Mihalis A. Nicolaou, Anima Anandkumar, and Stefanos Zafeiriou. Tensor methods in computer vision and deep learning. *Proceedings of the IEEE*, 109(5):863–890, 2021.

George Papamakarios, Theo Pavlakou, and Iain Murray. Masked autoregressive flow for density estimation. In *Advances in Neural Information Processing Systems 30 (NeurIPS)*, pp. 2338–2347. Curran Associates, Inc., 2017.

George Papamakarios, Eric Nalisnick, Danilo Jimenez Rezende, Shakir Mohamed, and Balaji Lakshminarayanan. Normalizing flows for probabilistic modeling and inference. *The Journal of Machine Learning Research (JMLR)*, 22(1):2617–2680, 2021.

Robert Peharz, Sebastian Tschiatschek, Franz Pernkopf, and Pedro Domingos. On theoretical properties of sum-product networks. In *Artificial Intelligence and Statistics*, pp. 744–752. PMLR, 2015.

Robert Peharz, Robert Gens, Franz Pernkopf, and Pedro Domingos. On the latent variable interpretation in sum-product networks. *IEEE transactions on pattern analysis and machine intelligence*, 39(10):2030–2044, 2016.

Robert Peharz, Robert Gens, Franz Pernkopf, and Pedro M. Domingos. On the latent variable interpretation in sum-product networks. *IEEE Transactions on Pattern Analalysis and Machine Intelligence*, 39(10): 2030–2044, 2017.

Robert Peharz, Antonio Vergari, Karl Stelzner, Alejandro Molina, Xiaoting Shao, Martin Trapp, Kristian Kersting, and Zoubin Ghahramani. RAT-SPN reference implementation, 2019. URL https://github.com/cambridge-mlg/RAT-SPN.

Robert Peharz, Steven Lang, Antonio Vergari, Karl Stelzner, Alejandro Molina, Martin Trapp, Guy Van Den Broeck, Kristian Kersting, and Zoubin Ghahramani. Einsum networks: Fast and scalable learning of tractable probabilistic circuits. In *37th International Conference on Machine Learning (ICML)*, volume 119 of *Proceedings of Machine Learning Research*, pp. 7563–7574. PMLR, 2020a.

Robert Peharz, Steven Lang, Antonio Vergari, Karl Stelzner, Alejandro Molina, Martin Trapp, Guy Van Den Broeck, Kristian Kersting, and Zoubin Ghahramani. EiNets reference implementation, 2020b. URL https://github.com/cambridge-mlg/EinsumNetworks.

Robert Peharz, Antonio Vergari, Karl Stelzner, Alejandro Molina, Xiaoting Shao, Martin Trapp, Kristian Kersting, and Zoubin Ghahramani. Random sum-product networks: A simple and effective approach to probabilistic deep learning. In *35th Conference on Uncertainty in Artificial Intelligence (UAI)*, volume 115 of *Proceedings of Machine Learning Research*, pp. 334–344. PMLR, 2020c.

David Pérez-García, F. Verstraete, Michael M. Wolf, and Juan Ignacio Cirac. Matrix product state representations. *Quantum Information and Computing*, 7(5):401–430, 2007. ISSN 1533-7146.

Knot Pipatsrisawat and Adnan Darwiche. New compilation languages based on structured decomposability. In *23rd Conference on Artificial Intelligence (AAAI)*, volume 8, pp. 517–522, 2008.

Hoifung Poon and Pedro Domingos. Sum-product networks: A new deep architecture. In *IEEE International Conference on Computer Vision Workshops (ICCV Workshops)*, pp. 689–690. IEEE, 2011.

Harsh Poonia, Moritz Willig, Zhongjie Yu, Matej Zečević, Kristian Kersting, and Devendra Singh Dhami. χSPN: Characteristic interventional sum-product networks for causal inference in hybrid domains. In *The 40th Conference on Uncertainty in Artificial Intelligence (UAI)*, 2024.

Lawrence Rabiner and Biinghwang Juang. An introduction to hidden Markov models. *IEEE ASSP magazine*, 3(1):4–16, 1986.

Tahrima Rahman, Prasanna Kothalkar, and Vibhav Gogate. Cutset networks: A simple, tractable, and scalable approach for improving the accuracy of chow-liu trees. In *Machine Learning and Knowledge Discovery in Databases: European Conference, ECML PKDD 2014, Nancy, France, September 15-19, 2014. Proceedings, Part II 14*, pp. 630–645. Springer, 2014.

Pengzhen Ren, Yun Xiao, Xiaojun Chang, Po-Yao Huang, Zhihui Li, Xiaojiang Chen, and Xin Wang. A comprehensive survey of neural architecture search: Challenges and solutions. *ACM Computing Surveys (CSUR)*, 54(4):1–34, 2021.

Elina Robeva and Anna Seigal. Duality of graphical models and tensor networks, 2017.

Yangjun Ruan, Karen Ullrich, Daniel S. Severo, James Townsend, Ashish Khisti, Arnaud Doucet, Alireza Makhzani, and Chris Maddison. Improving lossless compression rates via monte carlo bits-back coding. In *Proceedings of the 38th International Conference on Machine Learning*, volume 139 of *Proceedings of Machine Learning Research*, pp. 9136–9147, 2021.

Berkant Savas and Lars Eldén. Handwritten digit classification using higher order singular value decomposition. *Pattern Recognit.*, 40(3):993–1003, 2007.

Ulrich Schollwoeck. The density-matrix renormalization group in the age of matrix product states. *Annals of Physics*, 326:96–192, 2010.

Nimish Shah, Wannes Meert, and Marian Verhelst. *Efficient Execution of Irregular Dataflow Graphs*. Springer, 2023.

Xiaoting Shao, Alejandro Molina, Antonio Vergari, Karl Stelzner, Robert Peharz, Thomas Liebig, and Kristian Kersting. Conditional sum-product networks: Imposing structure on deep probabilistic architectures. In *International Conference on Probabilistic Graphical Models*, pp. 401–412. PMLR, 2020.

Xiaoting Shao, Alejandro Molina, Antonio Vergari, Karl Stelzner, Robert Peharz, Thomas Liebig, and Kristian Kersting. Conditional sum-product networks: Modular probabilistic circuits via gate functions. *International Journal of Approximate Reasoning*, 140:298–313, 2022.

Or Sharir, Ronen Tamari, Nadav Cohen, and Amnon Shashua. Tensorial mixture models. *ArXiv*, abs/1610.04167, 2017.

Amnon Shashua and Tamir Hazan. Non-negative tensor factorization with applications to statistics and computer vision. In *Proceedings of the 22nd international conference on Machine learning*, pp. 792–799, 2005.

Yujia Shen, Arthur Choi, and Adnan Darwiche. Tractable operations for arithmetic circuits of probabilistic models. In *Advances in Neural Information Processing Systems 29 (NeurIPS)*. Curran Associates, Inc., 2016.

Yaoyun Shi, Luming Duan, and Guifré Vidal. Classical simulation of quantum many-body systems with a tree tensor network. *Physical Review A*, 74:022320, 2005.

Amir Shpilka and Amir Yehudayoff. Arithmetic circuits: A survey of recent results and open questions. *Founddations and Trends in Theoretical Computer Science*, 5:207–388, 2010.

Sahil Sidheekh and Sriraam Natarajan. Building expressive and tractable probabilistic generative models: A review. *arXiv preprint arXiv:2402.00759*, 2024.

Sahil Sidheekh, Kristian Kersting, and Sriraam Natarajan. Probabilistic flow circuits: Towards unified deep models for tractable probabilistic inference. In *39th Conference on Uncertainty in Artificial Intelligence (UAI)*, volume 216 of *Proceedings of Machine Learning Research*, pp. 1964–1973. PMLR, 2023.

Nicholas D. Sidiropoulos, Lieven De Lathauwer, Xiao Fu, Kejun Huang, Evangelos E. Papalexakis, and Christos Faloutsos. Tensor decomposition for signal processing and machine learning. *IEEE Transactions on Signal Processing*, 65(13):3551–3582, 2017. doi: 10.1109/TSP.2017.2690524.

Le Song, Mariya Ishteva, Ankur Parikh, Eric Xing, and Haesun Park. Hierarchical tensor decomposition of latent tree graphical models. In *International Conference on Machine Learning*, pp. 334–342. PMLR, 2013.

Edwin Stoudenmire and David J Schwab. Supervised learning with tensor networks. In *Advances in Neural Information Processing Systems 29 (NeurIPS)*, pp. 4799–4807. Curran Associates, Inc., 2016.

Ping Liang Tan and Robert Peharz. Hierarchical decompositional mixtures of variational autoencoders. In *Proceedings of the 36th International Conference on Machine Learning*, volume 97 of *Proceedings of Machine Learning Research*, pp. 6115–6124. PMLR, 09–15 Jun 2019.

Alex Townsend and Lloyd N. Trefethen. Continuous analogues of matrix factorizations. *Proceedings of the Royal Society A: Mathematical, Physical and Engineering Sciences*, 471, 2015.

James Townsend, Thomas Bird, and David Barber. Practical lossless compression with latent variables using bits back coding. In *ICLR 2019*, 2019.

Volker Tresp, Sahand Sharifzadeh, Hang Li, Dario Konopatzki, and Yunpu Ma. The tensor brain: A unified theory of perception, memory, and semantic decoding. *Neural Computation*, 35:156–227, 2021.

L. R. Tucker. The extension of factor analysis to three-dimensional matrices. In *Contributions to mathematical psychology.*, pp. 110–127. Holt, Rinehart and Winston, 1964.

Ledyard R Tucker. Some mathematical notes on three-mode factor analysis. *Psychometrika*, 31:279–311, 1966.

Leslie G. Valiant. Negation can be exponentially powerful. In *11th Annual ACM Symposium on Theory of Computing*, pp. 189–196, 1979.

Emile van Krieken, Pasquale Minervini, Edoardo Ponti, and Antonio Vergari. On the independence assumption in neurosymbolic learning. In *Forty-first International Conference on Machine Learning*, 2024.

M. Alex O. Vasilescu and Demetri Terzopoulos. Multilinear image analysis for facial recognition. In *ICPR 2002*, pp. 511–514. IEEE Computer Society, 2002.

Joshua Vendrow, Jamie Haddock, and Deanna Needell. A generalized hierarchical nonnegative tensor decomposition. *IEEE International Conference on Acoustics, Speech and Signal Processing (ICASSP)*, pp. 4473–4477, 2021.

Antonio Vergari, Nicola Di Mauro, and Floriana Esposito. Simplifying, regularizing and strengthening sum-product network structure learning. In *Machine Learning and Knowledge Discovery in Databases: European Conference, ECML PKDD 2015, Porto, Portugal, September 7-11, 2015, Proceedings, Part II 15*, pp. 343–358. Springer, 2015.

Antonio Vergari, Robert Peharz, Nicola Di Mauro, Alejandro Molina, Kristian Kersting, and Floriana Esposito. Sum-product autoencoding: Encoding and decoding representations using sum-product networks. In *Proceedings of the AAAI Conference on Artificial Intelligence*, volume 32, 2018.

Antonio Vergari, Nicola Di Mauro, and Floriana Esposito. Visualizing and understanding sum-product networks. *Machine Learning*, 108(4):551–573, 2019a.

Antonio Vergari, Nicola Di Mauro, and Guy Van den Broeck. Tractable probabilistic models: Representations, algorithms, learning, and applications. *Tutorial at the 35th Conference on Uncertainty in Artificial Intelligence (UAI)*, 2019b.

Antonio Vergari, YooJung Choi, Anji Liu, Stefano Teso, and Guy Van den Broeck. A compositional atlas of tractable circuit operations for probabilistic inference. In *Advances in Neural Information Processing Systems 34 (NeurIPS)*, pp. 13189–13201. Curran Associates, Inc., 2021.

Maarten De Vos, Lieven De Lathauwer, Bart Vanrumste, Sabine Van Huffel, and Wim Van Paesschen. Canonical decomposition of ictal scalp EEG and accurate source localisation: Principles and simulation study. *Computational Intelligence and Neuroscience*, 2007, 2007.

Thomas Wedenig, Rishub Nagpal, Gaetan Cassiers, Stefan Mangard, and Robert Peharz. Exact soft analytical side-channel attacks using tractable circuits. In *International Conference on Machine Learning*, 2024a.

Thomas Wedenig, Rishub Nagpal, Gaëtan Cassiers, Stefan Mangard, and Robert Peharz. Exact soft analytical side-channel attacks using tractable circuits. In *International Conference on Machine Learning*, 2024b.

Han Xiao, Kashif Rasul, and Roland Vollgraf. Fashion-MNIST: a Novel Image Dataset for Benchmarking Machine Learning Algorithms. *ArXiv*, abs/1708.07747, 2017.

Mingxue Xu, Yao Lei Xu, and Danilo P. Mandic. Tensorgpt: Efficient compression of the embedding layer in llms based on the tensor-train decomposition. *CoRR*, abs/2307.00526, 2023.

Zhongjie Yu, Martin Trapp, and Kristian Kersting. Characteristic circuits. In *Thirty-seventh Conference on Neural Information Processing Systems (NeurIPS)*, 2023.

Zhe Zeng, Paolo Morettin, Fanqi Yan, Antonio Vergari, and Guy Van den Broeck. Scaling up hybrid probabilistic inference with logical and arithmetic constraints via message passing. In *International Conference on Machine Learning*, pp. 10990–11000. PMLR, 2020.

Honghua Zhang, Meihua Dang, Nanyun Peng, and Guy Van den Broeck. Tractable control for autoregressive language generation. In *40th International Conference on Machine Learning (ICML)*, volume 202 of *Proceedings of Machine Learning Research*, pp. 40932–40945. PMLR, 2023.

Han Zhao, Pascal Poupart, and Geoffrey J Gordon. A unified approach for learning the parameters of sum-product networks. *Advances in neural information processing systems*, 29, 2016.

A Proofs

A.1 Tucker as a Circuit

Proposition 1 (Tucker as a circuit)**.** Let $\boldsymbol{\mathcal{T}} \in \mathbb{R}^{I_1 \times \cdots \times I_d}$ be a tensor being decomposed via a multilinear rank-$(R_1, \ldots, R_d)$ Tucker factorization, as in Eq. (2). Then, there exists a circuit c over variables $\mathbf{X} = \{X_j\}_{j=1}^d$ with $\mathsf{dom}(X_j) = [I_j]$, $j \in [d]$ computing the same factorization. Moreover, we have that $|c| \in \mathcal{O}(d \prod_{j=1}^d R_j)$.

Proof. We prove it constructively by giving the structure and parameters of c. That is, we build a circuit c over variables $\mathbf{X}$ computing

$$c(\mathbf{X}) = c(x_1, \ldots, x_d) = \sum_{r_1=1}^{R_1} \cdots \sum_{r_d=1}^{R_d} w_{r_1 \cdots r_d} c_{1,r_1}(x_1) \cdots c_{d,r_d}(x_d). \tag{21}$$

Note that in Eq. (21) each product $c^{\mathsf{in}}_{1,r_1}(x_1) \cdots c^{\mathsf{in}}_{d,r_d}(x_d)$ can be computed by a product unit $c^{\mathsf{prod}}_{r_1 \cdots r_d}$ over variables $\mathbf{X}$. Moreover, we encode each c^{in}_{j,r_j} as an input unit, for all $j \in [d]$ and $r_j \in [R_j]$. In addition, the collection of sums $\sum_{r_1=1}^{R_1} \cdots \sum_{r_d=1}^{R_d}$ that are weighted by the $w_{r_1 \cdots r_d}$ can be computed by a single sum unit having $\prod_{j=1}^d R_j$ inputs, i.e., the products $c^{\mathsf{prod}}_{r_1 \cdots r_d}$ with $r_j \in [R_j]$ for all j. Since each product units has d inputs, we have that the overall circuit size is $|c| \in \mathcal{O}(d \prod_{j=1}^d R_j)$. Finally, we take $w_{r_1 \cdots r_d}$ as the entries of the core tensor $\boldsymbol{\mathcal{W}}$, and make each input unit c^{in}_{j,r_j} compute $c^{\mathsf{in}}_{j,r_j}(x_j) = v^{(j)}_{x_j,r_j}$ for the factor matrices $\{\mathbf{V}^{(j)}\}_{j=1}^d$ in the Tucker factorization. That is, $c(\mathbf{X})$ computes the same Tucker factorization given by hypothesis. □

A.2 Hierarchical Tucker as Deep a Circuit

Proposition 2 (Hierarchical Tucker as a deep circuit)**.** Let $\boldsymbol{\mathcal{T}} \in \mathbb{R}^{I_1 \times \cdots \times I_d}$ be a tensor being decomposed using hierarchical Tucker factorization according to a RG $\mathcal{R}$ (Def. 5). Then, there exists a circuit c over variables $\mathbf{X} = \{X_j\}_{j=1}^d$ with $\mathsf{dom}(X_j) = [I_j]$, computing the same factorization. Furthermore, given $\{\mathbf{Y}^{(i)}\}_{i=1}^m \subset 2^{\mathbf{X}}$ the set of all non-leaf region nodes $\mathbf{Y}^{(i)} \subseteq \mathbf{X}$ being factorized into $(\mathbf{Z}_1^{(i)}, \mathbf{Z}_2^{(i)})$ in $\mathcal{R}$, with corresponding Tucker factorization multilinear rank $(R_{\mathbf{Y}^{(i)}}, R_{\mathbf{Z}_1^{(i)}}, R_{\mathbf{Z}_2^{(i)}})$, we have that $|c| \in \mathcal{O}\left(\sum_{i=1}^m R_{\mathbf{Y}^{(i)}} R_{\mathbf{Z}_1^{(i)}} R_{\mathbf{Z}_2^{(i)}}\right)$.

Proof. Similarly to our proof for Proposition 1, we prove it constructively by giving the structure and parameters of c. That is, we rewrite the recursive rules used to define a hierarchical Tucker factorization showed in Def. 5 in terms of equivalent circuit computational units. For every leaf region $\mathbf{Z} = \{X_j\}$ in $\mathcal{R}$, we introduce the input units c^{in}_{j,r_j}, $r_j \in [R_{\mathbf{Z}}]$, each computing $c_{j,r_j}(x_j) = v^{(j)}_{x_j r_j}$ for the factor matrix $\mathbf{V}^{(j)}$ of the hierarchical Tucker factorization given by hypothesis. Next, we recursively introduce sum and product units by following the hierarchical variables factorization defined in $\mathcal{R}$. That is, for every non-leaf region node $\mathbf{Y} \subseteq \mathbf{X}$ being partitioned into $(\mathbf{Z}_1, \mathbf{Z}_2)$ in $\mathcal{R}$, we introduce sum and product units that encode a Tucker factorization related to the region node $\mathbf{Y}$. More formally, given $(R_{\mathbf{Y}}, R_{\mathbf{Z}_1}, R_{\mathbf{Z}_2})$ the multilinear rank associated to the region node $\mathbf{Y}$, we introduce the sum units $c^{\mathsf{sum}}_{\mathbf{Y},s}$, with $s \in [R_{\mathbf{Y}}]$. Moreover, we introduce the product units $c^{\mathsf{prod}}_{\mathbf{Y},r_1,r_2}$, with $r_1 \in [R_{\mathbf{Z}_1}]$ and $r_2 \in [R_{\mathbf{Z}_2}]$. Each sum unit $c^{\mathsf{sum}}_{\mathbf{Y},s}$ has the product units $\{c^{\mathsf{prod}}_{\mathbf{Y},r_1,r_2}\}_{r_1=1,r_2=1}^{R_{\mathbf{Z}_1},R_{\mathbf{Z}_2}}$ as inputs, and is parameterized by weights $\{w_{s,r_1,r_2}\}_{r_1=1,r_2=1}^{R_{\mathbf{Z}_1},R_{\mathbf{Z}_2}}$. Furthermore, we recursively define the inputs to each product unit $c^{\mathsf{prod}}_{\mathbf{Y},r_1,r_2}$ to be the pair of sum units $c^{\mathsf{sum}}_{\mathbf{Z}_1,r_1}$ and $c^{\mathsf{sum}}_{\mathbf{Z}_2,r_2}$, for all $r_1 \in [R_{\mathbf{Z}_1}]$ and $r_2 \in [R_{\mathbf{Z}_2}]$. By setting the parameters of each sum unit θ_{s,r_1,r_2} to be the entries of the core tensor $\boldsymbol{\mathcal{W}}^{(\mathbf{Y})}$ (see Eq. (6)), we recover that the constructed composition of sum and product units encodes the Tucker factorization associated to $\mathbf{Y}$. Finally, in the case of the root region $\mathbf{Y} = \mathbf{X}$ in $\mathcal{R}$, we have that $R_{\mathbf{Y}} = 1$ by hypothesis, and therefore the output of the circuit is given by the sum unit $c^{\mathsf{sum}}_{\mathbf{X},1}$. Since the circuit c built in this way consists of a composition of Tucker factorizations represented as circuits (Proposition 1), the circuit size is $|c| \in \mathcal{O}(\sum_{i=1}^m R_{\mathbf{Y}^{(i)}} R_{\mathbf{Z}_1^{(i)}} R_{\mathbf{Z}_2^{(i)}})$, with $\{\mathbf{Y}^{(i)}\}_{i=1}^m$ being the set of non-leaf regions in $\mathcal{R}$. □

B Many Tensorized PC Architectures can be Obtained through our Pipeline

We will consider one tensorized PC architecture at a time, and show how its construction can be understood in terms of simple design choices presented in our pipeline: (1) the region graph to parameterize (Section 4.1), (2) the sum and product layers chosen (Sections 4.2 and 4.3 and Section 5), and (3) whether the architecture is folded or not (Section 4.4).

Poon & Domingos circuits (Poon & Domingos, 2011) for image data follow the homonomous region graph structure. While the circuit is *not* tensorized, i.e., the computational units defined over the same variable scope are not replicated and tensorized into layers, we can still see them as a tensorized circuit where the width of each layer is 1. Furthermore, no folding is performed to the best of our knowledge.

Randomized-and-tensorized circuits (RAT-SPN) (Peharz et al., 2020c) are obtained by parameterizing a randomly-constructed binary tree region graph (named RND in this paper). In particular, in this architecture Kronecker product layers and sum layers are alternated, thus being equivalent to circuits with Tucker layers (Eq. (Tucker-layer)) in our pipeline. In the original implementation of RAT-SPNs (Peharz et al., 2019), layers are no folded.

Einsum networks (EiNets) (Peharz et al., 2020a) include a folded version of RAT-SPNs, as well as tensorized *and* folded circuits obtained by overparameterizing the PD region graph. See Peharz et al. (2020b) and Braun (2021) for known available implementations.

Hidden Chow-Liu Tree (HCLT) circuits (Liu & Van den Broeck, 2021b) are tensorized circuits obtained by compiling a tree-shaped graphical model that is learned with the Chow-Liu algorithm (Chow & Liu, 1968a). Therefore, it can be obtained in our pipeline by parameterizing the CL region graph with $\mathrm{CP}^\top$ layers whose parameter matrices encode conditional probability tables. HCLTs have been originally implemented within the Juice.jl Julia library (Liu & Van den Broeck, 2021a), which also includes a parallelization scheme using custom CUDA kernels that fuse sum and products operations.

Non-negative matrix-product states ($\mathbf{MPS}_{\mathbb{R}_{\geqslant 0}}$) have been shown to be equivalent to hidden-markov-models (HMMs) (Rabiner & Juang, 1986) up to renormalization (Glasser et al., 2019). Given a total ordering of variables $X_1, \ldots, X_d$, it is known we can compile an HMM into an equivalent structured decomposable circuit (Vergari et al., 2019b), which has the same structure of the tensorized circuit encoding an MPS showed in Fig. 8. Therefore, we can represent an $\mathrm{HMM}/\mathrm{MPS}_{\mathbb{R}_{\geqslant 0}}$ in our circuit construction pipeline by parameterizing a linear-tree region graph (called LT in this paper) with $\mathrm{CP}^\top$ layers.

Born machines (BM) (Han et al., 2018) **and Tensor-Train Density Estimators (TTDE)** (Novikov et al., 2021) are probabilistic models used to estimate probability mass functions and probability density functions, respectively. They are obtained by efficiently squaring an MPS, which is a structured decomposable tensorized circuit as for Proposition 3. Note that such a tensorized circuit can be obtained using the same region graph and tensorized layer used to construct a non-negative MPS, but instead just relax the non-negativity assumption over its parameters. It is known that squaring a MPS (resp. a structured decomposable tensorized circuit) yields a BM (resp. another structured decomposable tensorized circuit having the same layers but with a quadratic width increase). See e.g. Proposition 3 in Loconte et al. (2024a). Therefore, BMs and TTDEs can be retrieved through our circuit construction pipeline by overaparameterizing a linear-tree region graph (LT) with $\mathrm{CP}^\top$layers, followed by efficiently squaring the resulting circuit (Vergari et al., 2021).

Squared non-monotonic PCs (NPC^2) (Loconte et al., 2024a) are generalizations of BMs and TTDEs that also include the squaring of tensorized circuits obtained by overparameterizing a random binary tree region graph (as in RAT-SPNs above), as well as using Tucker layers instead of $\mathrm{CP}^\top$layers. Furthermore, the original implementation of NPC^2 allows circuits to be folded.

Tree Tensor Networks (TTNs) (Cheng et al., 2019) are tree-shaped hierarchical tensor factorizations represented through the tensor network formalism. TTNs factorizations are equivalent to hierarchical Tucker, but one choose a particular structure based on the data distribution being modelled. For image data, Cheng et al. (2019) proposed a TTN structure obtained by recursively splitting an image in half, alternating horizontal and vertical splits. This structure is analogous to our quad tree region graph (QT), but allowing splitting image patches in just two parts (rather than four).

C Sampling

In Algorithm C.1, we interpret the entries of each non-negative parameter matrix $\mathbf{W}^{S\times K}$ in c as the parameters of categorical distributions associated to S latent variables, each taking values in $\{1,\ldots,K\}$. Note that we can always normalize a PC s.t. its normalization constant is equal to 1 thus yielding parameter matrices that sum up to 1 along every row, as detailed in (Peharz et al., 2015). Then, sampling a data point $\mathbf{x}$ translates to iteratively sampling from such latent variables (see L8-13 of the algorithm) according to the hierarchical structure of the circuit, i.e. following a topological order like a breadth first search (BFS). Note that sampling the latent variables corresponding to a sum layer corresponds to choosing (i) a selection of the input layers on which recursively continue sampling, and (ii) a particular computational unit within each selected layer. The information (i) and (ii) for each layer is stored in dictionaries (see L1-4). Due to decomposability (Def. 8), sampling from a product layer $\boldsymbol{\ell}$ translates to choosing a selection of the input computational units, as they will be defined on different variables. Unlike sum layers where we sample from Categoricals to select such units, in product layers they are unequivocally determined by which product unit of $\boldsymbol{\ell}$ has been selected previously and whether $\boldsymbol{\ell}$ is an Kronecker or Hadamard layer (see L14-20). We sample all sum and product layers as explained below. Finally, it remains to sample from the input layers and assign values to the variables the PC is defined on. We sample from an input layer $\boldsymbol{\ell}$ when at least one input units within $\boldsymbol{\ell}$ has been selected by the sampling procedure above for sum and product layers. That is, given $X \in \mathbf{X}$ the variable on which $\boldsymbol{\ell}$ depends on and n_k the k-th input unit to sample from, we sample an assignment to X from n_k (see L21-25).

Algorithm C.1 $\mathsf{samplingTensorizedPC}(c, N)$

Input: A tensorized PC c over $\mathbf{X} = \{X_i\}_{i=1}^{D}$, a positive integer N.
Output: Samples $\mathbf{S} \in \mathbb{R}^{N\times D}$ drawn from c.
Assumptions: (1) c is normalized: all sum layer parameters sum up to 1 over the columns; (2) Each input layer is defined over a single RV; (3) the width of a layer is a multiple of K.
Notes: (1) All assignments preceded by the symbol $\forall$ can be parallelized; (2) $\mathsf{unravel\text{-}index}$ is the homonymous numpy function but whose indexing starts from 1 instead of 0.

1: $\mathcal{S} \leftarrow \{\boldsymbol{\ell} : [\,] \mid \forall \boldsymbol{\ell} \in c\}$ ▷ mapping layers to sample indices
2: $\mathcal{U} \leftarrow \{\boldsymbol{\ell} : [\,] \mid \forall \boldsymbol{\ell} \in c\}$ ▷ mapping layers to unit indices
3: $\mathcal{S}[c] \leftarrow [N]$
4: $\mathcal{U}[c] \leftarrow \mathbf{1}_N$
5: **for each** inner layer $\boldsymbol{\ell} \in \mathsf{BFS}(c)$ **do**
6: $\quad\mathcal{L} \leftarrow$ list of the L input layers of ℓ
7: $\quad$**if** $\mathcal{S}[\,\boldsymbol{\ell}\,]$ is empty **then skip**
8: $\quad$**else if** ℓ is a sum layer with $\mathbf{W} \in \mathbb{R}^{K\times KL}$ **then**
9: $\quad\quad\mathbf{v} \leftarrow$ vector of size $|\mathcal{S}[\,\boldsymbol{\ell}\,]|$ with values in $[KL]$
10: $\quad\quad v_i \leftarrow$ sample from categorical with $\mathsf{p} = \mathbf{w}_{\mathcal{U}[\ell]_i,:}$
11: $\quad\quad\mathsf{idx1}, \mathsf{idx2} \leftarrow \mathsf{unravel\text{-}index}(\mathbf{v}, (L, K))$
12: $\quad\quad\forall i \in [L] : \mathcal{S}[\mathcal{L}[i]].\mathsf{extend}(\mathcal{S}[\,\boldsymbol{\ell}\,][\,\mathsf{idx1} == i\,])$
13: $\quad\quad\quad\quad\mathcal{U}[\mathcal{L}[i]].\mathsf{extend}(\mathsf{idx2}[\,\mathsf{idx1} == i\,])$
14: $\quad$**else if** $\boldsymbol{\ell}$ is a Kronecker prod. layer **then**
15: $\quad\quad\mathsf{idx\text{-}list} \leftarrow \mathsf{unravel\text{-}index}(\mathcal{U}[\,\boldsymbol{\ell}\,], (K,)_{i=1}^{L})$
16: $\quad\quad\forall i \in [L] : \mathcal{S}[\mathcal{L}[i]].\mathsf{extend}(\mathcal{S}[\,\boldsymbol{\ell}\,])$
17: $\quad\quad\quad\quad\mathcal{U}[\mathcal{L}[i]].\mathsf{extend}(\mathsf{idx\text{-}list}[k])$
18: $\quad$**else if** ℓ is a Hadamard prod. layer **then**
19: $\quad\quad\forall i \in [L] : \mathcal{S}[\mathcal{L}[i]].\mathsf{extend}(\mathcal{S}[\,\boldsymbol{\ell}\,])$
20: $\quad\quad\quad\quad\mathcal{U}[\mathcal{L}[i]].\mathsf{extend}(\mathcal{U}[\,\boldsymbol{\ell}\,])$
21: $\mathbf{S} \leftarrow \mathbb{R}^{N\times D}$
22: **for each** input layer $\boldsymbol{\ell} \in c$ **s.t.** $\mathcal{S}[\ell] \neq [\,]$ **do**
23: $\quad j \leftarrow \mathsf{sc}(\boldsymbol{\ell})$
24: $\quad\mathsf{pairs} \leftarrow \mathsf{vstack}(\mathcal{S}[\boldsymbol{\ell}], \mathcal{U}[\boldsymbol{\ell}])$
25: $\quad\forall (i,k) \in \mathsf{pairs} : \mathbf{S}_{ij} \leftarrow$ sample k-th unit of $\boldsymbol{\ell}$
26: **return** samples $\mathbf{S}$

D Region Graphs: Quad-Graphs and Quad-Trees

Algorithm D.1 details the construction of our proposed RGs for image-data: QTs and QGs. The algorithm takes as input the height (H) and width (W) of the image, and a flag (isTree), which specifies whether to enforce the output RG to be a tree (QT) or not (QG). The algorithm builds a RG in a bottom-up fashion, merging regions associated to smaller patches to bigger patches, starting from the single pixels. Specifically, to build QTs—QT-4s to be precise—we merge regions using Algorithm D.2, whereas for QGs we merge regions using Algorithm D.3.

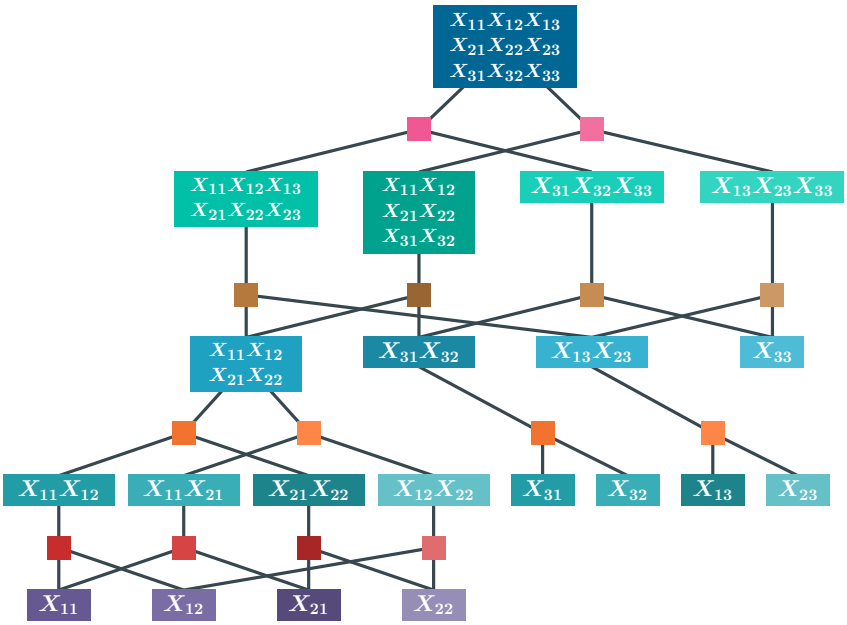

Figure D.1: **The quad graph (QG).** We illustrate the quad graph RG delivered by Algorithm D.1 passing $H = 3$, $W = 3$ and $\mathsf{isTree} = \mathsf{False}$ as input arguments. The region graph is *unbalanced* as the image size (3×3) is not a power of 2. Differently from our quad trees (QTs), QGs have regions partitioned in more than a single way (e.g., the root region node), and regions can be shared among partitions. For example, in a QT, the top region could only be partitioned in a single way into two or four subregions, respectively called QT-2 and QT-4 region graphs.

Algorithm D.1 $\mathsf{buildQuadGraph}(H, W, \mathsf{isTree})$

Input: Image height H, image width W, and whether to enforce the output RG to be a tree.
Output: a RG over $H \cdot W$ variables.

$\mathsf{S} \leftarrow \{\mathbf{Y}_{ij} = \{X_{ij}\} \mid (i,j) \in [H] \times [W]\}$
$\mathcal{R} \leftarrow$ a RG having leaf regions S
$h \leftarrow H;\ \ w \leftarrow W$
while $h > 1 \vee w > 1$ **do**
  $h \leftarrow \lceil h/2 \rceil;\ \ w \leftarrow \lceil w/2 \rceil;\ \ \mathsf{S}' \leftarrow \varnothing$
  for $i, j \in [h] \times [w]$ **do**
    $\Delta \leftarrow (\{2i-1, 2i\} \times \{2j-1, 2j\}) \bigcap ([H] \times [W])$
    if $|\Delta| = 1$ **then**
      Let $\mathbf{Y}_{pq} \in \mathsf{S}$ s.t. $(p,q) \in \Delta$
      $\mathsf{addRegion}(\mathcal{R}, \mathbf{Y}_{pq})$
    else if $|\Delta| = 2$ **then**
      Let $\mathbf{Y}_{pq}, \mathbf{Y}_{rs} \in \mathsf{S}$ s.t.
        $(p,q), (r,s) \in \Delta, \quad p < r, q < s$
      $\mathsf{addPartition}(\mathcal{R}, \mathbf{Y}_{pq} \cup \mathbf{Y}_{rs}, \{\mathbf{Y}_{pq}, \mathbf{Y}_{rs}\})$
    else $\quad \triangleright\ |\Delta| = 4$
      if isTree **then** $\mathsf{mergeTree}(\mathcal{R}, \Delta, \mathsf{S})$
      else $\mathsf{mergeDAG}(\mathcal{R}, \Delta, \mathsf{S})$
    $\mathbf{Y}_{ij} \leftarrow \bigcup_{(r,s) \in \Delta} \mathbf{Y}_{rs}$ s.t. $\mathbf{Y}_{rs} \in \mathsf{S}$
    $\mathsf{S}' \leftarrow \mathsf{S}' \cup \{\mathbf{Y}_{ij}\}$
  $\mathsf{S} \leftarrow \mathsf{S}'$
return $\mathcal{R}$

Algorithm D.2 $\mathsf{mergeTree}(\mathcal{R}, \Delta, \mathsf{S})$

Input: a RG $\mathcal{R}$, a set of four coordinates Δ, and a collection of regions S.
Behavior: It merges the regions indexed by Δ in $\mathcal{R}$ by forming a tree structure.

Let $\mathbf{Z}_{uv} = \mathbf{Y}_{p+u\ q+v} \in \mathsf{S}$ s.t.
  $(p+u, q+v) \in \Delta, \quad u, v \in \{0, 1\}$
$\mathbf{Y} \leftarrow \mathbf{Z}_{00} \cup \mathbf{Z}_{01} \cup \mathbf{Z}_{10} \cup \mathbf{Z}_{11}$
$\mathsf{addPartition}(\mathcal{R}, \mathbf{Y}, \{\mathbf{Z}_{00}, \mathbf{Z}_{01}, \mathbf{Z}_{10}, \mathbf{Z}_{11}\})$

Algorithm D.3 $\mathsf{mergeDAG}(\mathcal{R}, \Delta, \mathsf{S})$

Input: a RG $\mathcal{R}$, a set of four coordinates Δ, and a collection of regions S.
Behavior: It merges the regions indexed by Δ in $\mathcal{R}$ by forming a DAG structure.

Let $\mathbf{Z}_{uv} = \mathbf{Y}_{p+u\ q+v} \in \mathsf{S}$ s.t.
  $(p+u, q+v) \in \Delta, \quad u, v \in \{0, 1\}$
$\mathbf{Y} \leftarrow \mathbf{Z}_{00} \cup \mathbf{Z}_{01} \cup \mathbf{Z}_{10} \cup \mathbf{Z}_{11}$
$\mathsf{addPartition}(\mathcal{R}, \mathbf{Y}, \{\mathbf{Z}_{00} \cup \mathbf{Z}_{01}, \mathbf{Z}_{10} \cup \mathbf{Z}_{11}\})$
$\mathsf{addPartition}(\mathcal{R}, \mathbf{Y}, \{\mathbf{Z}_{00} \cup \mathbf{Z}_{10}, \mathbf{Z}_{01} \cup \mathbf{Z}_{11}\})$
$\mathsf{addPartition}(\mathcal{R}, \mathbf{Z}_{00} \cup \mathbf{Z}_{01}, \{\mathbf{Z}_{00}, \mathbf{Z}_{01}\})$
$\mathsf{addPartition}(\mathcal{R}, \mathbf{Z}_{10} \cup \mathbf{Z}_{11}, \{\mathbf{Z}_{10}, \mathbf{Z}_{11}\})$
$\mathsf{addPartition}(\mathcal{R}, \mathbf{Z}_{00} \cup \mathbf{Z}_{10}, \{\mathbf{Z}_{00}, \mathbf{Z}_{10}\})$
$\mathsf{addPartition}(\mathcal{R}, \mathbf{Z}_{01} \cup \mathbf{Z}_{11}, \{\mathbf{Z}_{01}, \mathbf{Z}_{11}\})$

We illustrate in Fig. D.1 the resulting QG obtained via Algorithm D.1 with $H = 3$, $W = 3$ and $\mathsf{isTree} = \mathsf{False}$. The QG is unbalanced as HW is not a power of 2.

E Additional Results

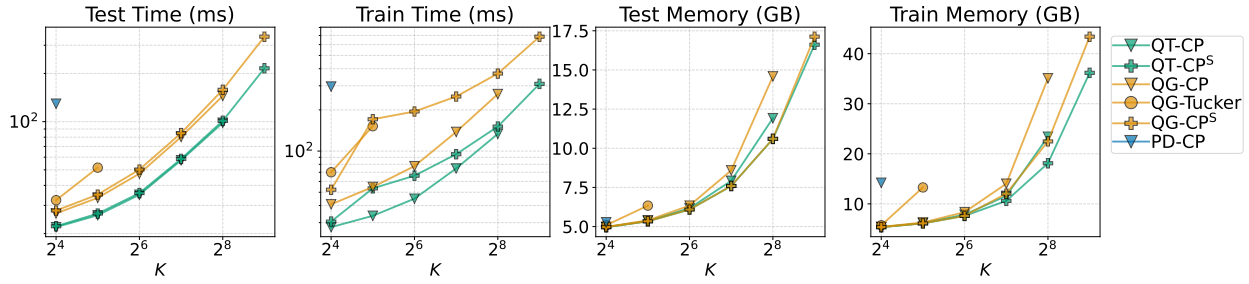

Figure E.1: **Benchmarking the role of RGs and composite layers in tensorized circuits on CelebA.** We report the average time (ms) and GPU memory usage (GiBs) to process a batch of samples for different tensorized architectures—listed in the legend on the right—at different values of K (x-axis). The stats are reported both at test and training time. The benchmark is conducted using the CelebA dataset with a batch size of 128.

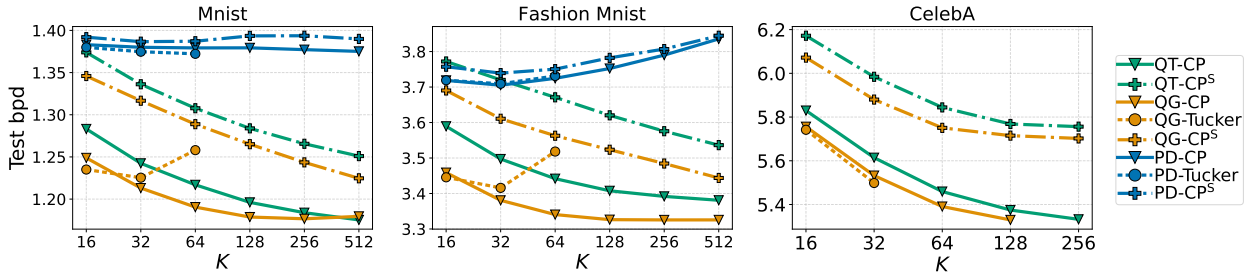

Figure E.2: **Overparameterizing tensorized architectures delivers better performing models when using QTs and QGs, but not when using PDs. Different from Fig. 20, we here learn the mixing layers in QG- and PD-based models.** We report the test-set bpd (y-axis) at different values of K (x-axis) for Mnist (left), FashionMnist (middle) and CelebA (right) averaged over 5 runs for different tensorized architectures, which we report in the legend on the right. We use a batch size of 256.

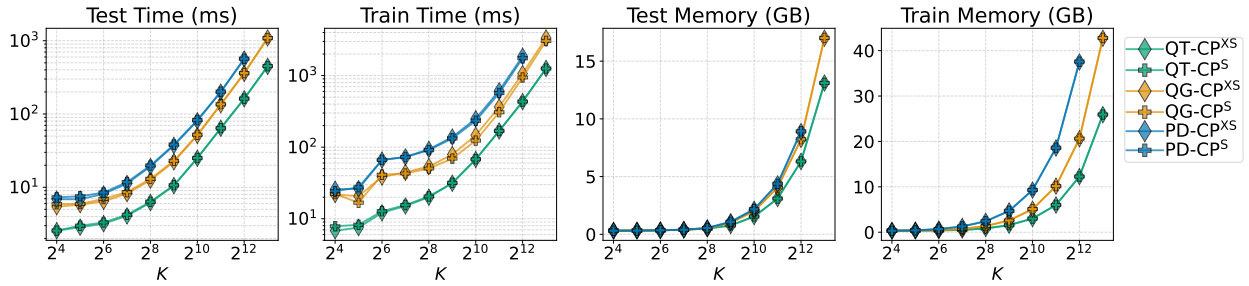

Figure E.3: **For the same choice of RG and K, CP^{S} and CP^{XS} layers require the same time/space resources, with CP^{XS} only being slightly faster at training-time.** We report time (ms) and GPU memory usage (GiBs) at different values of K (x-axis) at both test-time and training-time for different tensorized architectures listed in the legend on the right. The benchmark is conducted on Mnist using a batch size of 128.

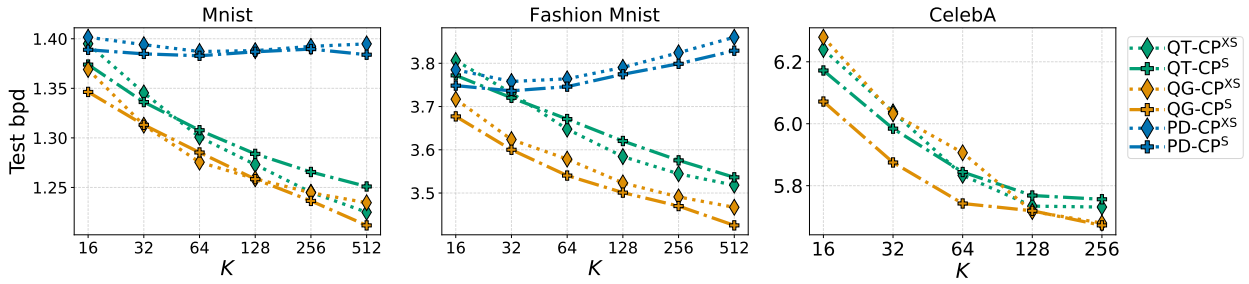

Figure E.4: **CP^{XS} and CP^{S} layers are equivalently accurate when used in different tensorized architectures.** We report the test-set bpd (y-axis) averaged over 5 runs for different tensorized architectures—listed in the legend on the right—at different values of K (x-axis). We use the MNIST, FASHIONMNIST and CELEBA datasets, and a batch size of 256.

Table E.1: **Mnist distribution estimation results.** Test-set bpd on MNIST averaged over 5 runs for different tensorized PC architectures. We report 3 standard deviations from the mean.

RG	Learn Mixing-Layer	K	CP	CP^{XS}	CP^{S}	Tucker
PD	Yes	16	1.383 ± 0.008	1.392 ± 0.008	1.392 ± 0.007	1.380 ± 0.006
		32	1.380 ± 0.007	1.387 ± 0.005	1.387 ± 0.008	1.375 ± 0.004
		64	1.379 ± 0.009	1.384 ± 0.005	1.387 ± 0.009	1.372 ± 0.004
		128	1.379 ± 0.003	1.386 ± 0.006	1.394 ± 0.006	OOM
		256	1.377 ± 0.005	1.386 ± 0.008	1.394 ± 0.009	OOM
		512	1.375 ± 0.009	1.385 ± 0.007	1.390 ± 0.011	OOM
PD	No	16	1.381 ± 0.007	1.402 ± 0.008	1.389 ± 0.006	1.377 ± 0.005
		32	1.381 ± 0.009	1.394 ± 0.011	1.385 ± 0.003	1.377 ± 0.004
		64	1.376 ± 0.002	1.387 ± 0.005	1.383 ± 0.004	1.381 ± 0.006
		128	1.375 ± 0.003	1.388 ± 0.004	1.387 ± 0.003	OOM
		256	1.373 ± 0.005	1.392 ± 0.006	1.390 ± 0.009	OOM
		512	1.370 ± 0.002	1.395 ± 0.014	1.384 ± 0.008	OOM
QT	N/A	16	1.283 ± 0.004	1.395 ± 0.008	1.374 ± 0.008	N/A
		32	1.242 ± 0.004	1.345 ± 0.030	1.336 ± 0.009	N/A
		64	1.217 ± 0.002	1.301 ± 0.019	1.308 ± 0.003	N/A
		128	1.196 ± 0.004	1.273 ± 0.028	1.284 ± 0.002	N/A
		256	1.184 ± 0.002	1.245 ± 0.028	1.266 ± 0.003	N/A
		512	1.175 ± 0.001	1.225 ± 0.010	1.251 ± 0.002	N/A
QG	Yes	16	1.249 ± 0.004	1.375 ± 0.014	1.346 ± 0.010	1.235 ± 0.012
		32	1.213 ± 0.003	1.334 ± 0.010	1.317 ± 0.004	1.225 ± 0.011
		64	1.190 ± 0.003	1.280 ± 0.017	1.289 ± 0.003	1.258 ± 0.005
		128	1.179 ± 0.001	1.240 ± 0.015	1.265 ± 0.004	OOM
		256	1.177 ± 0.004	1.218 ± 0.021	1.244 ± 0.003	OOM
		512	1.180 ± 0.009	1.205 ± 0.011	1.225 ± 0.004	OOM
QG	No	16	1.248 ± 0.003	1.369 ± 0.039	1.346 ± 0.004	1.233 ± 0.004
		32	1.212 ± 0.003	1.313 ± 0.027	1.313 ± 0.006	1.222 ± 0.004
		64	1.185 ± 0.002	1.276 ± 0.010	1.285 ± 0.006	1.257 ± 0.005
		128	1.171 ± 0.002	1.259 ± 0.011	1.258 ± 0.004	OOM
		256	1.173 ± 0.009	1.245 ± 0.009	1.236 ± 0.002	OOM
		512	1.177 ± 0.006	1.235 ± 0.010	1.212 ± 0.010	OOM

Table E.2: **FashionMnist distribution estimation results.** Test-set bpd on FashionMnist averaged over 5 runs for different tensorized PC architectures. We report 3 standard deviations from the mean.

RG	Learn Mixing-Layer	K	CP	CP^{XS}	CP^{S}	Tucker
PD	Yes	16	3.719 ± 0.014	3.757 ± 0.008	3.757 ± 0.011	3.719 ± 0.015
		32	3.705 ± 0.012	3.738 ± 0.011	3.739 ± 0.005	3.709 ± 0.004
		64	3.725 ± 0.011	3.749 ± 0.009	3.750 ± 0.007	3.731 ± 0.014
		128	3.752 ± 0.005	3.774 ± 0.009	3.782 ± 0.005	OOM
		256	3.790 ± 0.011	3.801 ± 0.013	3.807 ± 0.018	OOM
		512	3.836 ± 0.019	3.836 ± 0.024	3.845 ± 0.017	OOM
PD	No	16	3.715 ± 0.004	3.785 ± 0.010	3.748 ± 0.011	3.716 ± 0.007
		32	3.700 ± 0.017	3.758 ± 0.009	3.736 ± 0.005	3.709 ± 0.004
		64	3.721 ± 0.011	3.764 ± 0.012	3.746 ± 0.011	3.736 ± 0.006
		128	3.752 ± 0.012	3.791 ± 0.007	3.775 ± 0.010	OOM
		256	3.779 ± 0.012	3.824 ± 0.006	3.799 ± 0.014	OOM
		512	3.814 ± 0.012	3.860 ± 0.024	3.829 ± 0.015	OOM
QT	N/A	16	3.589 ± 0.005	3.806 ± 0.042	3.772 ± 0.031	N/A
		32	3.497 ± 0.003	3.731 ± 0.032	3.720 ± 0.007	N/A
		64	3.442 ± 0.003	3.648 ± 0.019	3.671 ± 0.005	N/A
		128	3.408 ± 0.003	3.584 ± 0.011	3.620 ± 0.009	N/A
		256	3.392 ± 0.001	3.544 ± 0.014	3.576 ± 0.013	N/A
		512	3.381 ± 0.002	3.518 ± 0.018	3.536 ± 0.007	N/A
QG	Yes	16	3.459 ± 0.004	3.741 ± 0.030	3.690 ± 0.019	3.446 ± 0.004
		32	3.381 ± 0.002	3.635 ± 0.026	3.611 ± 0.016	3.416 ± 0.006
		64	3.341 ± 0.004	3.555 ± 0.020	3.563 ± 0.020	3.518 ± 0.012
		128	3.326 ± 0.002	3.487 ± 0.018	3.523 ± 0.006	OOM
		256	3.326 ± 0.003	3.449 ± 0.018	3.484 ± 0.004	OOM
		512	3.326 ± 0.004	3.409 ± 0.011	3.444 ± 0.009	OOM
QG	No	16	3.464 ± 0.005	3.717 ± 0.051	3.677 ± 0.031	3.446 ± 0.008
		32	3.385 ± 0.004	3.624 ± 0.051	3.600 ± 0.011	3.417 ± 0.005
		64	3.339 ± 0.004	3.578 ± 0.032	3.540 ± 0.009	3.499 ± 0.006
		128	3.319 ± 0.004	3.523 ± 0.036	3.501 ± 0.017	OOM
		256	3.317 ± 0.002	3.491 ± 0.013	3.470 ± 0.005	OOM
		512	3.317 ± 0.005	3.467 ± 0.032	3.425 ± 0.010	OOM

Table E.3: **CelebA distribution estimation results (using RGB values).** Test-set bpd on CelebA averaged over 3 runs for different tensorized PC architectures. We report 3 standard deviations from the mean.

RG	Learn Mixing-Layer	K	CP	CP^{XS}	CP^{S}	Tucker
QT	N/A	16	5.828 ± 0.008	6.237 ± 0.026	6.171 ± 0.006	N/A
		32	5.612 ± 0.012	6.024 ± 0.032	5.981 ± 0.007	N/A
		64	5.457 ± 0.010	5.831 ± 0.022	5.843 ± 0.017	N/A
		128	5.374 ± 0.002	5.732 ± 0.044	5.766 ± 0.022	N/A
		256	5.332 ± 0.002	5.739 ± 0.037	5.753 ± 0.014	N/A
QG	Yes	16	5.756	6.161	6.072	5.742
		32	5.532	5.960	5.880	5.498
		64	5.391	5.816	5.751	OOM
		128	5.329	5.771	5.715	OOM
		256	OOM	5.731	5.702	OOM
QG	No	16	5.755 ± 0.010	6.292 ± 0.037	6.069 ± 0.006	5.738 ± 0.011
		32	5.528 ± 0.023	6.056 ± 0.072	5.875 ± 0.016	5.494 ± 0.023
		64	5.392 ± 0.026	5.906 ± 0.052	5.746 ± 0.010	OOM
		128	5.335 ± 0.027	5.742 ± 0.067	5.725 ± 0.039	OOM
		256	OOM	5.691 ± 0.034	5.667 ± 0.014	OOM

Table E.4: **CelebA distribution estimation results using lossless YCoCg transform.** Test-set bpd on CelebA over 1 single run for different tensorized PC architectures. We note how performance are consistently better than those in Table E.3, confirming that using the YCoCg transform helps. Note that results in this table are directly comparable with those in Table E.3 because the transformation used is lossless (and operates on discrete data, hence does not require a correction by the log-determinant).

RG	Learn Mixing-Layer	K	CP	CP^{XS}	CP^{S}	Tucker
QT	N/A	16	5.604	5.770	5.831	N/A
		32	5.447	5.656	5.648	N/A
		64	5.321	5.584	5.589	N/A
		128	5.248	5.570	5.549	N/A
		256	5.238	5.522	5.548	N/A
QG	No	16	5.541	5.840	5.757	5.541
		32	5.383	5.660	5.622	5.383
		64	5.273	5.544	5.510	OOM
		128	5.205	5.536	5.500	OOM
		256	OOM	5.579	5.489	OOM

E.1 Results on UCI Tabular Datasets

	D	Number of samples		
		train	validation	test
Power	6	1,659,917	184,435	204,928
Gas	8	852,174	94,685	105,206
Hepmass	21	315,123	35,013	174,987
MiniBooNE	43	29,556	3,284	3,648
BSDS300	63	1,000,000	50,000	250,000

Table E.5: **UCI dataset statistics.** Dimensionality D and number of samples of each dataset split after the preprocessing by Papamakarios et al. (2017).

Density estimation on tabular datasets. Following Papamakarios et al. (2017), we evaluate our tensorized architectures for density estimation on five tabular datasets. For each dataset, we randomly construct 8 binary tree region graphs (cf. Section 4.1), and build a mixture of tensorized PCs based of them. Specifically, following our mix-and-match approach Table 1, we build RND-CP and RND-Tucker architectures which we run for several model sizes K and learning rates (see below). Differently from images, all these datasets contain continuous features, which we model using input layers encoding Gaussian likelihoods. We train all PCs for up to 1000 epochs or until convergence, using Adam as optimizer and 512 as batch size. Furthermore, we perform the experiments using three different learning rates: 10^{-3}, $5 \cdot 10^{-3}$, and 10^{-2}, and report the best results according to the validation set log-likelihood.

Results. Fig. E.5 reports the best results from our models, where we see that Tucker layers outperform CP layers on the two lowest dimensional datasets – Power and Gas – which also have the highest number of training data points (see Table E.5). On the other hand, CP-based architectures outperform Tucker-based ones on the other three datasets (Hepmass, MiniBooNE and BSDS300), even though the latter have a much higher number of trainable parameters then the former for a fixed K (i.e., K^2 for CP while K^3 for Tucker). Our results suggest that the more aggressive over-parameterization of Tucker layers lead to a more difficult optimization for high-dimensional datasets and thus for deeper tensorized PCs.

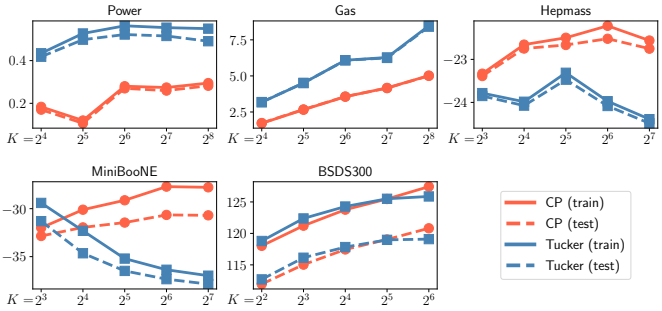

	Power	Gas	Hepmass	M.BooNE	BSDS300
MADE	-3.08	3.56	-20.98	-15.59	148.85
RealNVP	0.17	8.33	-18.71	-13.84	153.28
MAF	0.24	10.08	-17.73	-12.24	154.93
NSF	0.66	13.09	-14.01	-9.22	157.31
Gaussian	-7.74	-3.58	-27.93	-37.24	96.67
EiNet-LRS	0.36	4.79	-22.46	-34.21	—
TTDE	0.46	8.93	-21.34	-28.77	143.30
RND-CP	0.28	5.01	-22.52	-30.69	120.82
RND-Tucker	0.52	8.41	-23.47	-31.30	119.09

Figure E.5: **Tucker layers are harder to scale than CP layers on high-dimensional UCI datasets.** The **right table** is the one reported in Table 3. The **left plots** show the train and test log-likelihoods of our architectures as the size K of the layers increases. We observe that increasing K is generally beneficial for CP layers in all UCI datasets (left). However, increasing K in Tucker layers can decrease performances for higher-dimensional datasets, as shown for the cases of Hepmass and MiniBooNE. The left plots showing the train set log-likelihoods (dotted lines) are evidence that the decrease of performances of tensorized PCs with Tucker layers is not due to overfitting.

F How to implement (folded) layers?

In this section, we provide pytorch snippets to implement a folded Categorical input layer, as well as all the folded sum-product layers we introduced, i.e. Tucker (Eq. (Tucker-layer)), CP (Eq. (CP-layer)), CP$^\top$ (Eq. (CP$^\top$-layer)), CP$^\text{S}$ and CP$^\text{XS}$ (Eq. (CP$^\text{S}$-layer)). Our tensorized circuit architectures are nothing more than a sequential application of such layers. We will release our code upon acceptance.

```python
def categorical_layer(batch, param):
    """Evaluates a folded Categorical layer with C categories.

    :param batch: Input batch (num_folds, num_channels, batch_size)
    :param param: Raw parameters (num_folds, K, num_channels, C)
    :return log_prob: Output log prob (num_folds, K, batch_size)
    """
    cat_log_prob = param.log_softmax(-1)
    idx_fold = torch.arange(batch.size(0))[:, None, None]
    idx_channel = torch.arange(batch.size(1))[None, :, None]
    log_prob = cat_log_prob[idx_fold, :, idx_channel, batch].sum(dim=1)
    return log_prob.transpose(-1, -2)
```

Figure F.1: **Pytorch snippet for a folded categorical layer.** The snippet details the evaluation of a folded categorical layer, which can be used for any type of categorical variable. For instance, it can be used to evaluate the log-likelihood of pixels in image modeling as well as tokens in language modeling. Note how the raw input parameters (`param`) undergo a log-softmax reparameterization (Section 3.2) so as to model valid log-probabilities for many categorical distributions.

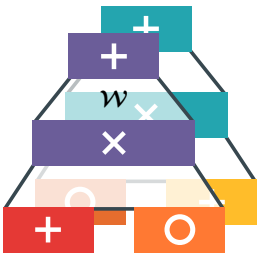


```python
def tucker_layer(log_prob, W):
    """Evaluates a folded Tucker layer with arity 2 via log-sum-exp.

    :param log_prob: Input log prob (num_folds, 2, K, batch_size)
    :param W: Layer weights in prob domain (num_folds, K, K, O)
    :return out_log_prob: Output log prob (num_folds, O, batch_size)
    """
    max_log_prob = log_prob.max(dim=2, keepdim=True).values
    exp_log_prob = torch.exp(log_prob - max_log_prob)
    out_log_prob = max_log_prob.sum(dim=1) + torch.einsum(
        "fib,fjb,fijo->fob",
        exp_log_prob[:, 0], exp_log_prob[:, 1], W).log()
    return out_log_prob
```

Figure F.2: **Pytorch snippet for a folded Tucker layer.** A folded Tucker layer $\boldsymbol{\ell}$ is parameterized by a tensor $\boldsymbol{\mathcal{W}}$ of shape $F \times O \times K^2$, and computes F Tucker layer (Eq. (Tucker-layer)) $\{\boldsymbol{\ell}^{(n)}\}_{n=1}^{F}$ *in parallel*. Specifically, the layer $\boldsymbol{\ell}$ computes

$$\boldsymbol{\ell}\left(\bigcup_{n=1}^{F} \mathbf{Y}^{(n)}\right)_{n:} = \mathbf{W}_{n::}\left[\boldsymbol{\ell}_1\left(\bigcup_{n=1}^{F} \mathbf{Z}_1^{(n)}\right)_{n:} \otimes \boldsymbol{\ell}_2\left(\bigcup_{n=1}^{F} \mathbf{Z}_2^{(n)}\right)_{n:}\right],$$

where $\boldsymbol{\ell}_1$ (resp. $\boldsymbol{\ell}_2$) denotes a folded layer computing the F left (resp. right) inputs to $\boldsymbol{\ell}^{(n)}$, each defined over variables $\mathbf{Z}_1^{(n)}$ (resp. $\mathbf{Z}_2^{(n)}$), and $\mathbf{W}_{n::} \in \mathbb{R}^{O \times K^2}$ is the parameter matrix of $\boldsymbol{\ell}^{(n)}$. Note that the snippet shapes the tensor $\boldsymbol{\mathcal{W}}$ as $F \times K \times K \times O$ for convenience with the einsum operation.

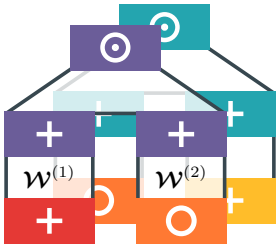


```python
def cp_layer(log_prob, W1, W2):
    """Evaluates a folded CP layer with arity 2 via log-sum-exp.

    :param log_prob: Input log probs, (num_folds, 2, K, batch_size)
    :param W1: Folded layer weights, (num_folds, K, O)
    :param W2: Folded layer weights, (num_folds, K, O)
    :return out_log_prob: Output log probs, (num_folds, O, batch_size)
    """
    max_log_prob = log_prob.max(dim=2, keepdim=True).values
    exp_log_prob = torch.exp(log_prob - max_log_prob)
    out_log_prob = max_log_prob.sum(dim=1) + torch.einsum(
        "fib,fjb,fio,fjo->fob",
        exp_log_prob[:, 0], exp_log_prob[:, 1], W1, W2).log()
    return out_log_prob
```

Figure F.3: **Pytorch snippet for a folded CP layer.** A folded CP layer $\boldsymbol{\ell}$ is parameterized by two equally-sized tensors $\boldsymbol{\mathcal{W}}^{(1)}$ and $\boldsymbol{\mathcal{W}}^{(2)}$ of shape $F \times O \times K$, and computes F CP layer (Eq. (CP-layer)) $\{\boldsymbol{\ell}^{(n)}\}_{n=1}^{F}$ *in parallel*. Specifically, the layer $\boldsymbol{\ell}$ computes

$$\boldsymbol{\ell}\left(\bigcup_{n=1}^{F} \mathbf{Y}^{(n)}\right)_{n:} = \left(\mathbf{W}^{(1)}_{n::}\, \boldsymbol{\ell}_1\left(\bigcup_{n=1}^{F} \mathbf{Z}_1^{(n)}\right)_{n:}\right) \odot \left(\mathbf{W}^{(2)}_{n::}\, \boldsymbol{\ell}_2\left(\bigcup_{n=1}^{F} \mathbf{Z}_2^{(n)}\right)_{n:}\right),$$

where $\boldsymbol{\ell}_1$ (resp. $\boldsymbol{\ell}_2$) denotes a folded layer computing the F left (resp. right) inputs to $\boldsymbol{\ell}^{(n)}$, each defined over variables $\mathbf{Z}_1^{(n)}$ (resp. $\mathbf{Z}_2^{(n)}$), and $\mathbf{W}^{(1)}_{n::}, \mathbf{W}^{(2)}_{n::} \in \mathbb{R}^{O \times K}$ are the parameter matrices of $\boldsymbol{\ell}^{(n)}$.

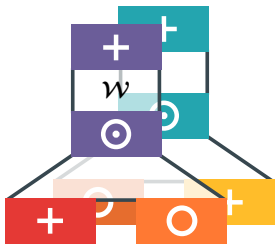


```python
def cpt_layer(log_prob, W):
    """Evaluates a folded CP-T layer with arity H via log-sum-exp.

    :param log_prob: Input log prob (num_folds, H, K, batch_size)
    :param W: Folded layer weights (num_folds, K, O)
    :return out_log_prob: Output log prob (num_folds, O, batch_size)
    """
    log_prob = log_prob.sum(dim=1, keepdim=True)
    max_log_prob = log_prob.max(dim=2, keepdim=True).values
    exp_log_prob = torch.exp(log_prob - max_log_prob)
    out_log_prob = max_log_prob.sum(dim=1) + torch.einsum(
        "fib,fio->fob",
        exp_log_prob[:, 0], W).log()
    return out_log_prob
```

Figure F.4: **Pytorch snippet for a folded CP$^{\top}$ layer.** A folded CP$^{\top}$ layer $\boldsymbol{\ell}$ is parameterized by tensor $\boldsymbol{\mathcal{W}}$ of shape $F \times O \times K$, and computes F CP$^{\top}$ layer (Eq. (CP$^{\top}$-layer)) $\{\boldsymbol{\ell}^{(n)}\}_{n=1}^{F}$ *in parallel*. Specifically, the layer $\boldsymbol{\ell}$ computes

$$\boldsymbol{\ell}\left(\bigcup_{n=1}^{F} \mathbf{Y}^{(n)}\right)_{n:} = \mathbf{W}_{n::}\left(\boldsymbol{\ell}_1\left(\bigcup_{n=1}^{F} \mathbf{Z}_1^{(n)}\right)_{n:} \odot \boldsymbol{\ell}_2\left(\bigcup_{n=1}^{F} \mathbf{Z}_2^{(n)}\right)_{n:}\right),$$

where $\boldsymbol{\ell}_1$ (resp. $\boldsymbol{\ell}_2$) denotes a folded layer computing the F left (resp. right) inputs to $\boldsymbol{\ell}^{(n)}$, each defined over variables $\mathbf{Z}_1^{(n)}$ (resp. $\mathbf{Z}_2^{(n)}$), and $\mathbf{W}_{n::} \in \mathbb{R}^{O \times K}$ are the parameter matrices of $\boldsymbol{\ell}^{(n)}$.

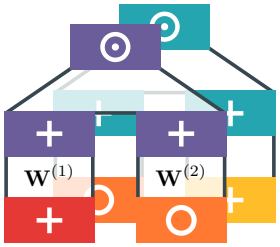


```python
def cpxs_layer(log_prob, W1, W2, D=None):
    """Evaluates a CP-XS layer with arity 2 via log-sum-exp.
       If D is None then evaluates a CP-S layer.

    :param log_prob: Input log probs, (num_folds, 2, K, batch_size)
    :param W1: Folded layer weights, (K, O)
    :param W2: Folded layer weights, (K, O)
    :param D: Optional weights (num_folds, O)
    :return out_log_prob: Output log probs, (num_folds, O, batch_size)
    """
    max_log_prob = log_prob.max(dim=2, keepdim=True).values
    exp_log_prob = torch.exp(log_prob - max_log_prob)
    out_log_prob = max_log_prob.sum(dim=1) + torch.einsum(
        "fib,fjb,io,jo->fob",
        exp_log_prob[:, 0], exp_log_prob[:, 1], W1, W2).log()
    if D:
        out_log_prob += D.log().unsqueeze(-1)
    return out_log_prob
```

Figure F.5: **Pytorch snippet for a CP$^{\mathbf{S}}$ layer.** A CP^{S} layer $\boldsymbol{\ell}$ is parameterized by two equally-sized matrices $\mathbf{W}^{(1)}$ and $\mathbf{W}^{(2)}$ of shape $O \times K$, and a matrix $\mathbf{D}$ of shape $F \times O$. The layer computes F CP layer (Eq. (CP^{S}-layer)) $\{\boldsymbol{\ell}^{(n)}\}_{n=1}^{F}$ *in parallel*, each parameterized by $\mathbf{W}^{(1)}$ and $\mathbf{W}^{(2)}$, and then weights their outputs by $\mathbf{D}$. Specifically, the layer $\boldsymbol{\ell}$ computes

$$\boldsymbol{\ell}\left(\bigcup_{n=1}^{F} \mathbf{Y}^{(n)}\right)_{n:} = \mathbf{d}_{n:} \odot \left(\mathbf{W}^{(1)}\, \boldsymbol{\ell}_1\left(\bigcup_{n=1}^{F} \mathbf{Z}_1^{(n)}\right)_{n:}\right) \odot \left(\mathbf{W}^{(2)}\, \boldsymbol{\ell}_2\left(\bigcup_{n=1}^{F} \mathbf{Z}_2^{(n)}\right)_{n:}\right),$$

where $\boldsymbol{\ell}_1$ (resp. $\boldsymbol{\ell}_2$) denotes a folded layer computing the F left (resp. right) inputs to $\boldsymbol{\ell}^{(n)}$, each defined over variables $\mathbf{Z}_1^{(n)}$ (resp. $\mathbf{Z}_2^{(n)}$), $\mathbf{W}^{(1)}, \mathbf{W}^{(2)} \in \mathbb{R}^{O \times K}$ are the parameter matrices of $\boldsymbol{\ell}^{(n)}$, and $\mathbf{D}$ as a folded-dependent parameter matrix. When $\mathbf{D} = \mathbf{1}$ we retrieve CP^{XS}.